Robot Assisted Asymmetric Incremental Sheet Metal Forming for Steep Wall Angle Parts

THESIS

Submitted in partial fulfilment
of the requirements for the degree of
DOCTOR OF PHILOSOPHY
By

SWAGATIKA MOHANTY
ID no :- 2012PHXF0534H

Under the Supervision of

Prof. Srinivasa Prakash Regalla

And Co-supervision of

Prof. Yendluri Venkata Daseswara Rao

BIRLA INSTITUTE OF TECHNOLOGY AND SCIENCE, PILANI

2018

BIRLA INSTITUTE OF TECHNOLOGY AND SCIENCE, PILANI

CERTIFICATE

This is to certify that the thesis entitled "**Robot Assisted Asymmetric Incremental Sheet Metal Forming for Steep Wall Angle Parts"** submitted by Swagatika Mohanty, ID. No. 2012PHXF0534H for the award of Ph. D degree of the institute embodies the original work done by her under our supervision.

Signature in full of the Supervisor -

Name in Capital block letters - Prof. SRINIVASA PRAKASH REGALLA

Designation -Professor

Signature in full of the Co-supervisor -

Name in Capital block letters - Prof. YENDLURI VENKATA DASESWARA RAO

Designation - Associate professor

ACKNOWLEDGEMENTS

First and foremost, I would like to thank God almighty for providing me the opportunity and strength to step in to the world of engineering research. I would like to express my gratitude to all those people who supported in this duration and made this research possible.

I would like to express my deepest gratitude to my supervisor **Prof. Srinivasa Prakash Regalla** who led me into this interesting field of research and for providing excellent guidance during the course of my candidature. His continuous assistance, invaluable advice, discussions and suggestions helped me in smoothly finishing the research. I would like to express my deepest appreciation to my co-supervisor **Prof. Yendluri Venkata Daseswara Rao** for his close guidance in robotics. His guidance and suggestions especially in designing control system helped me to complete my work efficiently.

I am highly grateful to my doctoral advisory committee members, **Prof. N. Suresh Kumar Reddy and Dr. Sabareesh Geetha Rajasekharan** for their valuable suggestions during semester presentation and for the valuable comments to improve my thesis. I am truly grateful to Prof. N. Suresh Kumar Reddy for allowing me to use the experimental facilities in workshop and his valuable comments on my thesis. I thank **Prof. Amit kumar Gupta**, Head of the Department, Mechanical engineering, BITS Pilani, Hyderabad campus and also other faculty members. I would like to thank **Dr. Kurra Suresh** for helping in conducting intial experiments and sharing his technical knowledge in research.

I am grateful to former vice-chancellor **Prof. Bijendra Nath Jain**, vice-chancellor **Souvik Bhattacharyya** of BITS Pilani, former director **Prof. V. S. Rao**, present director **Prof. G Sundar** of BITS Pilani Hyderabad Campus for allowing me to carry out my doctoral research work in the institute.

I would like to express my sincere thanks to **Prof. Vidya Rajesh**, former Associate Dean, and **Prof. Vamsi Krishna Venuganti**, Associate dean, Academic Research (Ph.D. Programme), **Prof. S. K.Verma**, Dean, Academic Research (Ph.D. Programme), BITS Pilani for their continuous support and encouragement during my research work.

Concerning the experimental work i performed, I am truly grateful to **Mr. Marri Bhaskar** for his patience with me and helping in performing experiments on CNC milling machines. I would also like to thank **Mr. Chandrasekhar, Mr. Jinu Paul and Mr. Sridhar** for investing their valuable time in setting up the designed set up on the CNC milling

machine. I would like to thank **M. Narsing Rao ,Mr. P. Mahendra Chary and Mr. K. Krishna Kumar** for preparing the blank and tool required for the experiments, **Mr. Laxman Bangaru** and **Mr. Srinivasa Rao** for their assistance in material testing lab and material procurement and **Mr. Suryanarayana** for his support in measuring surface roughness. Thanks to **Mr. Bali Reddy** for his interest in my experiments. I am highly grateful to **Mr.Rajat Bansal** for his timely help and effort in designing the control system part.

I would like to express my sincere thanks to **Mr. Rama Chandra Raju and Mr. Niranjan kumar** from S R Tooling systems for helping me out in manufacturing of the designed manipulator and timely delivery.

Finally I am grateful to my parents and my sister for their unfailing support, understanding and love over the years. I want to express my special gratitude to my husband for his patience and support. My heart-felt appreciations and thankfulness goes to all my friends who have been my family during my studies. I am obliged to thank all my friends Priyanka, Preeti, Sonia, Sai, Karthik, Shanmukh, Uday, Kiran, Pawan, Akhil, Hemanth and my department colleagues for being my source of motivation and thank you for making me feel at home.

I would like to thank Dr.Mohan, Punnya, Dr.Kalyana Rama, Pratyusha, Prof. Sridhar Raju, Aditya Gadepalli, Anook Immidisetty, Dr. Rajitha, Mr. Prakash Mohan, Dr. Radhika, Dr. Sabareesh for inspiring me and guiding me in leading a peaceful life through the knowledge of Bhagavad Gita.

Swagatika Mohanty

ABSTRACT

Incremental Sheet metal forming (ISF) is modern manufacturing process suitable for small batch production and new product development. For the growing need of customised products of geometric complexity, flexibility in manufacturing parts and low tool cost because it is die-less manufacturing process are the two core advantages for using ISF in industries. This die-less process can be carried out using a pre-existing vertical Computer numerical control (CNC) milling machine as well as by multi-axis robots. ISF enables higher formability than conventional sheet metal forming. Understanding the deformation mechanism in ISF needs deeper understanding of mechanics and parametric dependence to guarantee the reliability in using this method in industries.

For a given work piece geometry, ISF can be carried out either in a single stage, in which the total plastic strain required is achieved or in multi stage mode, where the plastic strain is suitably distributed among the stages. One major limitation of single stage incremental sheet metal forming is the maximum angle that can be obtained without excessive thinning (leading to subsequent failure) of the sheet metal. This contribution led to the concept of multi stag ISF. Multi stage ISF does enable steeper wall angles to be achieved at the expense of longer manufacturing time. A possible way to obtain steeper wall angles with reasonable manufacturing time is to orient the work piece with respect to the forming tool so that they always encounter each other at angles within the limits of, around 70^{o}, throughout the forming process. This can be achieved either by dedicated 5 or 6-axis CNC machine tool or by an innovative robotic manipulator tailor-made for the purpose. The latter is the main thrust in this present doctoral work. Since steep wall angle requirement can be only occasional on certain part geometries it is not justifiable to invest in a very expensive multi-axes CNC machines.

In this work, a more efficient and cost-effective solution in the form of a 2-DOF robotic fixture to support and dynamically orient the work piece is proposed and its use is investigated. In this robot assisted incremental forming process, the numerical control tool path is to be subdivided between the forming tool and the robotic fixture. The robotic fixture presents, at all instants the deformation zone of the work piece to the forming tool at effective wall angles far less than the presently known limiting wall angle of around 70^{o}. This enables the achievement of steeper wall angle parts by forming in a single stage and hence saving of manufacturing time in comparison to the multi stage incremental forming.

In the present work, robotic manipulator was designed using the kinematic and dynamic analysis. The developed manipulator was tested thoroughly, initially by forming only truncated circular cone. User programming based sub-division of numerical control part program between forming tool and robotic fixture was combined with finite element analysis to predict the surface roughness, sheet thinning, forming force and sheet failure at maximum wall angle. These results were compared with those found in experimental singe stage ISF. The scientific work in this thesis was focusing on investigating the behaviour of the commercial aluminium sheet Al-1100 by using the designed manipulator. Initially the effect of existing as well as additional process parameters on the responses were investigated using widely used numerical simulation. Adaptive meshing has been used in numerical simulation and the simulated results have been compared with the experimental results to confirm the adaptive meshing parameters. Formability, thickness distribution and forming force have been checked in numerical simulations. The responses have been validated experimentally in order to assess the level of accuracy between the results obtained in numerical prediction and experimental results. Surface roughness due to additional process parameters has also been investigated experimentally using the designed manipulator. Formability and surface finish in ISF can be improved by changing the orientation and rotation of the sheet. By further research, the proposed approach can be extended to form more complicated shapes that are highly in demand in various industries.

Keywords: Robot assisted incremental forming, Formability, Surface roughness, Thinning, Finite element simulation.

TABLE OF CONTENTS

LIST OF TABLES

LIST OF FIGURES

LIST OF ABBREVIATIONS

ADSIF: Accumulative Double-Sided Incremental Forming

ANN: Artificial Neural Network

ANOVA: Analysis of variance

CAD/CAM: Comuputer Aided Design/Computer Aided Manufacturing

CNC: Computer Numeric Control

DH: Denavit and Hartenberg

DOE: Design of experiments

DPIF: Duplex Incremental sheet metal Forming

FEM: Finite Element Modeling

FFLs: Fracture Forming Limit curves

FLC: Forming Limit Curve

FLD: Forming Limit Diagram

GA: Genetic Algorithm

ISF:Incremental sheet metal forming

LE: Euler_Lagrangian

MD: Monotonically decreasing curves

MSIF: Multi Stage Incremental Forming

NC: Numerical Control

NE Newton Euler

OA: Orthogonal array

PC: Polynomial curves

RAISF: Robot Assisted Incremental Sheet metal forming

RSM: Response surface methodology

S/N: Signal to Noise

SPIF: Single Point Incremental Sheet metal Forming

SS: Steady state force

SSIF: Single Stage Incremental Forming

SVR: Support Vector Regression

TPIF: Two Point Incremental Sheet metal Forming

WS: Work Space

LIST OF SYMBOLS

α: Part wall angle

A%: Percentage reduction in area

a: Link length

$\dot{c}$: Cartesian velocity of mass center

d: Link offset

d_{sf}: Scallop distance in ISF

d_{si}: Scallop distance in RAISF

F: Degree Of freedom

F_r: Radial force

F_t: Tangential force

F_z: Axial forming force in Z-direction

h: Number of higher pairs

H: Total depth to be formed

k: Strength coefficient

L: Lagrangian

l: Number of lower pairs

m_1: Mass of the link-1

m_2: Mass of the link-2

n: Number of links

p_i: Generalised coordinate

R_s: Radius of the cup

s: Step depth

T: Kinetic energy

t_f: Final thickness

t_o: Initial thickness

U: Potential energy

X_m, Y_m, Z_m: Machine coordinate system

X_{w1}, Y_{w1}, Z_{w1}: Work coordinate system

ε_t: Thickness strain

ε_θ: Tangential strain

ε_Φ: Meridional strain

θ_1: Inclination angle, first degree of freedom of the manipulator, rotational

θ_2=N_2 =End effector rotation, second degree of freedom of the manipulator, twist

$\dot{\theta}_2$: Rotational speed of end effector

σ: Equivalent stress

σ_t: stress in thickness direction

σ_θ: Tangential stress

σ_Φ: Meridional stress

τ_i: Generalised force

ω: Angular velocity of the link

CHAPTER 1

INTRODUCTION

Metal forming has been in demand in automotive, aerospace and other industries. To meet the customer need for new technologies, especially in automotive and aerospace industries, new forming methods have been evolved currently. Currently most widely used processes for metal forming in these industries are stamping and deep drawing, which involve large initial investment. In stamping unique dies need to be manufactured which makes it profitable for mass production but unyielding in terms of process.

In the midst of today's fierce competition in the industrial world, there is a demand for more and more complex products yet for saving in manufacturing time and cost. In order to meet this tough objective and the requirements of geometrically complex sheet metal parts, the traditional rout of sheet stamping using expensive dies becoming an avoidable option, search started for less expensive process of manufacturing sheet metal parts with complex asymmetric geometry in batch production without dies. The answer to this search has been incremental sheet metal forming (ISF). The conventional deep drawing and sheet stamping processes need part-dependent tooling in the form of punches, dies and blank holders, which prove expensive in terms of time and money as the part's geometric complexity increases.

This doctoral work creates an innovative methodology to form complex geometry sheet metal incrementally using an integrated automation system. In aerospace and automotive industries mostly, sheet metal of 0.5-1.5mm thickness is used depending on the application. Most commonly sheet metal panels are produced using stamping and deep drawing to improve production rates. However due to use of dies, these processes lack flexibility, which is essential for producing customized products and new trial products. Use of fixed fixture for incremental forming restricts the process flexibility which leads to non-uniform thinning of the sheet. Limitation of formed wall angle is also a disadvantage of ISF. This has increased the need for the research in this field. Automated manufacturing system has been widely used to achieve increasing production rate and production demands. Since then, robot has been used as an integral part of manufacturing system. Accuracy of the parts has been increased along with precision, leading to minimal errors. In a shorter lead time, robot has also been used to produce customized products. Using a robotic manipulator for incremental sheet metal forming improves the process flexibility, formable wall angle limits, more uniform thickness distribution and surface quality. A flexible metal forming approach is required to provide ever-changing customer requirements and to enable the production of

proto designs at lower production cost. This development will also reduce the time consuming laborious repetitive wok. This research is focused on developing a flexible manufacturing approach by integrated manufacturing systems. In this work, a robotic manipulator has been designed to manipulate the sheet with respect to existing vertical hemispherical tool attached to computer numeric control (CNC) vertical milling machine.

1.1 Background

In many manufacturing industries, dies are used for sheet metal forming operation. But production of dies involves high manufacturing cost and time to meet necessary standards. In proto phase and in trial phase of manufacturing, it is quite possible that part may fail. Failure of part or design modification in part will lead to modifying the existing die or completely scrapping the die in these phases which incurs extra cost. Producing low volume parts, complicated panels and proto parts are not feasible using die due to lack of flexibility and high manufacturing cost. High forming force is needed for precise part production in stamping. In order to produce such high forces, die forming machines are built in huge size which can occupy considerable space in a shop floor. Therefore to replace the part dependent dies in these two phases of production, part independent technologies have been proposed for sheet metal forming.

Some of the technologies in sheet metal forming which have come into existence to improve the flexibility are electro-magnetic forming, hydro forming, and laser forming as shown in Figure 1.1 But in achieving the accuracy and precision in sheet metal forming, ISF has shown better results than other processes. In ISF, the net area of contact between the tool and blank at any time during the process is small, just a small fraction of the total surface area of the blank and hence the overall required plastic deformation is achieved incrementally, making the mechanics of incremental forming also distinct. The ISF is one of the emerging flexible sheet metal forming technologies. The incremental forming concept is not new as conventional and shear spinning processes also involve the principles of incremental forming. However, these processes can achieve only symmetric parts and use a mandrel as a simple die whereas ISF can achieve both symmetric and asymmetric parts without the use of any dies.

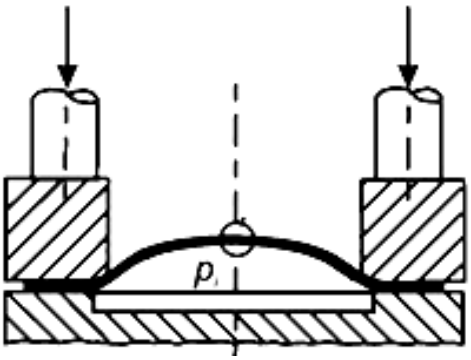

(a)

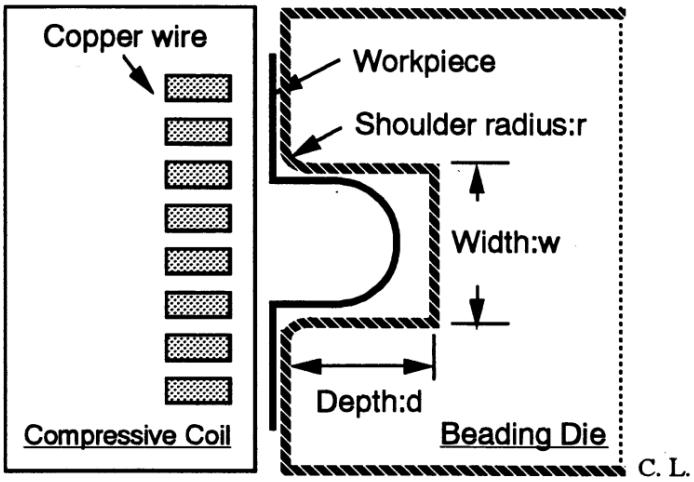

(b)

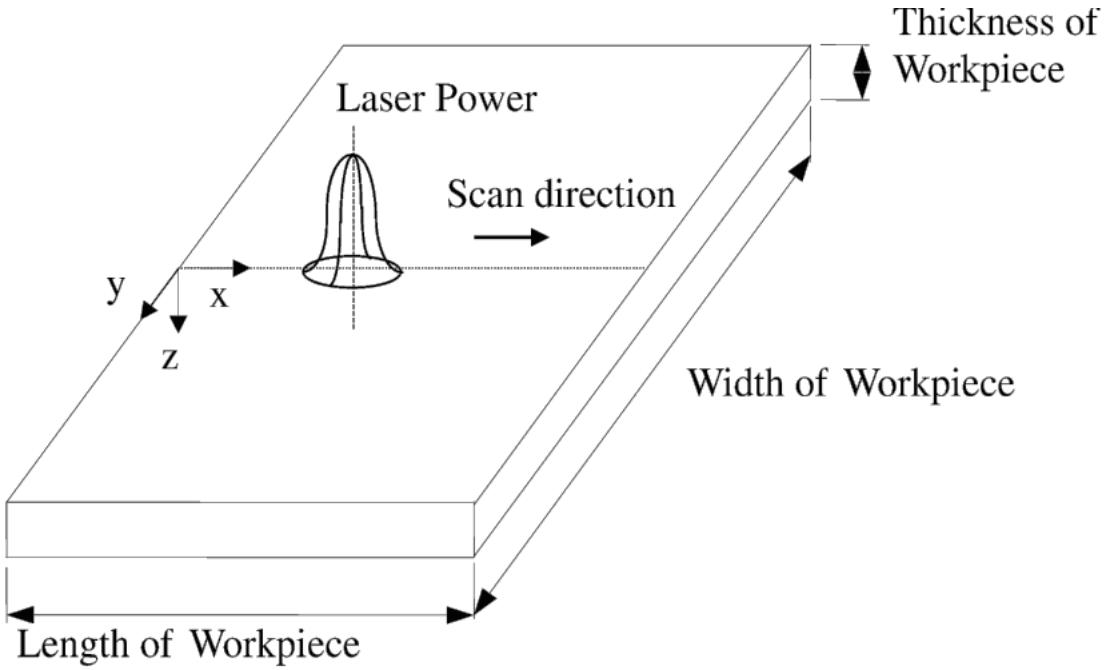

(c)

Figure 1.1 (a) Hydroforming [1] (b) Electro-magnetic forming [2] (c) Laser forming [3]

Most of the ISF processing, as per the current status of technology, is carried out on a computer numerical control machine tool. In single point ISF (SPIF), the cutting tool is replaced with a narrow spherical surface ended forming tool moved by numerical control path program and on the work table, a simple sheet metal holding fixture is used. On the other hand, in the two point ISF (TPIF), in addition to the main forming tool, an additional similar narrow support tool is imparted exactly on the opposite of the sheet metal and moving in synchronization with the main forming tool, in order to provide support to the sheet metal, much like a partial die. Figure 1.2 shows the schematic diagram for stamping, SPIF, TPIF with a tool and a partial die. Due to the need of costlier die and punch in stamping and to reduce the initial cost, punch is replaced by a hemispherical forming tool as shown in Figure 1.2(d) To improve the process flexibility further, die is removed in SPIF as shown in Figure 1.2(b). Due to variable thinning in SPIF, another tool was added to SPIF. Simultaneous movement of two tools through the wall of the sheet improves the thickness distribution.

In most applications of ISF, the blank edge is clamped and does not move inwards. The sheet is formed by having a tool follow the required shape in space, mostly by a succession of planar contours or a single spiral contour programmed into the G & M numerical control program. In the ISF, the wall thickness reduces considerably because the forming process involves combined bending and stretching of sheet metal. The absence of work piece rotation allows an independent *X* and *Y* control allowing the manufacturing of asymmetric shapes. The important process parameters in ISF are step size, diameter of the tool, rotational speed, thickness of the sheet, friction between the tool and sheet, lubrication and tool path. The dependent quality parameters that most researchers previously pursued are thinning, surface finish, and maximum wall angle, maximum depth before fracture, plastic strain distribution and force variation during forming. One of the most well understood limitations of ISF is the limiting wall angle, wherein walls having an inclination more than around 65^{o} to 75^{o} (depending upon the sheet material and thickness) cannot be formed without failure or without significant sheet thinning as per the sine rule of incremental forming [4]

$$\frac{t_f}{t_o} = \sin\phi = \sin\left(\frac{\pi}{2} - \alpha\right) \tag{1.1}$$

Here t_f is the final sheet thickness, t_o is the initial sheet thickness, ϕ and α are indicators of the wall angle as shown in Figure 1.3. It is important to note that the beyond a wall angle of about 70°, thickness have thinned down to 20% of the original value.

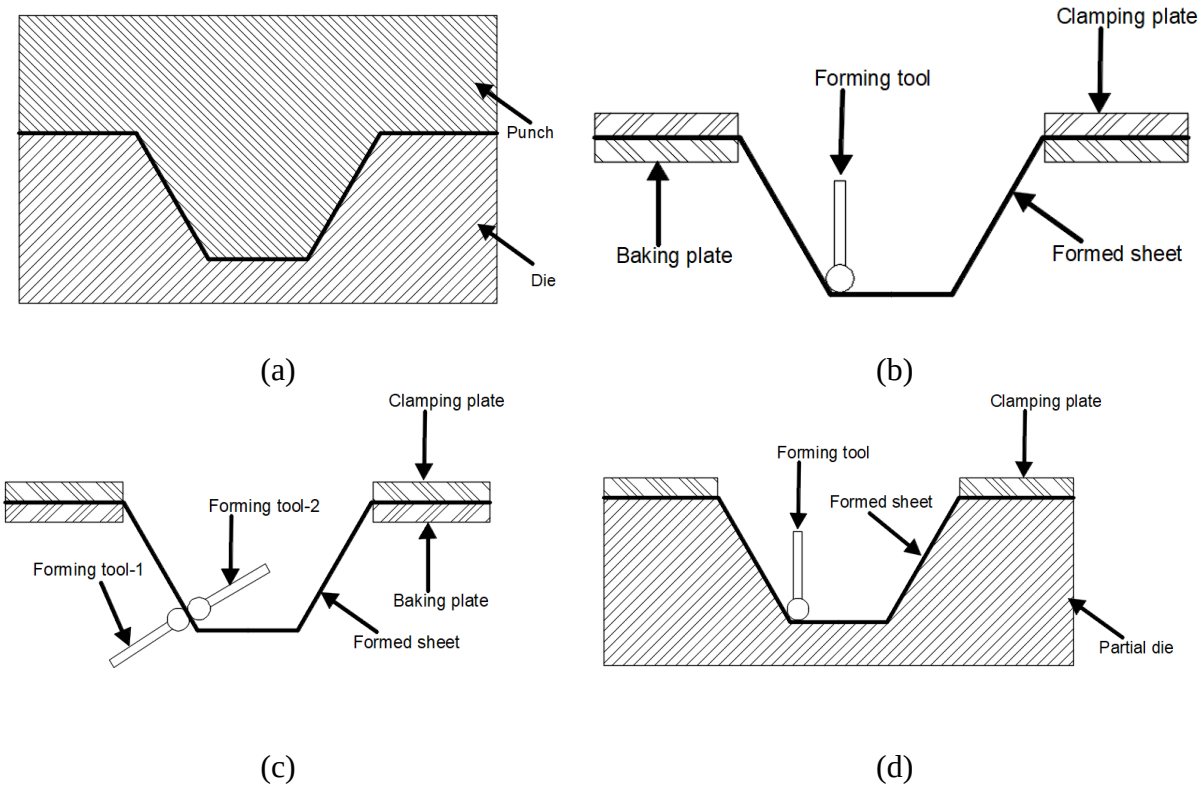

Figure 1.2. (a) stamping (b) Single point incremental forming (c) Two point incremental forming by two tools, and (d) Two point incremental forming with tool and partial die

In order to improve upon the maximum wall angle limitation of the single stage ISF, the multi-stage ISF has been proposed in the literature. In the multi-stage ISF, the total angle of the inclination of a wall of the part is achieved in multiple numbers of stages, where a limited angle is completed in each stage. Due to this, the net amount of thinning (t_f/t_o) is limited in each stage and hence a net larger wall angle becomes achievable.

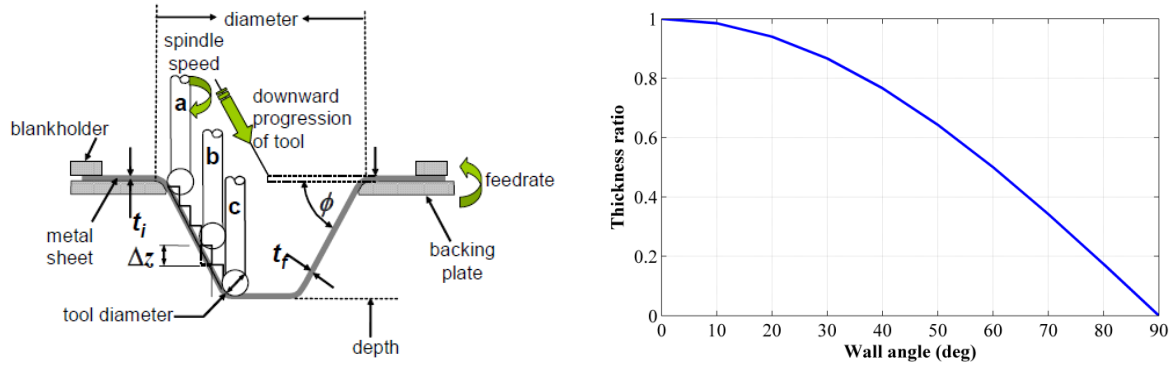

Figure 1.3. (a) The terminology of angles given in (1.1, and (b) the graphical interpretation of sine rule of incremental forming.[4]

Another direction of improvement in complex geometry sheet metal forming is the availing of robot assistance in sheet metal forming. Robot assistance enables the use of numerical control path planning with the help of which it becomes possible to automatically orient the sheet metal blank in front of the tool as per a pre-planned path planning resulting in multiple complex features without interference being achieved. For example, the robot assistance in sheet metal bending was found to make the complex geometry sheet metal forming process more efficient and practical. In the following chapter, the state of art on single stage ISF (SPIF) and robot-assisted ISF(RAISF) as well as the existing research gaps leading to formulation of objectives are explained.

1.2 Thesis Overview

The research work is presented in eight chapters as follows.

Chapter 1: The first chapter of the thesis introduces the research background and also a summarized review of the Incremental sheet metal forming and its variants. The process concept has been introduced and practical aspects have been explained. Along with research objective, main research topics have been covered.

Chapter 2: The second chapter presents the current state of the art in incremental forming processes, numerical simulations involved in ISF, various process parameters and different types of ISF by examining existing literature. A brief overview of comparison of existing methods and research gaps are also presented in this paper.

Chapter 3: The third chapter presents a detailed discussion on the design of a robotic manipulator for incremental sheet metal forming process to improve part quality as well as process flexibility. Design of manipulator includes concept generation and modeling, kinematic and dynamic analysis of the manipulator, mechanism selection and simulation as well as the control system design for complete mechanism. This chapter also explains tool path planning algorithm developed for ISF for designed manipulator.

Chapter 4: The fourth chapter presents the development of the numerical simulation model for ISF in single stage as well as robot assisted forming (RAISF) for Al1100. This also explains the forming force and surface quality obtained experimentally in RASIF and SPIF for Al1100. Here finite element modeling (FEM) analysis has been used to study the deformation behavior, effect of various process parameters on formability and forming force so that number of experiments can be reduced.

Chapter 5: The fifth chapter focuses on surface roughness obtained in ISF as well as RAISF experiments. Effect of existing process parameters in surface roughness as well as forming

time has been investigated for Al1100 in single stage ISF. Additional two process parameters due to sheet manipulation have also been investigated for RAISF. The results obtained from both SPIF and RAISF have been compared.

Chapter 6: The sixth chapter explains the experimental investigation of forming force in ISF. Effect of various process parameters on forming force has been investigated. Along with existing process parameters, effect of tilting angle and rotational angle on forming force has been investigated for RAISF. Forming force obtained in both ISF and RASIF has been compared.

Chapter 7: The seventh chapter focuses on formability and deformation behavior of the Al-1100 sheet in ISF and RAISF. This study has been done for a conical frustum in ISF and RAISF. Effect of various process parameters along with tilting angle and rotational angle on sheet thinning and formability have been compared for ISF and RAISF.

Chapter 8: The eighth chapter presents a conclusion of the research work by explaining the results obtained in both numerical simulation and experiments for both ISF and RAISF. Recommendation for future work has also been discussed.

CHAPTER 2

STATE OF THE ART

Most widely used processes in the sheet metal industry are stamping and deep drawing which involve huge initial investment and expensive part-dependent dies. ISF is one of those die less forming techniques that involve less initial cost and part-independent tooling. This chapter presents the detailed review of the ISF process and the need of more flexible technique in ISF. The review covers single point incremental forming, two-point incremental forming, roboforming, forming strategies, deformation technique, forming force, formability, surface roughness and finite element studies in ISF.

2.1 Single Point Incremental Forming (SPIF)

Several ISF techniques have been developed to make use of CNC machine. SPIF is one of those techniques in which a narrow-area smooth blunted tip forming tool is attached to CNC milling machine for sheet metal forming. In this method, sheet is edge-clamped in a clamping system and forming contour is controlled by the NC tool path plan supplied to the CNC machine. Basic principle of SPIF is shown in the Figure 2.1. The hemispherical tool attached to CNC machine deforms the sheet incrementally along the given contour tool path to create a desired shape. The geometrical accuracy is the key element in this process and it can be achieved by optimizing tool path [5].

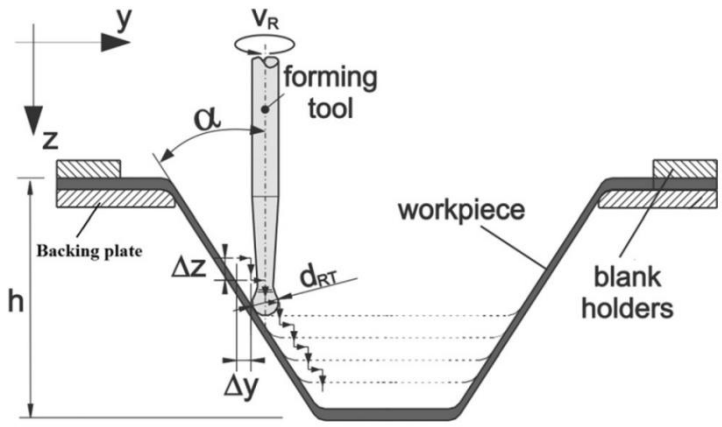

Figure 2.1.Basic principle of single point incremental forming [6]

2.2 Two-point incremental forming (TPIF)

TPIF process may involve either a static support or a kinematic support for ISF. Static support involves either a generic support (partial die) or a part-dependent support (full die) along with a forming tool as shown in Figure 2.2(a) for forming operation. For a full part-dependent support, a new die has to be manufactured for each type of part which is a less

flexible process. In both the cases, supports are fixed while the clamping system along with sheet moves along the direction perpendicular to tool. Although a better part accuracy can be achieved by this process, due to its higher forming time, complex tool path and higher material cost, this method has been replaced by roboforming or duplex forming. TPIF with kinematic support uses two forming tools instead of die and tool combination as shown in Figure 2.2 (b, c). This process is called duplex incremental sheet metal forming (DPIF). In DPIF, a supporting tool moves at the back side of the sheet following the forming tool, at the top of which helps in better thickness distribution in this process. Similar to DPIF, in roboforming, the sheet deformation can be altered either by manipulating the tool motion using a robot or by manipulating the sheet with the help of a robotic manipulator.

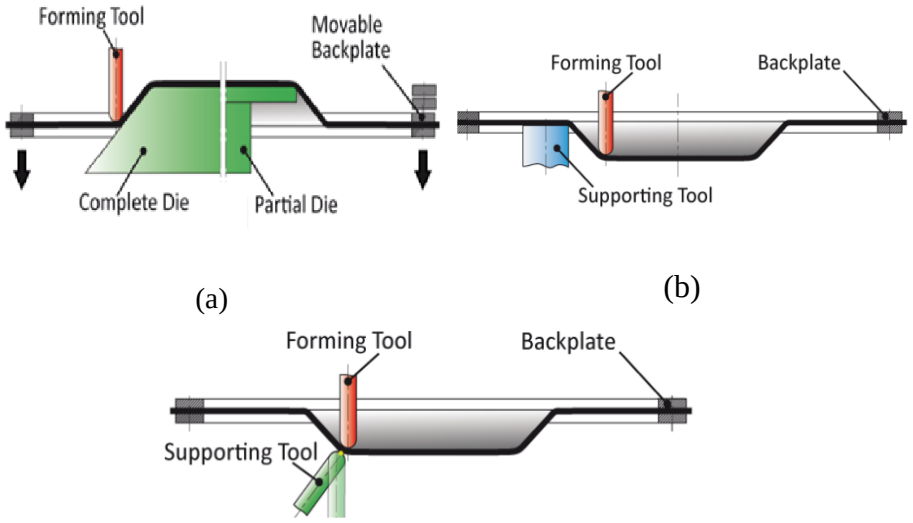

Figure 2.2 Forming Strategies [4]

2.3 Roboforming

Roboforming is very useful in small batch production and when the part is in proto or pilot phase. In these two phases modified part or new customized parts are designed and tested for final production. The number of parts to be tested is very less in these phases as compared to final production phase. Thus the aim of all industries is to reduce the cost of manufacturing of the part in these two phases.

In initial phases is very expensive to acquire special die, because parts may fail at any time. In order to reduce the manufacturing cost by eliminating conventional sheet metal forming process in initial phase ISF was introduced [7]. ISF uses tooling which is mostly part dependent. Many recent forming processes use ISF in order to reduce the cost [4], [7]–[11].One of the most admired processes is RAISF which can be used for asymmetric shapes with less cost and time as compared to MSIF [11].To reduce the cost of manufacturing in

introduction phase, incremental sheet metal forming was introduced so that instead of full die, partial die can be used for forming. To make the process more flexible robot was included, so that any complex shapes can be manufactured easily. It reduces the overall production cost by completely eliminating die in MSIF. Figure 2.3 compares the difference between the different sheet metal forming processes and highlights the advantages of ISF.

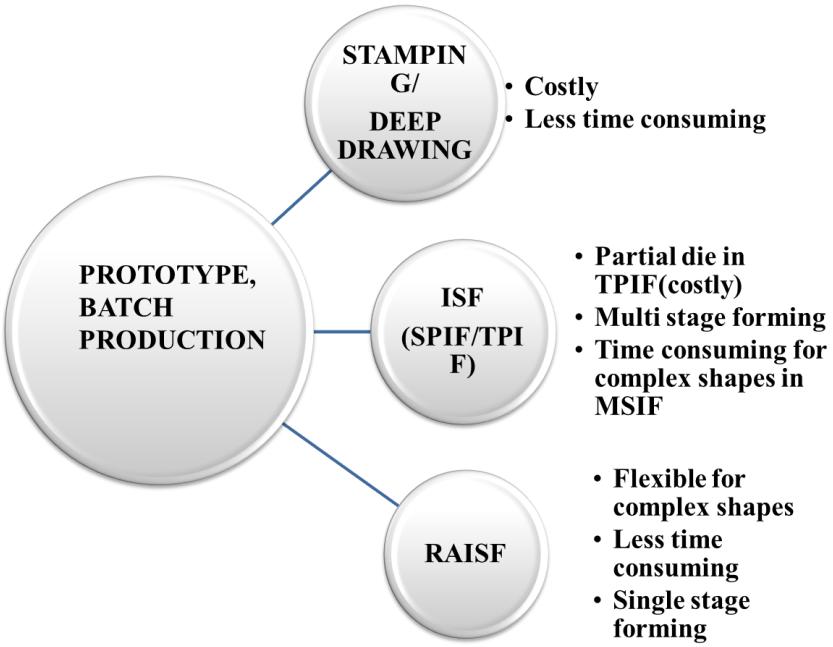

Figure 2.3 Difference between different sheet metal forming processes and advantages

Industrial robots neither have the stiffness nor the accuracy that are generally required for the incremental forming operation [10], but parallel kinematics machines were designed so as to show good features from this point of view. Authors [7] used non-axisymmetric mandrel and force feedback control instead of 3-axis CNC milling machine to produce axi-symmetric shapes. The process of spinning operation was applied to non-axisymmetric parts by using force feedback control. A non-axisymmetric mandrel of a desired shape was used, the pushing force of forming roller was controlled and the material was forced onto the mandrel as shown in the Figure 2.4.The roller follows the contour of the mandrel to fit the material to the mandrel. This enables fabrication of a non-axisymmetric product of the same shape as the mandrel.

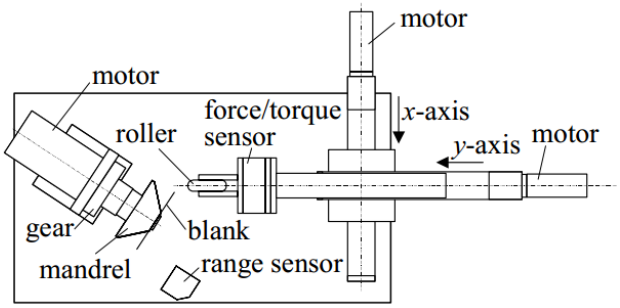

Figure 2.4. Shear Spinning [7]

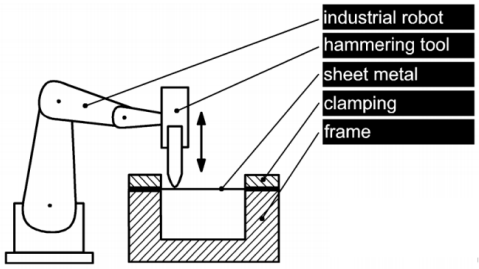

Figure 2.5.Incremental hammering by industrial robot [12]

Though total time for the whole operation was reduced, for complicated parts replacement of mandrel is required. Robots are used as a tool holder in place of CNC machine to make the process more flexible. In previous research work, authors [12] developed a forming method in which a hammering tool was moved by the robot over a sheet of metal held in a frame and the forming is done by punching the sheet metal using the hammering tool. The hammering tool was moved by robot along a predetermined path. The principle of hammering using an industrial robotics is shown in Figure 2.5.The advantages of this hammering method is that deformation forces are that of the inertia forces of the punch and not by the robot itself. Small area of deformation and lack of friction forces in the feed direction are additional advantages of this method .However, vibration in the sheet metal was the main disadvantage of this process. Two robot assisted incremental forming methods namely; by pressing and hammering were compared in the earlier research work[13]. These two methods were performed on two types of test geometries, on cone (A) and square pyramid (D) .The true strains were measured on both of these geometries using both the processes and graph was plotted as shown in Figure 2.6. It was concluded that strains developed in both the processes were very close to each other in the direction of major strain. The material formability was higher in hammering and vibration of the sheet during forming can cause earlier fracture.[14]and [15]used six-axis robot with a hybrid structure which has a serial wrist mounted on top of a parallel shoulder. A pneumatic gripper holding a punch was attached to the robot's flange and various tools with spherical tips of different radii were used. The die and the blank were clamped together using several clips and the die with the supporting frame was mounted on the same base plate where the robot was mounted as shown in the Figure 2.7.

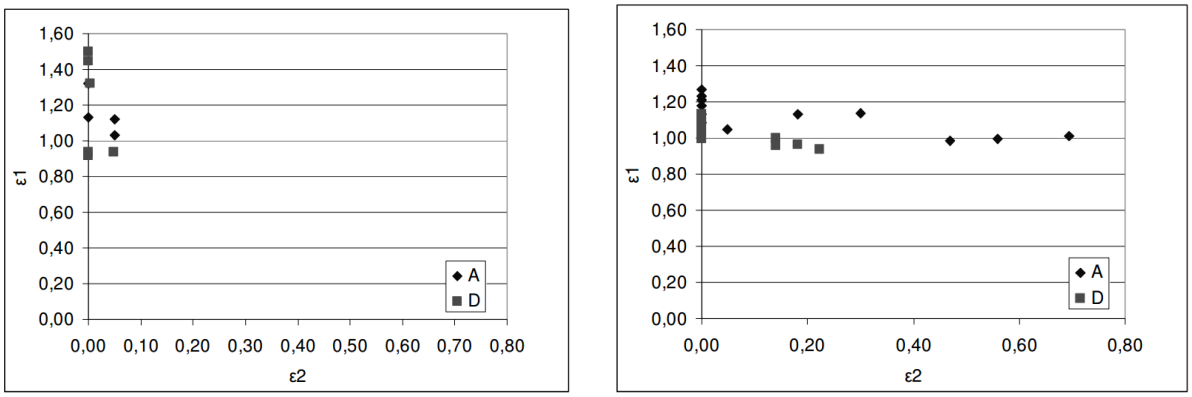

(a) (b)

Figure 2.6 (a) True strains with pressing for both the geometries (b) True strains with hammering for both the geometries

The steps necessary for incremental hammering forming using an industrial robot that are applicable for both convex and concave geometries has been discussed in the literature [16]. Sensor-based and model-based strategies was tried to improve the part accuracy in Roboforming [17].

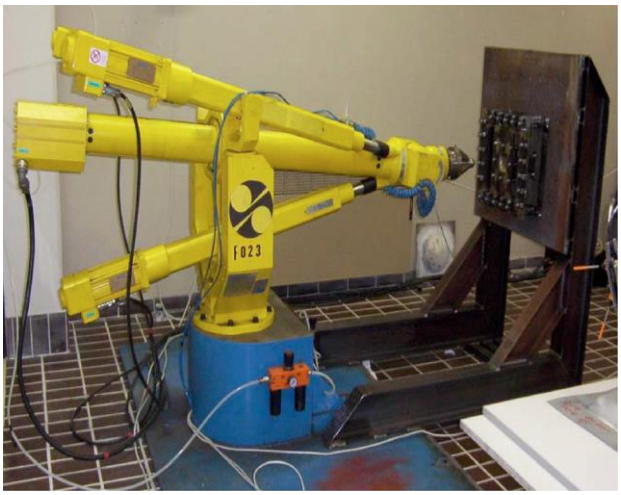

Figure 2.7.Roboforming [18]

Figure 2.8.Roboforming with 6-DOF robots [19]

The model-based approach is an alternative to regular optimization process in identifying geometrical inaccuracies. It reduces the number of forming iterations by supporting or substituting the sensor based approach. An integrated CAx (CAD/CAM) process chain including diverse blocks for Roboforming was introduced to quickly realize the path planning and raise the geometric accuracy using different compensation methods[18]. But calculation time was more and large and complex geometries were not tried. Different methods have been proposed to improve the accuracy of the part and to reduce the processing

time. To improve the dimensional accuracy, the sheet was formed using two 6-axis robots [19]. To reduce the spring back effect, integration of Finite element model and optimization was done. But computation time was very high and path deviation was observed .Work hardening was not considered in FEM to reduce spring back effect. DELMIA software package has been used for designing, simulating and generating the tool path [20]. The experimental set up for this forming operation used is as shown in the Figure 2.8.This set up includes a six-degrees of freedom robot, a custom blank holder, a custom tool holding unit and the forming tool. Researchers [21] compared two methods of forming operation, namely, forming by industrial serial robot and forming by three axis milling machine. Comparison of measured force is as shown in Figure 2.9. Then coupling of FEA of the forming process and elastic modeling of the robot was adopted through post-processor approach. Due to correlation between numerical and experimental forces of a SPIF operation, error was reduced to 80%. A 4-DOF robot with a linear actuator equipped with C-Frame support can replace two sided incremental sheet forming set up [22], where optimal supporting force could be achieved with the force control of tools. The suggested set up is as shown in Figure 2.10.

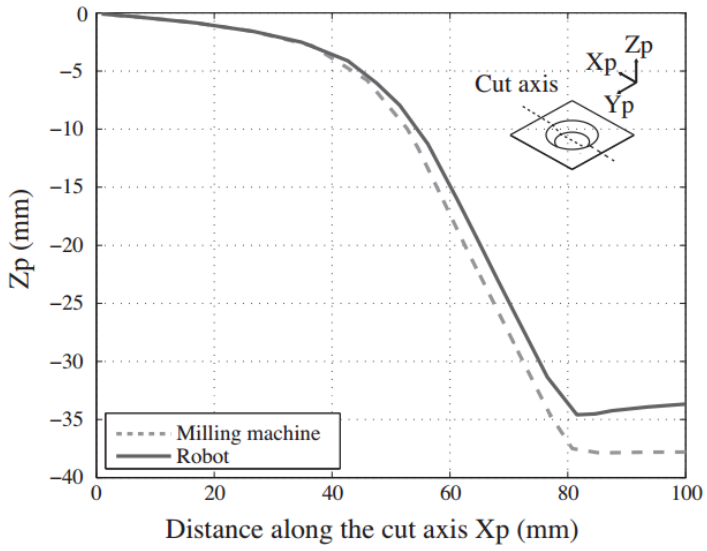

Figure 2.9 Comparison of the measured force in milling machine and industrial robot [21]

Figure 2.10 Experimental set up[22]

Major limitations in forming complex parts by MSIF are cost and time and flexibility in forming complex parts. In MSIF achieving steeper wall angles is difficult. To reduce the production cost, reduction in operation time and elimination of partial die are necessary. Multi axis CNC machine can be a solution to this problem. However, since steep wall angle

requirement and complex parts are only occasional on certain part geometries, it is not justifiable to invest on very expensive multi-axis CNC machines for this. As like in TPIF, use of two robots will cost more in RISF. So, future work can be concentrated on integrating a robot and 3-axis CNC machine to form complex shapes which will help in reduction in cost and manufacturing time. Prior to robot design for sheet manipulation, it is essential to discuss the deformation techniques in existing ISF processes and the effect of various parameters on sheet deformation which will help to design the manipulator to improve the sheet deformation.

2.4 Deformation techniques

ISF is a die-less sheet metal forming process allowing easily forming asymmetric geometric parts with computer based numerical control (CNC) part programing on a typical pre-existing CNC machine with the cutting tool replaced by a custom designed spherical-ended cylindrical forming tool. It is becoming popular in automotive, aerospace and biomedical sectors as it is particularly suitable for low volume production because tooling cost is low and asymmetric shapes can be easily obtained. Extensive academic and industrial research done in this area and largely made available in literature is the main enabler to get the ISF to such fruition. Understanding of fracture mechanism and fundamental material deformation has great importance for achieving material formability, uniform sheet thickness and geometric accuracy. Both experimental[23], [24] and analytical[25], [26] investigation has been done by previous researchers. In ISF sheet metal can be stretched more than conventional stamping process and beyond common forming limit curve. Localized deformation in ISF is mainly due to three mechanisms i.e. shear mechanisms, contact stress and bending under tension. But hydrostatic stress, geometrical instability and cyclic straining play important role in postponing the growth of necking[27]. In ISF, deformation occurs at the contact region of the tool and sheet. The deformation mechanics in the ISF has been investigated both analytically and experimentally[23]–[25], [28], [29] and has also been proved that ISF has higher formability than conventional forming[30][31] due to its highly localized deformation. A closed form analytical model was presented which shows an insight to the fundamentals behind the fracture and enhanced formability in ISF. The deformation mechanism in ISF is shear and stretching along the plane parallel to the tool direction. Shear strain along the tool moving direction was the greatest strain[23]. Direct strain perpendicular to the tool motion is the major deformation mode in ISF. The strain in forming direction alternates at smaller value and the strain values depend on the bending direction of the

sheet[32]. Sheet fracture can either be caused by deformation instability or by material ductility. The main cause of ISF formability is bending which can delay the deformation instability and strain hardening effect is surpassed by bending effect[33]. Contact stress, bending under tension, cyclic straining, hydrostatic stress, shear and geometric inability are the six mechanisms that enable stable deformation[27]. However, still some gaps unaddressed with regard to understanding of deformation mechanics, which is critical in determining product quality.

2.5 Forming force

Deformation behavior in ISF is a combination of stretching, bending and shearing and the dominant deformation mechanism can be seen to contribute most to the direct strain perpendicular to the tool motion. Largest strain values are normally found at the lower end of the inclined wall of the cup-shaped formed part [32], [34], [35]. Since ISF is a process with localized plastic deformation zone, the forming force is one of the most significant parameters to predict the deformation behavior as well as the failure. Forming force in incremental forming is dependent on various process parameters such as wall angle, step depth, sheet thickness and spindle speed. Effect of some of the process parameters have been shown in literature[36], [37].

Wall angle is the single most critical parameter because it is associated with the functional design of the part and hence cannot be compromised. In sheet metal parts with the wall angles up to a threshold, there was no distinguishable and specific peak force throughout the forming process, rather only a steady state force was found to prevail. On the other hand, for all parts with wall angle beyond this threshold value, other process parameters being the same, a distinguishable peak force was observed and moreover the steady state force values decreased. Further, a proportionate increase in peak force and decrease in steady state force were also observed for wall angles beyond this threshold value [35]. Increase of the normal force was found slower at higher wall angles. Tangential and radial component of the forces were found smaller and nearly constant. Forming force also increases with increase in tool diameter and sheet thickness[38]. Wall angle, step depth, sheet thickness, spindle speed are the main process parameters which affect forming force.

Tool path also has significant effect on forming forces. Previous research works reveal that, spiral tool path gives smoother force curve than profile tool path. In spiral tool path, as the vertical step depth increases, normal force increases and when sheet thickness increases, forming force increases linearly[39]. As the sheet thickness increases, deformation energy

required to deform the sheet is more, and required force will be more. Tool path strategy has great impact on forming force. Three types of tool path strategies have been experimented by earlier researchers to check force variation on the sheet. Decrease in maximum force is 23% in case of spiral tool path as compared to pressed strategy and 14% compared to the successive press strategy [40].

Strain increment and total equivalent plastic strain are affected by both step depth and tool diameter. Strain increment increases when the forming tool passes over a point and remains unchanged when it moves away from that point. So step depth effects strain increment. Forming force in normal direction increases when tool diameter increases due to larger contact area of sheet with tool [41], [42]. Lubrication doesn't have significant effect on forming force but it affects surface quality [41]. Spindle speed can be used to control local heating of the blank. As the spindle speed increases, friction between tool and blank increases which leads to decrease in forming force and increase in temperature [43], [44]. Spindle speed mainly helps in reducing forming force and also increases material formability[45].

Shape of the part and grain sizes are also important parameters to be considered while measuring forming force. In geometry with corners (pyramids), it was found that forming force is more as compared to oblique wall of the pyramid. Forming force in normal plane is more than horizontal plane [46]. But vector sum of forces in three direction for a pyramid shape part and conical shape part are same [47]. Material properties and grain size change as the material is heat treated. With increase in grain size, hardness and yield stress decrease and plasticity and ductility increase. Forming force decreases with increase in grain size[48].

Force also varies due to bending at initial steps in ISF and stretching at later stage. In first phase of ISF, force trends are due to bending effect of the sheet. But in second phase, due to combined effects of thinning and strain hardening, force remain steady till the fracture[34]. Deforming forces in conventional bending is higher than that required to deform a sheet in incremental forming and forces induced in stretch forming is 10 times higher than ISF [49].

Many attempts have been made to reduce the force on the sheet. Use of ultrasonic sheet metal equipment is one of the equipment, in which forming force can be varied by varying ultrasonic vibration. Increase in vibration frequency caused a decrease in mean axial force. But frequency higher than 50kHz produced larger axial force than without ultrasonic vibration[50].

Study of forming forces in ISF provides insights into deformation mechanics. It is difficult to form steeper wall angle parts in single stage incremental sheet metal forming

(SSIF). But research works shows that, these parts can be formed in multi stage incremental forming (MSIF) [51]. Deformation variation between these two processes is the main key point. From literature survey, it is learnt that deformation variation changes due to induced forming forces by tool on the sheet. A good amount of research work has been done on force variation in single stage incremental sheet metal forming.

2.6 Formability

Over the recent years, many studies have been conducted to understand and improve the formability of the sheet in ISF. Formability of the material is the ability of the sheet metal to deform until failure. Fracture forming limit curves (FFLs) has been used instead of forming limit curve (FLC). Other formability indicators like maximum forming angle and maximum forming depth can also be used to assess formability. FLD obtained in ISF is different from than conventional forming[52] and forming limit curve (FLC) is a line with negative slope in positive region of the minor strain. Deformation in ISF occurs due to shearing [53] and some believes it is due to stretching[28]. Forming limit diagram (FLD) is used to investigate the formability of the material in SPIF and FFLC is employed to investigate the straining limit before failure. To improvise the thickness distribution and formability in single stage forming, double pass forming was proposed[30]. Using a tool with freely rotating ball, shows different formability behavior[52]. Increasing the number of forming stages, the minimum thickness rises and thickness distribution improves. Maximum thickness reduction drops initially and improves as the forming angle increment increases [54]. Many factors affect the formability of the sheet material in ISF. Forming angle, sheet thickness, step depth, spindle speed, feed rate, tool size, tool path and forming temperature are the main parameters which affect formability more.

Sheet thickness is one of the process parameters which affect the sheet formability. Sine law has been widely used to explain the effect of thickness, in which thickness distribution is related to forming angle. Smaller diameter forming tools gives better formability as sheet strains concentrate under the forming tool. However, larger forming tool distributes strain at more extended area which reduces the formability.

Formability decreases with increase in step depth [55]. However, some authors argued that, step depth has negligible effect on sheet formability [56] and some authors have proved experimentally that formability increases with increase in step depth [34]. The main reason behind the variation in observation is that of the step depth range selection. Smaller step

depth ranging from 0.1 mm to 1 mm [57] and larger step depth more than 0.7 mm [4], [55] were used in previous research. Therefore, with increase in step depth by a smaller value, formability increases however by larger step depth increase leads to reduction in formability.

Various researches have been done to investigate the effect of forming temperature on formability of the sheet metal in ISF. By creating a heating spot at the contact zone of tool and sheet using a laser based heating system, formability of the sheet increases [58]. Hot incremental forming using electrical current to improve the formability of the sheet in ISF was proposed in previous research [59]. It was observed that, with increase in electrical current, formability of the sheet increases and yield strength at the tool and sheet contact zone reduces. So the maximum achievable forming angle increases due to increase in formability. Electric assisted ISF by using cooling channels in the ISF tooling to form Ti6Al4V sheets to increase formability was developed [60].

In incremental forming, forming angle or wall angle is the most important parameter to be considered which affects the formability of the sheet. Effect of process parameters on formable wall angle on AI5052 was investigated [55]. It was found that formability decreases with increase in tool diameter step depth and decrease in sheet thickness, but feed rate has no significant effect on formable wall angle. Spiral tool path yields greater formable angle than conventional tool path [61].

Spindle speed has considerable effect on formability of the sheet. It directly affects the frictional condition of the tool sheet contact zone. With increase in spindle speed, relative rotational speed between tool and sheet interface increase. Increase in relative speed increases friction between tool and sheet. Higher friction between sheet and tool increases contact heat between sheet and tool. Due to increase in contact heat, formability of the sheet increases. The effect of frictional heat on formability on AA3003 sheet was investigated. Due to high tool rotational speed, heat at contact zone was more which improves the formability of the sheet[56]. Tool rotational speed has more influence on formability, when tool rotational speed increases, formability decreases which is contradicting from previous researches. A method for poor formability material was proposed to improve formability by increasing spindle speed [62]. The result shows that there was an improvement in drawing angle by 7.5° and 12.5° due to increase in spindle speed. Tool size and shape affects the formability of the sheet. Smaller tool diameter enables higher formability. For larger tool diameter, contact area between tool and sheet increases. Due to increase in contact zone, forming force increases.

A slower feed rate improves the formability of the part [4]. Feed rate has different effect on heat treated sheet. A slower feed rate on aged sheet improves formability and it has no effect on annealed sheet [56], [63]. An optimum value of feed rate increases the contact temperature and formability increases [64]. Some researchers however found that formability increases with increase in feed rate [45]. It has been observed that feed rate has possible influence on formability as well as forming time. Therefore, optimization would be required if trade-off between these two parameters are necessary. Optimization of the process parameters to improve the formability of the sheet may alter the surface quality after forming operation. Therefore, study of effect of various process parameters on surface roughness is a necessary for a quality output.

2.7 Surface roughness

SPIF is one of the ISF forming techniques in which shape of the part is controlled by axis movement of CNC machine or any robot. In this process, quality of the part surface is an important concern for customer. Surface roughness is one of the parameters which help in improving quality of the surface. In ISF, there are many parameters which affect surface roughness directly or indirectly. These parameters include feed rate, spindle speed, step depth, cutting condition, tool material, sheet material and machine vibration. But last four parameters are uncontrollable parameters. Various methods have been proposed in literature to study roughness and quality of the surface [65]. Effect of tool depth increment and spindle speed variation on surface roughness of Al3003 sheet was investigated and roughness was measured using white light interferometer [66]. It was found that spindle speed has little effect on roughness. Tool path has also great impact on surface roughness. Tool path is a function of time, step depth and scallop height. By varying these three parameters tool path has been optimized for quality surface finish in two point asymmetric incremental forming [67]. Thinning analysis and formability analysis has been done by varying wall angle and keeping other parameters constant [68]. Other parameters like tool radius, vertical step and forming angle were varied to check change in surface quality [69]. Ten points mean roughness, absolute roughness and RSM values were checked experimentally as well as analytically. Effect of parameters like vertical step, feed rate, spindle speed, tool diameter on surface roughness was investigated on Al1050 sheet metal. It was found that tool with larger diameter has positive effect on surface roughness but adverse effect on accuracy. Lower value of step depth gave better surface finish and higher value of feed rate and spindle speed has positive effect on accuracy and surface roughness of the part [70].

Using response surface methodology surface quality and forming time were optimized by varying three input parameters i.e. spindle speed, feed rate and tool size on AA5052 sheet [71]. Wall thickness and surface roughness were predicted as a function of three parameters using a second order quadratic model. By changing sheet thickness along with feed rate, step depth and tool diameter, surface roughness changes [72]. Impact of these four parameters was predicted by response surface methodology with multi-objective function and Box-Behnken design. Sheet thickness had maximum influence on roughness and then step down. Feed rate and tool diameter had little effect on surface quality. Many optimization techniques have been employed to optimize process parameters till the date. Artificial neural network (ANN), support vector regression (SVR) and genetic algorithm (GA) were used to optimize parameters in ISF [73]. ANN and SVR performed better than GA and predicted results were in very good agreement with experimental value. Sheet thickness is also a key parameter for formability and forming time. Optimum Spindle speed and sheet thickness for achieving maximum formability and in minimum forming time for AA-3003 sheet was reported [74]. Surface roughness decreases with increase in tool radius, decrease in step depth and decrease in sheet thickness. Lubrication has also influence on surface roughness, dry and cool lubricant increases roughness as compared to grease [75], [76]. Roughness value also depends on tool path direction and is better in tool advancing direction than perpendicular one [77]. Tool shape and tool-sheet contact condition change surface quality [78]. Vertical pitch and feed rate have more effect on forming time than tool diameter [79]. Tool material and coating affects the forming force and surface roughness. Higher surface roughness was resulted by using acetal tool but more isotropic finish was achieved as compared to carbide tool [57].

2.8 Finite element studies

Due to high nonlinearities at the changing contact area between tool and the sheet surface and due to high nonlinear behavior of the material in ISF, numerical simulation has been in high demand. Due to this nonlinear behavior, modeling implicit and explicit FE codes has been a time consuming process. To reduce the computational time in FE simulation of SPIF, a model has been developed with fine meshing at small contact zone with continuum elements and through-thickness shear was predicted using this method which was closer to experimental results. For truncated pyramids, FE model was used to investigate various characteristics and validated using experimental results [80]. FE modeling simulation with solid element is better than shell element to investigate the deformation in ISF [81]. Some

researchers found that modelling FE simulation with shell element is not suitable for all tool path strategies to find out the transverse shear behaviour [82].

For predicting geometrical accuracy in a cone wall, anisotropic yield criterion is not a key factor [83]. Sheet metal orientation has no significant effect on predicting straining history with an anisotropic constitutive law [84]. Three different hardening laws (i) Von Mises plasticity with isotropic hardening (ii) Von Mises plasticity with combined kinematic and isotropic hardening (iii) Hill'48 plasticity with isotropic hardening have been tested for simulation of axi-symmetric components for SPIF. The mixed hardening law gave more accurate prediction than other laws, however geometric accuracy was better when kinematic hardening was considered [85]. Combined effect of hydrostatic pressure, plastic strain and shear was embedded in to FEM model in LS-dyna and the predicted results and experimental results were in good agreement in terms of fracture depth, thinning and forming force [86].

Accumulative double-sided incremental forming (ADSIF) and SPIF was simulated in LS-dyna using solid element and was concluded that ADSIF has higher hydrostatic pressure, greater plastic strains and through thickness shear[87]. To reduce the computational time, a new algorithm was proposed [88], [89],70% reduction in calculation time was achieved in stretching a spherical cup. However, only 4% improvement was observed at high contact nonlinearity zone. To further reduce the computational time, adaptive meshing strategy [90], [91] and time scaling and mass scaling [92] was implemented. It was observed that simulating time could be reduced up to 80% with acceptable loss of accuracy. It was observed from the literature that the FE simulations are good in predicting forming force, strains, thinning and deformed profile during forming in ISF. The advantages and disadvantages of ISF from literature review have been highlighted below.

- Smaller force due to incremental deformation
- No use of dies, so set up cost can be largely reduced [5].
- Design changes can be easily done
- Dimension of the part is limited by the forming tool
- Process is not part dependent
- Conventional CNC machine can be used to control the tool path and by optimization of tool path, product shape can be changed [93].
- Material formability is higher than conventional stamping [5].
- Good surface finish
- Amount of lubricant used in ISF is lesser than conventional forming processes [93].

Some of the drawbacks of this process are as follows.

- Takes more time due to gradual deformation in the desired tool path direction. [5].
- Restricted to small batch production
- Difficult to form steep wall angle parts and can be formed using multi stage forming.
- Accuracy of the part is inferior to conventional stamping due to spring back occurring during tool movement.
- Less geometric accuracy in bending edge area

An extensive review of the incremental forming process including different major forming aspects has been provided in this chapter. Contributions and challenges in each aspect have been highlighted in the literature. The literature survey reveals that forming of steeper wall angle parts has been a difficult task in ISF. However, forming of steeper parts is possible through MSIF. Higher forming time in MSIF is the main drawback. By improving the formability, steeper parts can be produced with more uniform thickness distribution by improvising the process.

The present study addresses the limitations of ISF by manipulating the sheet metal by adding a two degree of freedom manipulator to the existing CNC milling machine. A manipulator has been designed to manipulate the sheet. A detailed analysis of the manipulator has been explained in the thesis. Deformation mechanism, surface roughness, forming force and sheet thinning of the sheet due to sheet manipulation are the main focused area in the present thesis. The detailed numerical as well as experimental investigation has also been performed to understand the mechanism. The effect of various process parameters on surface quality, forming force and sheet thinning are being provided in the subsequent chapters.

2.9 Aim and Objective

iterature review reveals that research carried out in Incremental sheet metal forming doesn't provide flexibility to the process. Only up to certain angle and up to certain depth, a sheet can be formed in this process. To improve the process flexibility, robotic manipulator has been designed and added to ISF. In this work, focus is to investigate the existing incremental sheet metal forming and to develop a manipulator to improve the flexibility in the existing process. Achieving steeper wall angle parts and better surface finish within less interval of time in single stage forming using the manipulator is the main aim of this research. Main objectives of this research are as follows.

- To investigate into the numerical control (NC) tool path planning strategies that enable robot assisted incremental sheet metal forming to achieve steep wall angles up to 90^o in the asymmetric part geometry
    a. Tool path planning
    b. Design of manipulator
    c. Coding for Numerical analysis and experiments
- To estimate using finite element method the sheet metal thinning, formability limit curves and failure in robot-assisted incremental sheet metal forming and compare with experimental results
    a. Finite element analysis for RAISF and SPIF
- Comparison of forming time and part quality obtained using robot-assisted asymmetric incremental forming with those obtained using multi-pass incremental forming
    a. Manipulator Fabrication
    b. SPIF experiments
    c. RAISF experiments
    d. Comparison of results

2.10 Methodology

The methodology adopted for this research work is shown in Figure 2.11. The main objective of this research work involves designing of the manipulator to improve the process flexibility in the existing ISF processes. In this research commercial aluminium Al1100 sheet has been used for the analysis of incremental sheet metal forming process. This study is restricted to conical shape using 3-axis CNC milling machine and designed manipulator. Single stage incremental forming has been analyzed using numerical simulation. Numerical simulation has been carried out using LS-dyna. Validation of the results has been done experimentally without using manipulator.

In RAISF, to investigate the deformation mechanism, the process has been simulated numerically. The manipulator has been designed to manipulate the sheet and numerical simulation results have been validated experimentally using designed manipulator. Strain distribution, formability depth achieved at steep wall angle parts, surface roughness and forming forces have been investigated at different process parameters such as tilting angle, sheet rotation and wall angle in RAISF. Finally, the results obtained in SPIF and RAISF process was compared.

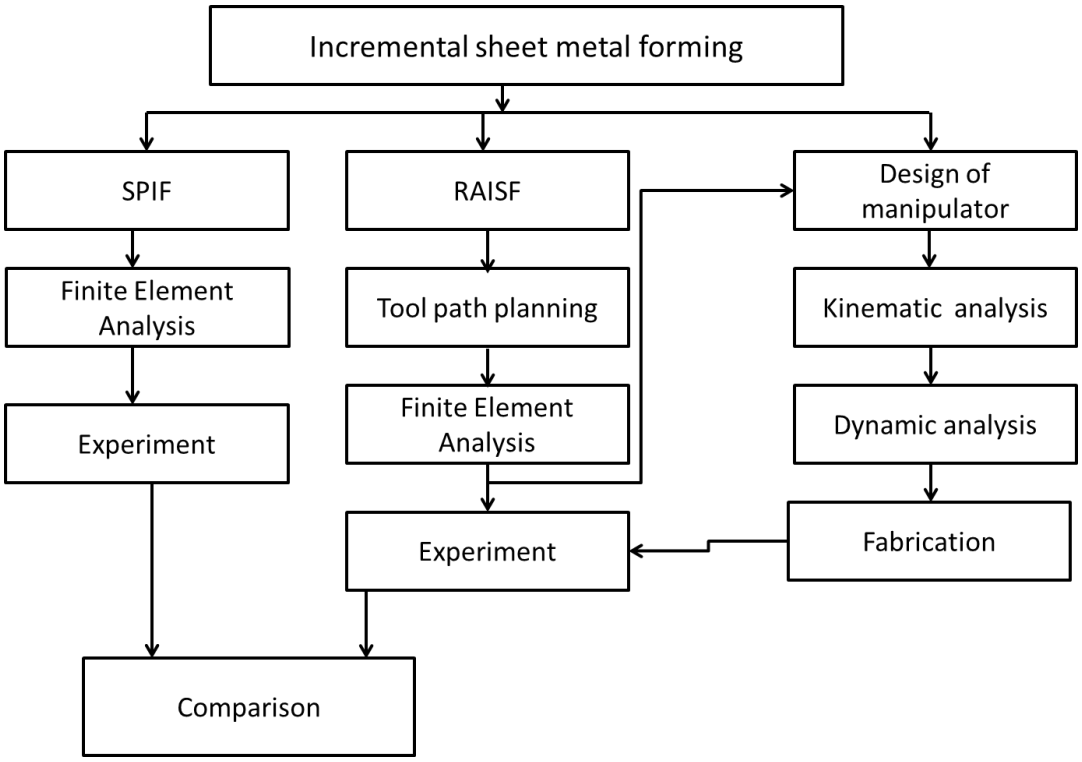

Figure 2.11. Methodology in the present work

To improve the formability, surface quality and to reduce forming time in single stage forming, a manipulator has been designed to manipulate the sheet. First step in design of manipulator includes selection of links and joints to achieve required tool path. Kinematic analysis is the subsequent step through which feasibility of selected links and joints to achieve required trajectory are checked. Due to application of external force by the forming tool, manipulator will have dynamic behavior which can be analyzed by dynamic analysis. By dynamic analysis, control system for the manipulator can be designed. Through dynamic analysis, torque at the joints and links can be calculated which helps in selecting the driving system for the joints. Designed manipulator is achieved by fabrication using the selected links, joints and control system. Experiments have been conducted using the fabricated manipulator to investigate the formability, thickness distribution, surface finish and forming time. The results obtained from both RAISF experiments and ISF experiments are then compared.

CHAPTER 3

ANALYSIS AND DESIGN OF THE ROBOTIC MANIPULATOR

The objective of the current research is to overcome the research gaps in the existing literature mentioned in chapter-2. To improve the process flexibility and material formability, sheet metal manipulation in ISF is necessary. The current research work introduces a novel test rig which can improve the sheet thinning, formability, surface quality and forming force by changing the sheet position with respect to vertical forming tool. The design and analysis of a manipulator to manipulate the sheet for ISF has been described in this chapter.

Both the kinematic and dynamic analysis is used to design, simulate and control the manipulator. Kinematic analysis is essential for motion planning and dynamic model. Dynamic analysis calculates the behavior of joints and links due to application of external forces. Here in this chapter along with kinematic and dynamic analysis, selection of joints, links, mechanism and control system has also been discussed.

3.1 Modeling of robotic manipulator

In the present work, a manipulator has been designed to improve the process flexibility as well as the product quality by manipulating the sheet in ISF. The manipulator design involves prior analysis to maintain the stiffness as well as for long run use. Figure 3.1 shows the block diagram giving the steps involved in designing a manipulator. Trajectory planning is one of the most important steps in metal forming which directly affects the surface quality, formability and sheet thinning. Therefore, first step in manipulator design is to do trajectory analysis. In the ISF as the spiral tool path gives more formability, better surface quality, therefore, the same is obtained by integrating 3-axis milling machine and manipulator in the present work.

Kinematic analysis is the second step through which position of the end effector can be known if link and joint parameters are known (forward kinematics) and when a desired position is known, joint and link parameters can be calculated (inverse kinematics). As in the current research, trajectory is known, link length, position and joint angle can be determined by inverse kinematics. In this position analysis is an important part of the robot analysis as this will identify the joint angle movement and link translation. Velocity of each link can affect the kinetic energy of the assembly which will directly impact sheet metal forming. Therefore, it is also necessary to conduct the velocity and acceleration analysis of each link and joint of the manipulator. To sustain externally applied load by tool on the sheet,

manipulator should be stiff enough. To improve the stiffness of the joints and links, adequate joint torque need to be calculated. To find out the joint torque and behaviour of the manipulator when external force is applied on the effector, dynamic analysis is necessary.

3.2 Number Synthesis

Number synthesis includes Number of links and joints required to get a desired path. As 2- DOF manipulator is going to be integrated with CNC milling tool, so number of links and joints should be selected in such a way that, final result will have desired path and 2-DOF. 3 links and 2 joints have been selected for robotic manipulator.

According to Gruebler's equation [12]:

$$F = 3(n-1) - 2l - h, \tag{3.1}$$

where

F= Degree Of freedom

n= Number of links

l= Number of lower pairs

h=Number of higher pairs

For the robotic manipulator of relevance to the present work, since two rotational degrees of freedom are required to achieve the objective, it has been concluded that manipulator can be designed to have the number links to be 3, joints to be 2 with both kinematics pairs being lower pairs.

3.3 Type synthesis

Suitable joints are very much required to give a proper path to work piece so that after integrating CNC tool and manipulator, required trajectory will form the final part. Selection of suitable mechanism for desired output is the main focused area in this phase. In ISF to improve the sheet formability and reduce the forming force, sheet has to be inclined so that the relative wall angle between tool vertical axis and sheet could be reduced. To control the friction between tool and sheet, sheet has to be given rotation with respect to tool. By this manner, additional two degrees of freedom (2-DOF) manipulator would be required. To provide additional 2-DOF to a manipulator, appropriate joints need to be selected. Out of all the joints, hinge joints and cylindrical joint are selected for manipulator motion. In the

present manipulator, in cylindrical joint translation motion is locked as vertical (Z-direction) motion is not required. Vertical motion or z-axis motion is given as input to CNC milling machine tool. To rotate work piece, cylindrical joint is given in z-axis so that all the sides of work piece will be formed by contacting tool. Hinge joint is given in Y-axis to rotate work piece in certain direction.

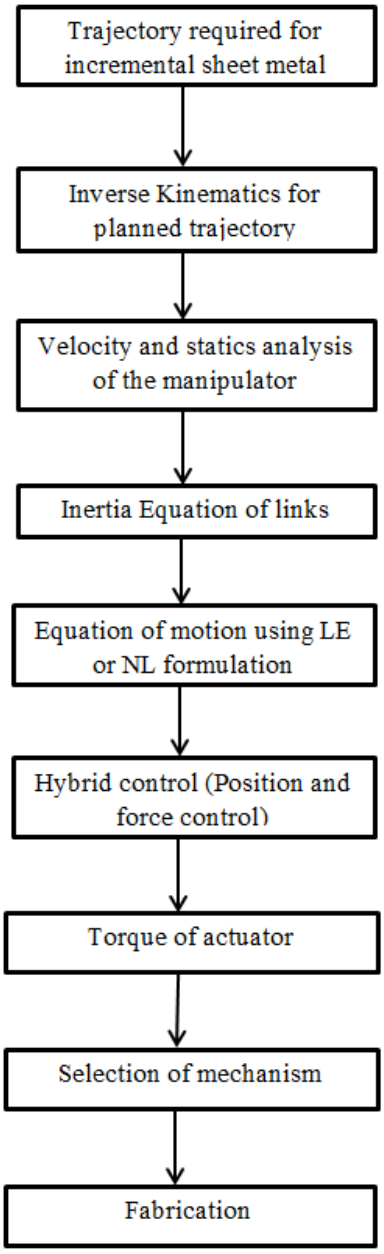

Figure 3.1.Steps involved in Manipulator design

3.4 Path planning

The path planning has been analyzed with reference to the inclined working plane or rotated coordinate system with respect to machine coordinate system. Path planning in combined two DOF manipulator and vertical CNC milling machine has been explained in the following section. Generally, a three axis milling machine has three linear axes. In Figure 3.2 *X*, *Y* linear motion has been shown in machining bed and vertical *Z* motion has been shown on tool which is attached to CNC vertical milling machine. A two degree of freedom manipulator has been attached to the machining bed which has θ_1 and θ_2 rotation as shown in the Figure 3.2.

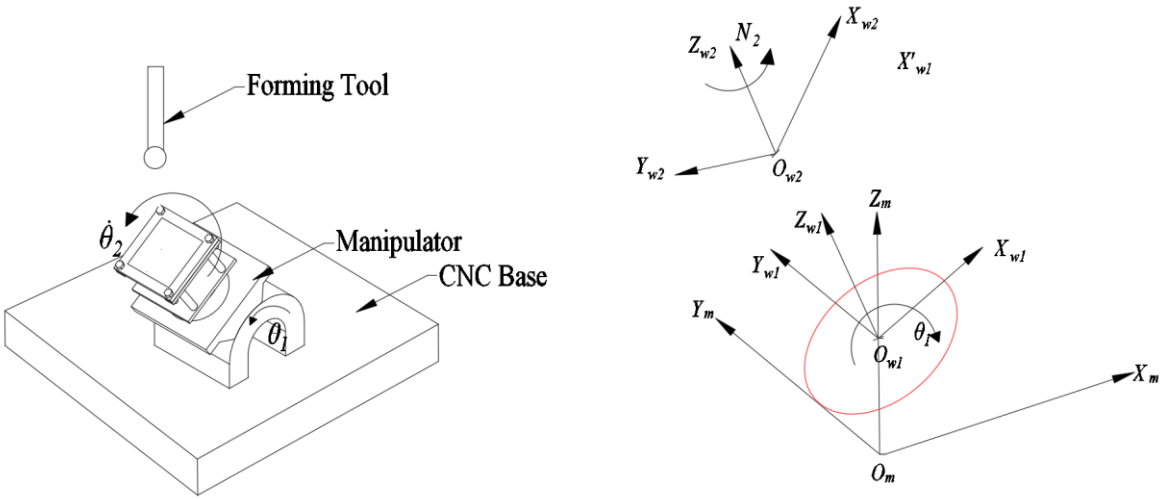

Figure 3.2. Coordinate transformation for synchronized CNC machine and manipulator

In the figure 3.2, X_m, Y_m, Z_m indicates machine coordinate system. X_{w1}, Y_{w1}, Z_{w1} indicates work coordinate system after first inclination θ_1 which is at a height of z_1 from the machine coordinate system. θ_2 indicates angular rotation given to sheet about inclined Z_1. O_1 represents origin shifting of manipulator after first inclination. O_2 represents rotated origin of the end effector. Homogenous transformation matrix due to first inclination (θ_1) of the sheet and translation by Z_1 can be obtained as follows.

$$R_1 = \begin{bmatrix} \cos\theta_1 & 0 & \sin\theta_1 & 0 \\ 0 & 1 & 0 & 0 \\ -\sin\theta_1 & 0 & \cos\theta_1 & z_1 \\ 0 & 0 & 0 & 1 \end{bmatrix} \qquad (3.2)$$

$$Where -40° \le \theta_1 \le 40°$$

Initial point coordinates along the radius of the cup are

$$\begin{bmatrix} x_2 \\ 0 \\ z_2 \\ 1 \end{bmatrix}$$

Let the height of the cup be H and wall angle be α. Tool movement in x-direction can be obtained using following equation.

$$m = n_i \times \tan(90 - \alpha)$$

$$0 \le n_i \le H \tag{3.3}$$

Parametric equation for tool path can be obtained by combining homogenous transformation matrix, initial coordinate of the point as follows

$$\begin{bmatrix} \cos\theta_1 & 0 & \sin\theta_1 & 0 \\ 0 & 1 & 0 & 0 \\ -\sin\theta_1 & 0 & \cos\theta_1 & z_1 \\ 0 & 0 & 0 & 1 \end{bmatrix} \begin{bmatrix} x_2 \\ 0 \\ z_2 \\ 1 \end{bmatrix} - \begin{bmatrix} m \\ 0 \\ n_i \\ 1 \end{bmatrix} = \begin{bmatrix} x_{i+1} \\ y_{i+1} \\ z_{i+1} \\ 1 \end{bmatrix}$$

$$\begin{aligned} x_{i+1} &= x_2 \times \cos\theta_1 + z_2 \times \sin\theta_1 - t_i \times \tan(90 - \alpha) \\ z_{i+1} &= -x_2 \times \sin\theta_1 + z_2 \times \cos\theta_1 + z_1 - n_i \end{aligned} \tag{3.4}$$

Using parametric equation and angular rotation of the end effector, tool path trajectory was generated using MATLAB for circular cone, square cup and asymmetric cup as shown in Figure 3.3. But practically, 1st joint of the manipulator can be inclined to limited angle to avoid interference between end effector and machine bed. Tool rotation is also not possible in all direction to avoid interference between tool shank and sheet during forming. Therefore, all the process parameters for two degree of freedom manipulator have to be found out to maintain proper surface finish without any interference.

3.5 Kinematic Analysis

Kinematic analysis involves study of position, velocity and acceleration. The main aim of this section is to find out the optimum velocity and position of the link and joints to follow a specific trajectory. If path to be followed by the end effector and number of joints and links to be used in manipulator are known, position orientation and velocity of the links and joints can be easily calculated using kinematic analysis. This can be analyzed in two ways, one using inverse kinematics and other using forward kinematics. In forward kinematics, joint angle in revolute joints, displacement of the link in prismatic joints are prescribed and using

these parameters, end effector configuration is to be obtained. But in incremental sheet metal forming tool path trajectory is known and joint and link configuration need to be calculated to obtain desired trajectory. For this, inverse kinematics has to be done. The forward kinematics problem helps in solving the end-effector pose when complete set of joint variables are known. But the inverse kinematics problem helps in finding joint variables for known end-effector pose. In incremental sheet metal forming, tool path trajectory is shown below in Figure 3.4.

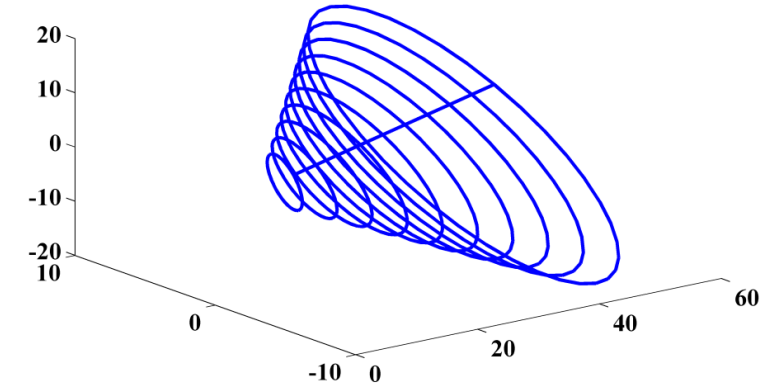

(a)

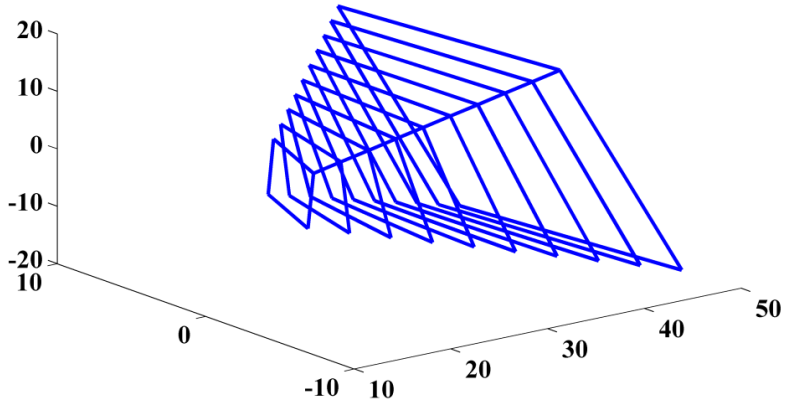

(b)

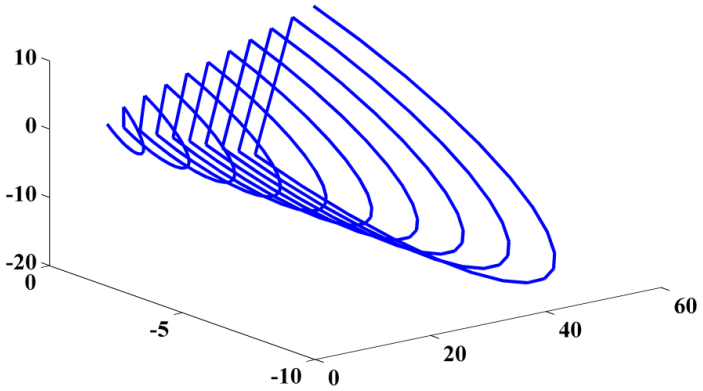

(c)

Figure 3.3 Trajectory for (a) circular cone (b) square cup (c) asymmetric cup

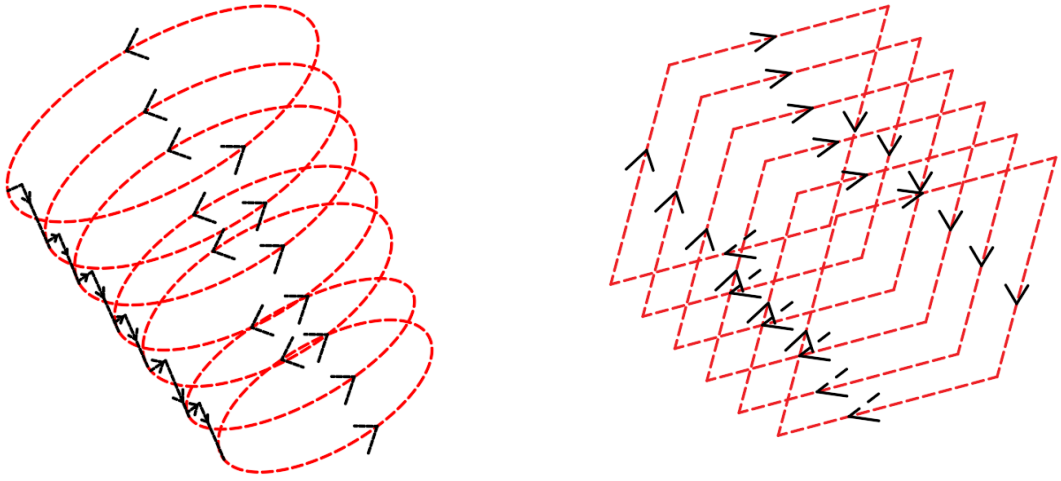

(a) (b)

Figure 3.4. Tool path in RAISF for (a) circular cone (b) square cup

To achieve optimal performance and accuracy, accurate design methodologies for ISF should be selected. The methodologies mostly used by the researchers are jacobian matrix which relates end effector velocity with joint speeds. jacobian matrix linearly maps end effector velocity and joint velocities, which makes jacobian matrix a structure dependent matrix. In isotropic Jacobian matrix, each actuator provides equal effort in all direction. So to design a robotic manipulator for good kinematic performance, structural parameter should be selected in such a way that jacobian matrix will be isotropic. In design of manipulator, both the kinematic analysis and dynamic analysis require frame transformation of the model.

The basic configuration selected is similar to joint arm configuration. Since the purpose is to provide rotational degrees of freedom to work piece, joint arm configuration is the simplest configuration. Multiple numbers of task points *P* can be used to define task description that the manipulator is supposed to reach with a specified movement (translation/orientation). Let *P* be the set of m task points that define the manipulator's performance requirements.

$P = \{p_1, p_2, p_3 \ldots\ldots, p_n\} \epsilon\ WS$

All these points define position and orientation of the end-effector work Space (*WS*). Each point in the Work Space (WS) can be given as:

$P_i = \{x, y, z, \theta_1, \theta_2\}$,

where

x, y, z = three degree of freedom in CNC milling machine

θ_1, θ_2= Two degree of freedom given to robotic manipulator

Figure 3.5 shows manipulator with two degree of freedom in which one link is fixed. Pin joint or rotational degree of freedom is given to second link and cylindrical joint with translation lock is given to third link. Work piece frame will be fixed to end effector.

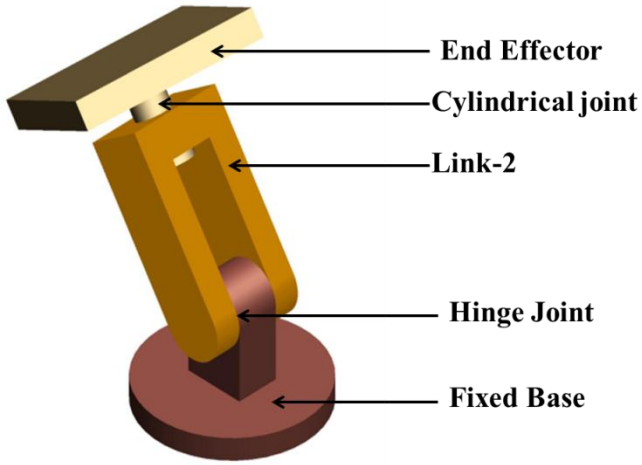

Figure 3.5. CAD model of 2-DOF manipulator

3.5.1 Frame Assignment

Frame assignment of the link is the first step for developing a mathematical model for robot. In frame assignment, following basic rules need to be followed.

a. Z vector is always on the joint axis direction

b. The X vector of the frame lies along the common perpendicular to Z_{i-1} and Z_i

Frame assignment for 2-DOF manipulator has been shown in the Figure 3.6.

{0} = Fixed Link

{1}= joint-1(Pin joint) and Link-2

{2}=Joint-2(Cylindrical joint) and Link-3

J_1= joint-1(Cylindrical joint with translation lock)

J_2= joint-2(Pin joint)

L_1= Length of link-1

L_2=length of the link-2

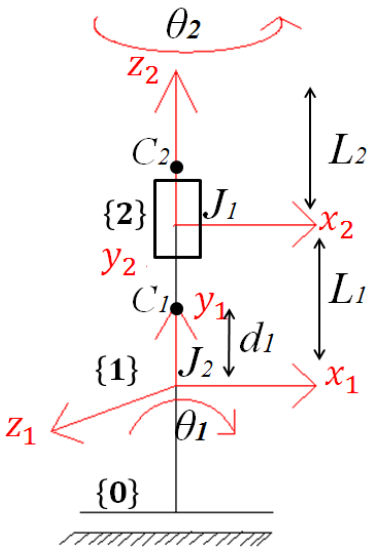

Figure 3.6.Frame assignment

The θ_1 has rotation about Z_1 axis which will give Y-axis rotation to sheet metal on the CNC milling machine. Hinge rotation schematic diagram is shown in Figure 3.7. This shows end effector rotation of J_2 about Z_2 axis which will give rotation of end effector about an arbitrary axis. Arbitrary axis is the axis after pin joint rotation at certain angle.

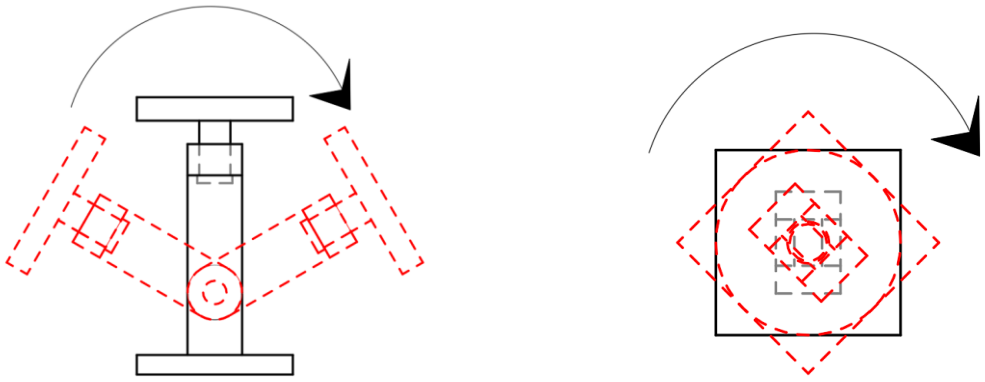

(a) (b)

Figure 3.7 (a) First rotational degree of freedom, inclination (θ_1), and (b) second rotational degree of freedom, twist of the robotic manipulator (θ_2)

A serial robot of N links has N+1 serially mounted rigid bodies connected by N joints. The N rigid bodies are numbered from 0 to N. 1st rigid body is fixed to base and end effector is connected to N^{th} rigid body. Rigid bodies are also called as link and are actuated by motors (hydraulic/pneumatic/electrical) via transmission mechanism. Joints are numbered from 1 to N and the i^{th} joint connects i-1 and i^{th} links. Position and orientation of the end effector can be controlled fully. Configuration of the manipulator can be described by joint angle or angular

position vector. Figure-5 shows the frame transformation of the manipulator. In this case, 1st link is fixed to base. So it has been assigned as frame {0}. 2nd link has been connected to fixed 1st link by revolute joint and is assigned as frame {1}. 1st revolute joint is denoted as J_1. End effector or the sheet metal holder is connected to 1st link by revolute joint J_2. End effector is assigned as frame {2} as shown in Figure-5. The θ_1 is the angular rotation by J_1 or rotation of second link about first link. The mathematical description of the robotic manipulator is usually represented using Denavit and Hartenberg (DH) parameters [12]. The DH parameters include link offset (d), link length (a), link angle (α) and link twist (θ). The θ is a variable when joint is revolute and constant when joint is translational. When joint is revolute, parameter d is a constant and is variable when joint is prismatic. The d is the translation distance along z axis. The θ is the rotation angle about z-axis. The a is the translational distance along x-axis. The α is the rotation angle about x-axis. For above mentioned frame, DH parameters are as shown below in Table 3.1.

Table 3.1. Denavit-Hartenberg Parameters

Link	***d***	***a***	***α***	***θ***	**Type**
1	L_1	L_1	0	θ_1	Revolute
2	L_2	L_2	90	θ_2	Revolute

3.5.2 Linear and angular velocities

Position and orientation of the links and joints can be obtained by inverse kinematics. Linear velocity and angular velocity can be defined as time derivative of position vector and rotation matrix of rigid body. Linear velocity of an arbitrary point on rigid link undergoing translation and rotation with respect to base frame has to be calculated first. Using this linear velocity, both linear and angular velocity of the links and joints can be calculated as follows. Before calculating linear and angular velocities, homogeneous transformation matrices for all joints need to be obtained.

The transformation matrices of frames 1 and 2 with respect to reference frame are:

$$T_0^1 = \begin{bmatrix} \cos\theta_1 & 0 & \sin\theta_1 \\ 0 & 1 & 0 \\ -\sin\theta_1 & 0 & \cos\theta_1 \end{bmatrix} \tag{3.5}$$

$$T_1^2 = \begin{bmatrix} \cos\theta_2 & -\sin\theta_2 & 0 \\ \sin\theta_2 & \cos\theta_2 & 0 \\ 0 & 0 & 1 \end{bmatrix} \quad (3.6)$$

where T_j^i is transformation matrix of frame i with respect to frame j.

$$T_0^2 = T_1^2 T_0^1$$

$$T_0^2 = \begin{bmatrix} \cos\theta_2 & -\sin\theta_2 & 0 \\ \sin\theta_2 & \cos\theta_2 & 0 \\ 0 & 0 & 1 \end{bmatrix} \begin{bmatrix} \cos\theta_1 & 0 & \sin\theta_1 \\ 0 & 1 & 0 \\ -\sin\theta_1 & 0 & \cos\theta_1 \end{bmatrix}$$

$$T_0^2 = \begin{bmatrix} \cos\theta_1\cos\theta_2 & -\cos\theta_1\sin\theta_2 & \sin\theta_1 \\ \sin\theta_2 & \cos\theta_2 & 0 \\ -\sin\theta_1\cos\theta_2 & -\sin\theta_1\sin\theta_2 & \cos\theta_1 \end{bmatrix} \quad (3.7)$$

Using equations (3.5) ,(3.6),(3.7), the linear velocity can be calculated as follows:

$$V_i^i = T\,{}_{i-1}^{i}\left(V_{i-1}^{i-1} + \omega_{i-1}^{i-1} \times O_i^{i-1}\right), \quad (3.8)$$

where V_j^i is velocity of link i in frame j.

Angular velocity can be calculated as follows:

$$\omega_i^i = T\,{}_{i-1}^{i}\omega_{i-1}^{i-1} + \dot{\theta}_i \{0 \quad 0 \quad 1\}^T \quad (3.9)$$

For fixed frame {0},

i=0

$$V_0^0 = 0 \quad (3.10)$$

$$\omega_0^0 = 0 \quad (3.11)$$

For frame {1},

i=1

$$V_1^1 = T\,{}_0^1(V_0^0 + \omega_0^0 \times O_1^0) = 0 \quad (3.12)$$

$$\omega_1^1 = T\,{}_{i-1}^{i}\omega_{i-1}^{i-1} + \dot{\theta}_i \{0 \quad 0 \quad 1\}^T = \{0 \quad 0 \quad \dot{\theta}_1\}^T \quad (3.13)$$

For frame {2},

i=2

$$V_2^2 = T\,{}_1^2(V_1^1 + \omega_1^1 \times O_2^1) = \begin{Bmatrix} -\sin\theta_2 l_1\dot{\theta}_1 \\ \cos\theta_2 l_1\dot{\theta}_1 \\ 0 \end{Bmatrix} \quad (3.14)$$

$$\omega_2^2 = T\,{}_1^2\omega_1^1 + \dot{\theta}_2 \{0 \quad 0 \quad 1\}^T = \{0 \quad 0 \quad \dot{\theta}_1 + \dot{\theta}_2\}^T \quad (3.15)$$

Linear and angular velocities of the end effector are given by

$$\omega_E^E = \{0 \quad 0 \quad \dot{\theta}_1 + \dot{\theta}_2\}^T$$

$$V_E^E = \begin{Bmatrix} -\sin\theta_2 l_1 \dot{\theta}_1 \\ \cos\theta_2 l_1 \dot{\theta}_1 \\ 0 \end{Bmatrix}$$

The linear velocity of the end effector in the fixed coordinate system can be calculated by multiplying the rotation matrix with $V_{\mathrm{E}}^{\mathrm{E}}$. Angular velocity will be same as there is no joint connection in the end effector.

ω_j^i is angular velocity of link j with respect to frame i.

$$\omega_E^0 = \{0 \quad 0 \quad \dot{\theta}_1 + \dot{\theta}_2\}^T \tag{3.16}$$

$$V_E^0 = \begin{bmatrix} \cos\theta_1\cos\theta_2 & -\cos\theta_1\sin\theta_2 & \sin\theta_1 \\ \sin\theta_2 & \cos\theta_2 & 0 \\ -\sin\theta_1\cos\theta_2 & -\sin\theta_1\sin\theta_2 & \cos\theta_1 \end{bmatrix} \times \begin{Bmatrix} -\sin\theta_2 l_1 \dot{\theta}_1 \\ (\cos\theta_2 l_1 + l_2)\dot{\theta}_1 \\ 0 \end{Bmatrix} =$$

$$\begin{bmatrix} -\cos\theta_2 \sin\theta_2 \dot{\theta}_1 (\cos\theta_1 l_1 + l_2) \\ \dot{\theta}_1 [l_1(\cos\theta_2 - \sin^2\theta_2) + \cos\theta_2 l_2] \\ -\sin\theta_1 \sin\theta_2 \, l_2 \dot{\theta}_1 \end{bmatrix}$$

$$V_E^0 = \begin{bmatrix} -\cos\theta_2 \sin\theta_2 \dot{\theta}_1 (\cos\theta_1 l_1 + l_2) \\ \dot{\theta}_1 [l_1(\cos\theta_2 - \sin^2\theta_2) + \cos\theta_2 l_2] \\ -\sin\theta_1 \sin\theta_2 \, l_2 \dot{\theta}_1 \end{bmatrix} \tag{3.17}$$

The velocity and acceleration of the end effector by quasi-static analysis have been measured in CREO parametric and the results are shown in Figure 3.8 and Figure 3.9.

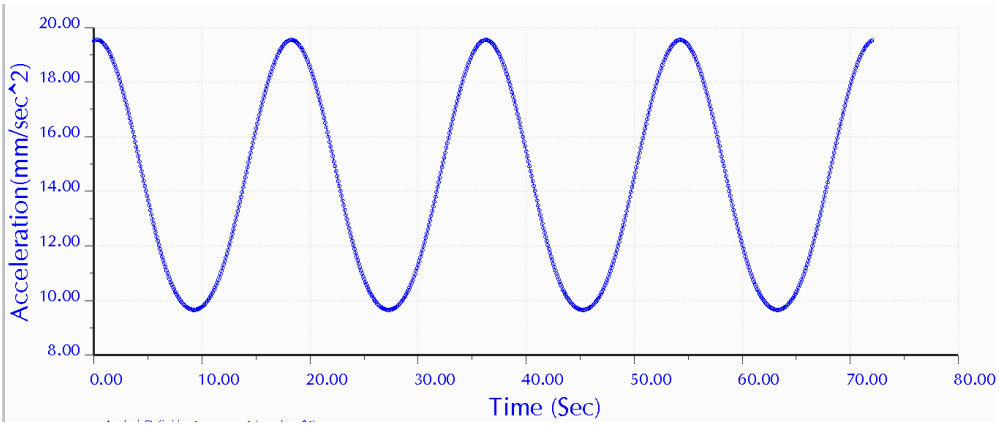

Figure 3.8.Acceleration analysis

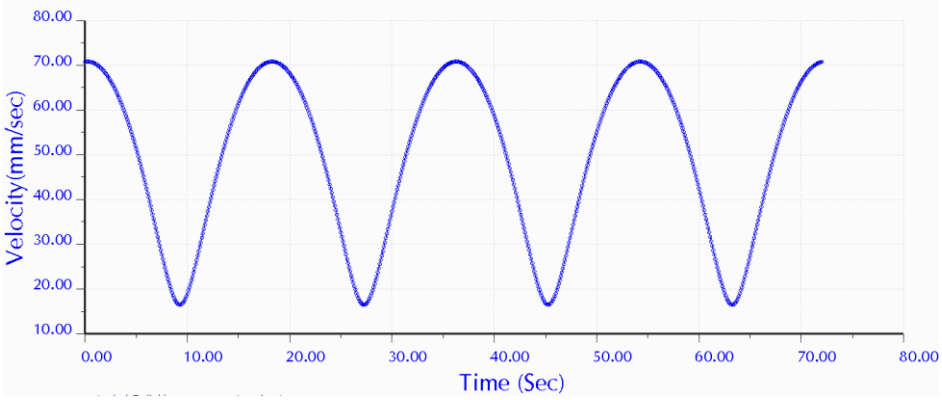

Figure 3.9.Velocity analysis

3.6 Dynamic Analysis

The objective of this section is to analyse the behaviour of the link and joint variables when end effector undergoes external forces. When the manipulator is intended for high speed application or high torque application or when external force application is high, dynamic analysis plays an important role. Dynamic analysis results will give maximum torque value experienced by each link and joint as well as dynamic stress due to application of external force. There are several ways to derive dynamic equation of motion of a manipulator. Equation of motion can be generated using the NE formulation, the LE formulation, D'Alembert's principle and Hamilton's principle. Kane's formulation has also been used by few researchers. Kane's formulation can be applied to any frame which can be represented in Newtonian's frame in terms of generalised coordinates. Two additional parameters are involved in this formulation, partial angular velocity and partial velocity.

NE and LE formulation are two widely used formulations for dynamic analysis.NE formulation requires linear and angular momentum to be estimated. Here manipulator is intended for high forming load. So results of dynamic analysis provide input for the required actuator torque as well as the dynamic stress that will occur in the link members. This work represents dynamic analysis of a serial spatial manipulator using LE formulation.

3.6.1 Euler-Lagrange (EL) Formulation

In the EL formulation of the present work, the kinetic energy and the potential energy of each link of the manipulator is computed first. By applying Lagrange's equation to the kinematic model, the dynamic equations are derived. In this model, a massive forming force is assumed and gravitational and inertia effects are considered.

The dynamic equations are derived for this 2-DOF manipulator using Lagrange's formulation. In this formulation, the input joint angles are chosen as per the consistent

generalized coordinate system. The Lagrangian, which is a function of generalised coordinates, depends on potential energy as well as kinetic energy of the manipulator. Therefore, position and velocity analysis as done in kinematic analysis are required in this analysis. This approach is advantageous as it removes internal constraint forces from the equation. Here Lagrange multipliers can also be used to inspect stress in the manipulator link induced by the external forces. The dynamic equation of motion of our 2-DOF manipulator can be derived using the EL formulation as follows.

The robotic manipulator's generalised coordinate is

$$\theta = \{\theta_1, \theta_2\}^T$$

Equations of motion of the manipulator according to EL formulation are as follows:

$$\frac{\mathrm{d}}{\mathrm{dt}}\left(\frac{\partial \mathrm{L}}{\partial \dot{\mathrm{p}}_\mathrm{i}}\right) - \frac{\partial \mathrm{L}}{\partial \mathrm{p}} = \tau_{\mathrm{i},} \tag{3.18}$$

where L is Lagrangian, p_i is the generalised coordinate, τ_i is generalised force. Here $L=T-U$, T is kinetic energy and U is potential energy.

$$T = \frac{1}{2}\left(m_i \dot{c_i}^T \dot{c_i} + \omega_i{}^T I_i \omega_i\right), \tag{3.19}$$

where

$\dot{c} =$ cartesian velocity of mass center

$\omega =$ angular velocity of the link.

$$\overrightarrow{\omega_i} = \overrightarrow{\omega_{i-1}} + \dot{\theta_i}\overrightarrow{e_i} \tag{3.20}$$

$$\dot{\overrightarrow{c_i}} = \dot{\overrightarrow{c_{i-1}}} + \omega_{i-1} \times r_{i-1} + \omega_i \times d_i \tag{3.21}$$

Equation of motion for link-1 can be calculated as follows

$$\overrightarrow{c_1} = \begin{bmatrix} \frac{l_1}{2}\cos\theta_1 \\ \frac{l_1}{2}\sin\theta_1 \\ 0 \end{bmatrix} \qquad \dot{\overrightarrow{c_1}} = \begin{bmatrix} -\frac{l_1}{2}\sin\theta_1\dot{\theta_1} \\ \frac{l_1}{2}\cos\theta_1\dot{\theta_1} \\ 0 \end{bmatrix}$$

$$\left(\dot{\overrightarrow{c_1}}^T \dot{\overrightarrow{c_1}}\right) = \frac{{l_1}^2}{4} sin^2\theta_1 \, \dot{\theta_1}^2 + \frac{{l_1}^2}{4} cos^2\theta_1 \, \dot{\theta_1}^2 + \frac{{l_1}^2}{4} \, \dot{\theta_1}^2 = \frac{{l_1}^2}{4} \, \dot{\theta_1}^2$$

$$\text{Kinetic Energy due to linear motion} = \frac{1}{2} m_1 \frac{{l_1}^2}{4} \dot{\theta_1}^2$$

$$\text{Kinetic Energy due to rotational motion} = \frac{1}{2} \overrightarrow{\omega_i}^T I_i \overrightarrow{\omega_i}$$

$$\overrightarrow{\omega_1} = \dot{\theta_1} \, \overrightarrow{e_1}$$

$$\overrightarrow{\omega_1} = \dot{\theta}_1 \begin{bmatrix} 0 \\ 0 \\ 1 \end{bmatrix} = \begin{bmatrix} 0 \\ 0 \\ \dot{\theta}_1 \end{bmatrix}$$

$$I = \begin{bmatrix} I_{xx} & I_{xy} & I_{xz} \\ I_{yx} & I_{yy} & I_{yz} \\ I_{zx} & I_{zy} & I_{zz} \end{bmatrix}$$

$$I\overrightarrow{\omega_1} = \begin{bmatrix} I_{xx} & I_{xy} & I_{xz} \\ I_{yx} & I_{yy} & I_{yz} \\ I_{zx} & I_{zy} & I_{zz} \end{bmatrix} \begin{bmatrix} 0 \\ 0 \\ \dot{\theta}_1 \end{bmatrix} = \begin{bmatrix} I_{xz}\dot{\theta}_1 \\ I_{yz}\dot{\theta}_1 \\ I_{zz}\dot{\theta}_1 \end{bmatrix}$$

$$\frac{1}{2}\overrightarrow{\omega_1}^T I\overrightarrow{\omega_1} = \frac{1}{2}[0 \quad 0 \quad \dot{\theta}_1] \begin{bmatrix} I_{xz}\dot{\theta}_1 \\ I_{yz}\dot{\theta}_1 \\ I_{zz}\dot{\theta}_1 \end{bmatrix} = \frac{1}{2} I_{zz}\dot{\theta_1}^2 = \frac{1}{2}\frac{m_1 {l_1}^2}{12}\dot{\theta_1}^2$$

$$T_1 = \frac{1}{2} m_1 \frac{{l_1}^2}{4}\dot{\theta_1}^2 + \frac{1}{2}\frac{m_1 {l_1}^2}{12}\dot{\theta_1}^2 = \frac{m_1 {l_1}^2}{6}\dot{\theta_1}^2, \tag{3.22}$$

where

$m_1 =$ mass of the link $- 1$

U= Potential Energy

$$U_1 = -m_1(-g)\left(\frac{l_1}{2} - \frac{l_1}{2}\cos\theta\right)$$

$$U_1 = m_1 g \frac{l_1}{2}(1 - \cos\theta_1) \tag{3.23}$$

From Equation (3.22) (3.23), L_1 can be calculated as mentioned below.

$$L_1 = T_1 - U_1 = \frac{m_1 {l_1}^2}{6}\dot{\theta_1}^2 - m_1 g \frac{l_1}{2}(1 - \cos\theta_1) \tag{3.24}$$

Equation of motion for link-2 can be calculated as follows

$$\dot{\overrightarrow{c_2}} = \dot{\overrightarrow{c_1}} + \vec{\omega}_1 \times r_1 + \vec{\omega}_2 \times d_2 = e_1 \times (l_1 + d_2)\dot{\theta}_1 + e_2 d_2 \dot{\theta}_2$$

$$\vec{\omega}_2 = \vec{\omega}_1 + \dot{\theta}_2\, e_2 = \begin{bmatrix} 0 \\ 0 \\ \dot{\theta}_1 \end{bmatrix} + \dot{\theta}_2 \begin{bmatrix} \sin\theta_2 \\ 0 \\ \cos\theta_2 \end{bmatrix}$$

$$\vec{\omega}_2 = \begin{bmatrix} (\sin\theta_2)\dot{\theta}_2 \\ 0 \\ (\cos\theta_2)\dot{\theta}_2 + \dot{\theta}_1 \end{bmatrix}$$

$$\dot{\overrightarrow{c_2}} = \begin{bmatrix} 0 \\ 0 \\ 1 \end{bmatrix} \times \left(l_1 + \frac{l_2}{2}\right)\dot{\theta}_1 + \dot{\theta}_2 \frac{l_2}{2} \begin{bmatrix} \sin\theta_2 \\ 0 \\ \cos\theta_2 \end{bmatrix}$$

$$\dot{\overrightarrow{c_2}} = \begin{bmatrix} (\sin\theta_2)\dot{\theta}_2 \frac{l_2}{2} \\ 0 \\ \left(l_1 + \frac{l_2}{2}\right)\dot{\theta}_1 + (\cos\theta_2)\dot{\theta}_2 \frac{l_2}{2} \end{bmatrix}$$

Kinetc Energy due to linear motion

$$T_l = \frac{1}{2} m_2 \dot{\overrightarrow{c_2}}^T \dot{\overrightarrow{c_2}}$$

$$= \frac{1}{2} m_2 \left[(\sin\theta_2)\dot{\theta}_2 \frac{l_2}{2} \quad 0 \quad \left(L_1 + \frac{l_2}{2}\right)\dot{\theta}_1 + (\cos\theta_2)\dot{\theta}_2 \frac{l_2}{2} \right] \begin{bmatrix} (\sin\theta_2)\dot{\theta}_2 \frac{l_2}{2} \\ 0 \\ \left(l_1 + \frac{l_2}{2}\right)\dot{\theta}_1 + (\cos\theta_2)\dot{\theta}_2 \frac{l_2}{2} \end{bmatrix}$$

$$T_l = \frac{1}{2} m_2 \left[\frac{{l_2}^2}{4} \left({\dot{\theta}_1}^2 + {\dot{\theta}_2}^2 + \dot{\theta}_1 \dot{\theta}_2 \cos\theta_2 \right) + {l_1}^2 {\dot{\theta}_1}^2 + l_1 l_2 \dot{\theta}_1 \left(\dot{\theta}_1 + \frac{\dot{\theta}_2}{4} \cos\theta_2 \right) \right], \qquad (3.25)$$

where

$m_2 =$ mass of the link $- 2$

Kinetic energy due to rotational motion

$$T_r = \frac{1}{2} \overrightarrow{\omega_2}^T I_2 \overrightarrow{\omega_2}$$

$$I_2 \vec{\omega}_2 = \begin{bmatrix} I_{xx} & I_{xy} & I_{xz} \\ I_{yx} & I_{yy} & I_{yz} \\ I_{zx} & I_{zy} & I_{zz} \end{bmatrix} \begin{bmatrix} (\sin\theta_2)\dot{\theta}_2 \\ 0 \\ (\cos\theta_2)\dot{\theta}_2 + \dot{\theta}_1 \end{bmatrix}$$

$$= \begin{bmatrix} I_{xx}(\sin\theta_2)\dot{\theta}_2 + I_{xz}\left[(\cos\theta_2)\dot{\theta}_2 + \dot{\theta}_1\right] \\ I_{yx}(\sin\theta_2)\dot{\theta}_2 + I_{yz}\left[(\cos\theta_2)\dot{\theta}_2 + \dot{\theta}_1\right] \\ I_{zx}(\sin\theta_2)\dot{\theta}_2 + I_{zz}\left[(\cos\theta_2)\dot{\theta}_2 + \dot{\theta}_1\right] \end{bmatrix}$$

$$T_r = \frac{1}{2} \overrightarrow{\omega_2}^T I_2 \overrightarrow{\omega_2}$$

$$= \frac{1}{2} \left[(\sin\theta_2)\dot{\theta}_2 \quad 0 \quad (\cos\theta_2)\dot{\theta}_2 + \dot{\theta}_1 \right] \begin{bmatrix} I_{xx}(\sin\theta_2)\dot{\theta}_2 + I_{xz}\left[(\cos\theta_2)\dot{\theta}_2 + \dot{\theta}_1\right] \\ I_{yx}(\sin\theta_2)\dot{\theta}_2 + I_{yz}\left[(\cos\theta_2)\dot{\theta}_2 + \dot{\theta}_1\right] \\ I_{zx}(\sin\theta_2)\dot{\theta}_2 + I_{zz}\left[(\cos\theta_2)\dot{\theta}_2 + \dot{\theta}_1\right] \end{bmatrix}$$

$$= \frac{1}{2} \left[I_{xx}(\sin^2\theta_2){\dot{\theta}_2}^2 + 2 I_{zx} \sin\theta_2 \dot{\theta}_2 \left[(\cos\theta_2)\dot{\theta}_2 + \dot{\theta}_1\right] + I_{zz}\left[(\cos\theta_2)\dot{\theta}_2 + \dot{\theta}_1\right]^2 \right]$$

$$T_2 = T_l + T_r = \frac{1}{2}m_2\left[\frac{{l_2}^2}{4}\left({\dot{\theta}_1}^2 + {\dot{\theta}_2}^2 + \dot{\theta}_1\dot{\theta}_2\cos\theta_2\right) + {l_1}^2{\dot{\theta}_1}^2 + l_1 l_2\dot{\theta}_1\left(\dot{\theta}_1 + \frac{\dot{\theta}_2}{4}\cos\theta_2\right)\right] + \frac{1}{2}\left[I_{xx}(\sin^2\theta_2){\dot{\theta}_2}^2 + 2I_{zx}\sin\theta_2\dot{\theta}_2\left[(\cos\theta_2)\dot{\theta}_2 + \dot{\theta}_1\right] + I_{zz}\left[(\cos\theta_2)\dot{\theta}_2 + \dot{\theta}_1\right]^2\right] \quad (3.26)$$

$$U_2 = -m_2(-g)\left(\frac{l_1 + l_2}{2} - \frac{l_1 + l_2}{2}\cos\theta_1\right) \quad (3.27)$$

Using Equation (3.26) and (3.27), L_2 can be calculated as follows

$$L_2 = T_2 - U_2 = \frac{1}{2}m_2\left[\frac{{l_2}^2}{4}\left({\dot{\theta}_1}^2 + {\dot{\theta}_2}^2 + \dot{\theta}_1\dot{\theta}_2\cos\theta_2\right) + {l_1}^2{\dot{\theta}_1}^2 + l_1 l_2\dot{\theta}_1\left(\dot{\theta}_1 + \frac{\dot{\theta}_2}{4}\cos\theta_2\right)\right] + \frac{1}{2}\left[I_{xx}(\sin^2\theta_2){\dot{\theta}_2}^2 + 2I_{zx}\sin\theta_2\dot{\theta}_2\left[(\cos\theta_2)\dot{\theta}_2 + \dot{\theta}_1\right] + I_{zz}\left[(\cos\theta_2)\dot{\theta}_2 + \dot{\theta}_1\right]^2\right] - -m_2(-g)\left(\frac{l_1 + l_2}{2} - \frac{l_1 + l_2}{2}\cos\theta_1\right) \quad (3.28)$$

The τ_1 and τ_2 can be calculated using Lagrangian equation for manipulator obtained from equations (3.24) and (3.28) as mentioned below.

$$\frac{d}{dt}\left(\frac{\partial L_1}{\partial\dot{\theta}_1}\right) - \frac{\partial L_1}{\partial\theta_1} = \tau_1, \frac{d}{dt}\left(\frac{\partial L_2}{\partial\dot{\theta}_2}\right) - \frac{\partial L_2}{\partial\theta_2} = \tau_2$$

$$\tau_1 = \frac{1}{3}m_1{l_1}^2\ddot{\theta}_1 + \frac{1}{2}m_1 g l_1\sin\theta_1 \quad (3.29)$$

$$\tau_2 = \frac{m_2}{4}{l_2}^2\ddot{\theta}_2 + I_{zz}\ddot{\theta}_2\cos\theta_2 - \frac{m_2}{4}\left[{l_2}^2\dot{\theta}_2\ddot{\theta}_2 + (l_2 + l_1)\times\frac{l_2\dot{\theta}_1}{2}\left(\ddot{\theta}_2\cos\theta_2 - \dot{\theta}_2\sin\theta_2\right) - \frac{I_{zz}}{2}\left(2\left(\ddot{\theta}_2\cos\theta_2 - \dot{\theta}_2\sin\theta_2\right)\left(\ddot{\theta}_2\cos\theta_2 + \dot{\theta}_1\right)\right)\right] \quad (3.30)$$

Equations (3.29) and (3.30) show the Lagrangian formulation for manipulator which is difficult to solve analytically hence numerical method of solution was resorted to using COMSOL multibody dynamic analysis module.

3.6.2 Multibody dynamic analysis

Multibody dynamic analysis is one of the methods to know the interaction between each moving rigid body parts and with environment in any mechanical system. Mechanical and structural systems with large translational and rotational displacement are being analysed in multibody dynamic analysis. Under influence of external as well as internal forces, analysis of behaviour of the mechanism is done in MBD analysis and this analysis is called forward dynamics. The analysis of forces required to move the mechanism in a specific manner is called inverse dynamics. In this mechanism, external force due to forming tool on manipulator is known to us. Due to this external force, change in position, velocity and reaction forces with time can be analysed using MBD. MBD analysis has been done using COMSOL multibody dynamics module in this section. Inputs in MBD analysis are: mass and inertia of the rigid bodies, joint constraints, external forces, contact force, friction force, gravitational force, initial conditions, and boundary conditions. Outputs in MBD analysis are: joint moment and forces, position and velocity of each joint and link, reaction forces etc.

In general, in multibody dynamic analysis, it is required to formulate equation of motion using mass, inertia tensor and centre of mass and interaction conditions. These equations of motion are then integrated and solved by differential equations.

Dynamic analysis of the mechanism shows us how our design will respond to dynamic forces (friction/gravity). Before creating physical prototype, dynamic analysis can be conducted in design phase. Kinematic and dynamic simulation of a rescue robot has been done using MATLAB and ADAMS previously. Here in our manipulator, links are connected by two joints which restrict their relative motion. Multibody dynamic analysis shows dynamic behaviour of a manipulator or links and joints, when an external force is applied. Displacement and velocity analysis of 2-DOF manipulator has been done in COMSOL multiphysics. In COMSOL, the EL equation is the governing equation for dynamic analysis. Maximum force has been calculated by conducting ISF experiments without using manipulator. Force plot has been shown in the Figure 3.10. Here vertical Z force is higher as compared to X and Y forces. Therefore, while carrying out the simulation, only the Z force has been considered. Z force was found to be less than 1000 N in experiments, hence in the simulation; the maximum load has been taken to be 1000 N. The sheet metal is made of

Aluminium alloy AA-1100 and the angular velocity was chosen as 200 rad/s, as mentioned in Table 3.2. Material properties used in the simulation are shown in Table 3.2. Simulation results are given in Figure 3.11 and Figure 3.12.

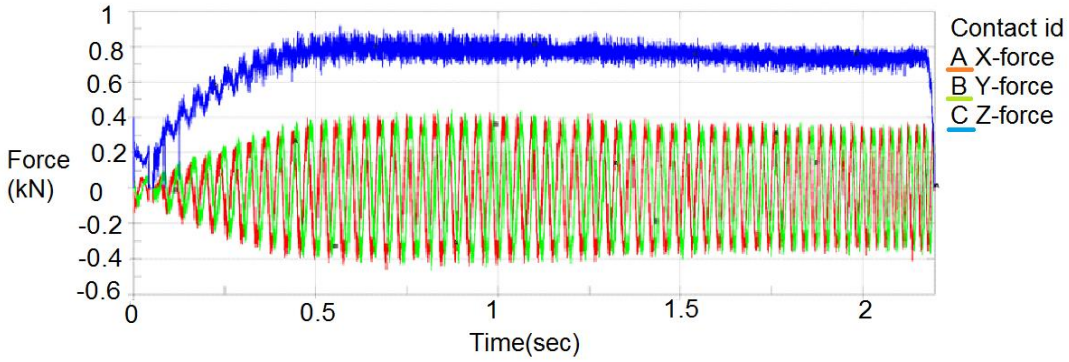

Figure 3.10. Experimental force distribution obtained from ISF

Table 3.2.Parameters used for simulation		
Parameter Name	Value	Description
F	1000 N	Total forming force
Angular speed	25 rad/s	Speed of workpiece (second rotational degree of freedom)

The manipulator was modelled in CREO as an assembly of three links and then was imported into COMSOL. In COMSOL, the appropriate settings were made to declare the manipulator as assembly so that the interfaces of individual links are recognized. Structural properties of the manipulator material are selected as shown in the Table 3.3.

Table 3.3.Material properties		
Name	Value	Unit
Density	7850	kg/m^3
Young's modulus	200	GPa
Poisson's ratio	0.33	-

The COMSOL Multi-physics simulation gave the displacement at end effector to be maximum, which is 0.54 m at 1.0 sec and when the end effector is at its maximum position. Velocity is also maximum on the end effector. Displacement at intermediate stages is plotted

in Figure 3.11, which shows that as the end effector moves up, due to application of external force, the displacement reduces.

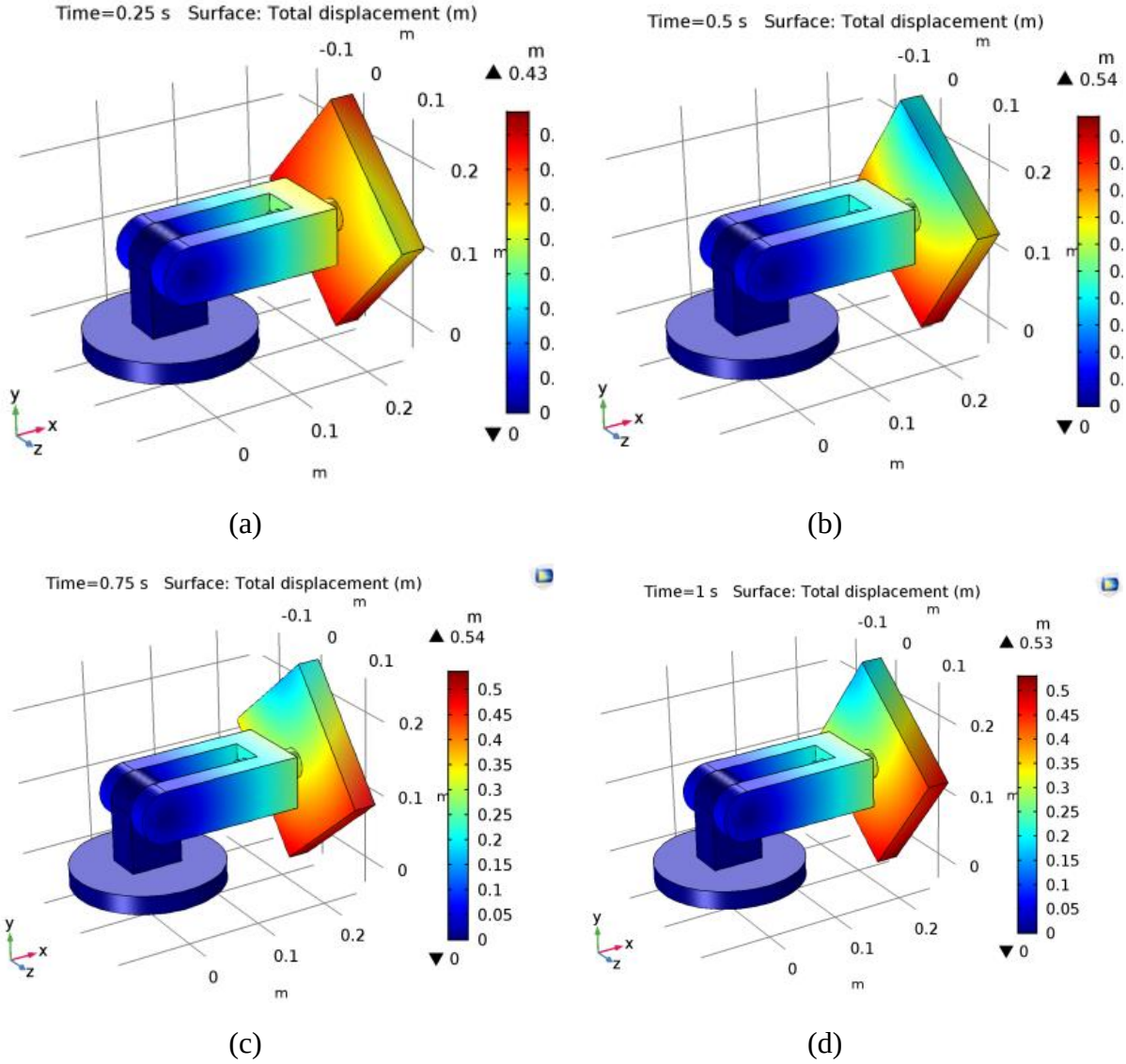

Figure 3.11.Displacement results from multibody dynamic analysis, at (a) 0.25sec, (b) 0.5sec, (c) 0.75sec and (d)1.0 sec

T

he Figure 3.12 shows the velocity at intermediate time steps.

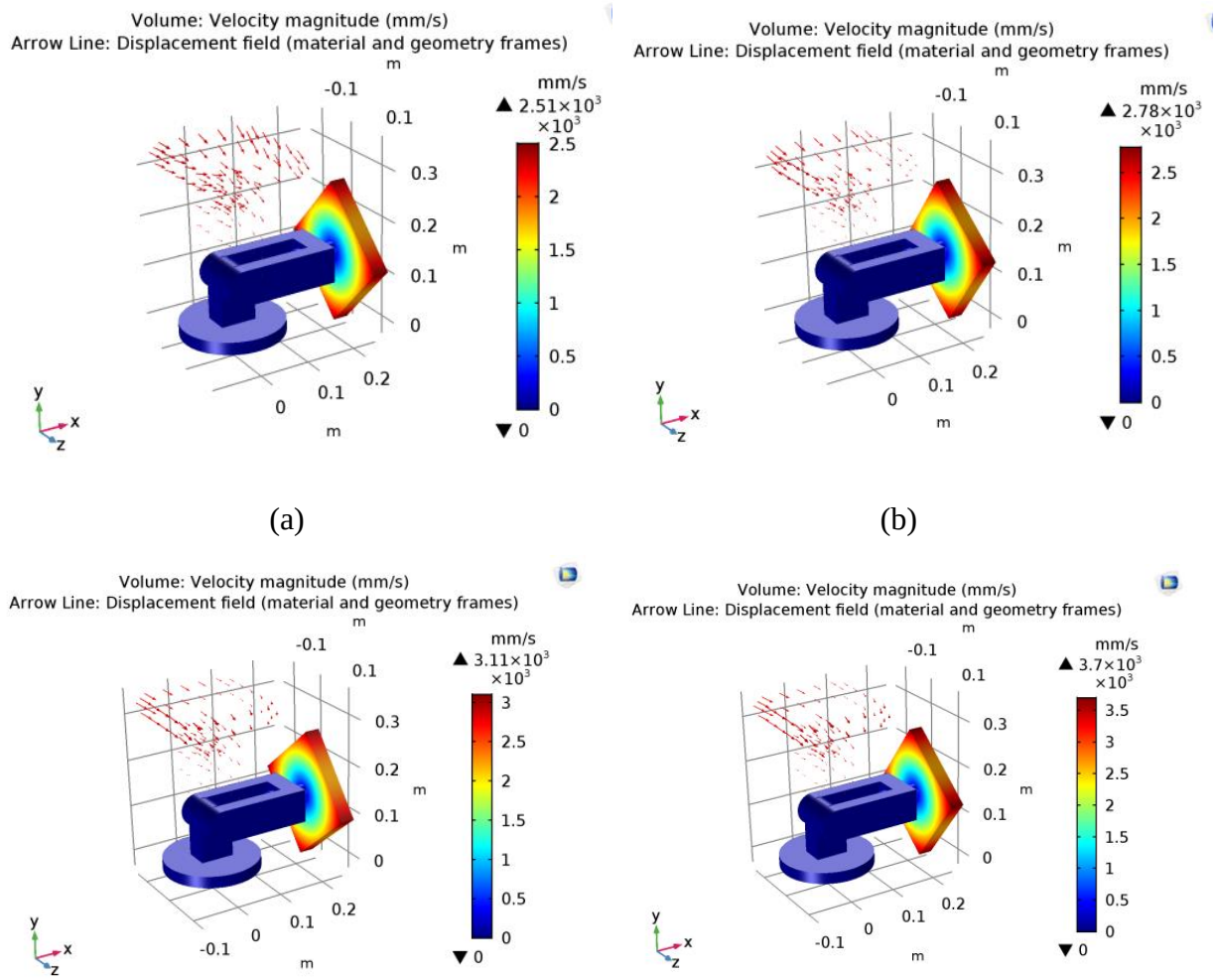

Figure 3.12. Velocity results from multibody dynamic analysis of the robotic manipulator at (a) 0.25 sec, (b) 0.5 sec, (c) 0.75 sec and (d) 1.0 sec

3.7 Mechanism

3.7.1 Design specifications and technical requirements

According to kinematic and dynamic analysis, a 2-DOF manipulator is sufficient to incline and rotate the sheet. However, design of the manipulator should be executed in such a way that it should be able to sustain the tool force as well as it can fit inside the space available on 3-axis vertical CNC milling machine. The tool length, X and Y travel limit of the machine bed should also be considered while designing the manipulator. For existing FANUC 3-axis CNC milling machine, the specification is given below in Table 3.4.

Table 3.4.Specification of CNC machine

Controller	Fanuc-I series GX 600
Working Surface	750 mm x 750 mm x 540 mm
Spindle speed	8000 rpm
Feed rate	12 m/min
Spindle power	15 KW

Considering the available workspace for the CNC milling machine and the forming tool dimension, manipulator dimension was restricted to 700 mm x 700 mm x 500 mm.

3.7.2 Selection of mechanism for the joints

Hinge in the first joint can be operated by a simple servo motor; however the motor should be chosen to handle the top frame weight as well as tool forming force. To rotate the second joint either a customized gear box or a servo/stepper motor would be an option. Therefore, first selection would be the mechanism for top joint which will rotate the sheet about an inclined axis and where end effector and second link will be connected to each other. ISF experimental results on AL1100 sheet shows that maximum forming force exerted by forming tool on sheet is 600-800N. So, second joint should be able to sustain minimum of 1500N vertical forming force.

The maximum tilting angle of the first joint was ±45° in clockwise and anticlockwise direction. Therefore, the maximum torque at the second joint is approximately 70Nm. However, end effector rotation should be low to maintain the proper contact as well as friction between sheet and tool. To reduce the cost of high torque motor, gear box has to be designed. High torque and low speed output can be achieved by a high speed reduction gearbox. Planetary gear box and Worm and worm wheel gear box are mainly used for higher gear ratio applications.

However, planetary gear box requires more installation space than worm and worm wheel gear box. The advantage of worm and worm wheel gear box over other gear boxes is high speed reduction, less backlash, less workspace, high efficiency. Therefore, worm and worm wheel gear box was chosen for the manipulator design. Depending on the availability of the motor with low torque and high speed, gear ratio was chosen for the mechanism. Table 3.5 shows the specification of the gearbox and the motor.

Table 3.5.Gearbox and motor specification			
Gear Box	Worm and Worm wheel	50:1 Gear ratio	Duplex worm and spiral gear
Motor	High torque stepper motor	300 kg-cm holding torque	Bipolar

Fixture used to clamp the sheet was designed similar to ISF fixture with an additional shaft which was connected to the spiral gear of the worm gearbox. The entire gearbox and end effector assembly as shown in Figure 3.13(a) was fixed in a casing to protect the gear tooth from external dust particle. The stepper motor was attached to the worm shaft and fixed on the tilting table as shown in the Figure 3.13(b). Figure 3.13(c) shows the manipulator design after assembly.

The stepper motor has been connected to the control system as shown in the Figure 3.14. The microcontroller Arduino uno board, which has programmable circuit board and software to write the program to the board has been used in the system.

To improve the performance of the stepper motor with low noise and low temperature rise as well as low vibration, a micro stepping driver has been used. A 120V transformer was used to transmit and distribute power, to change impedance and to provide electrical isolation. To control the steeper motor speed, a keyboard has been used and a program has been created which reads the keyboard key presses. To display the inputs, a 16X2 LCD display has been added to the circuit.

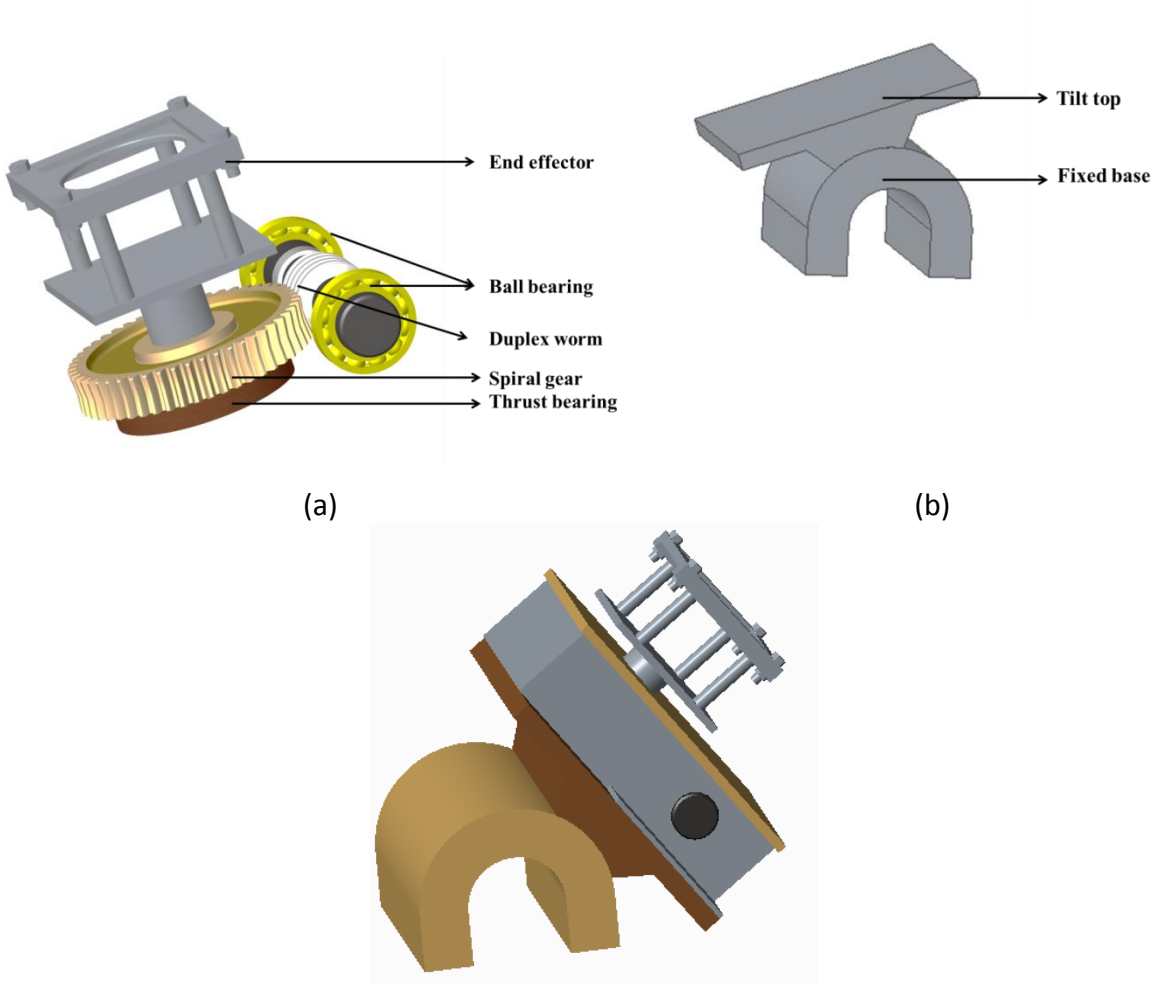

Figure 3.13 (a)Gearbox with end effector (b) Tilting table (c) Assembly

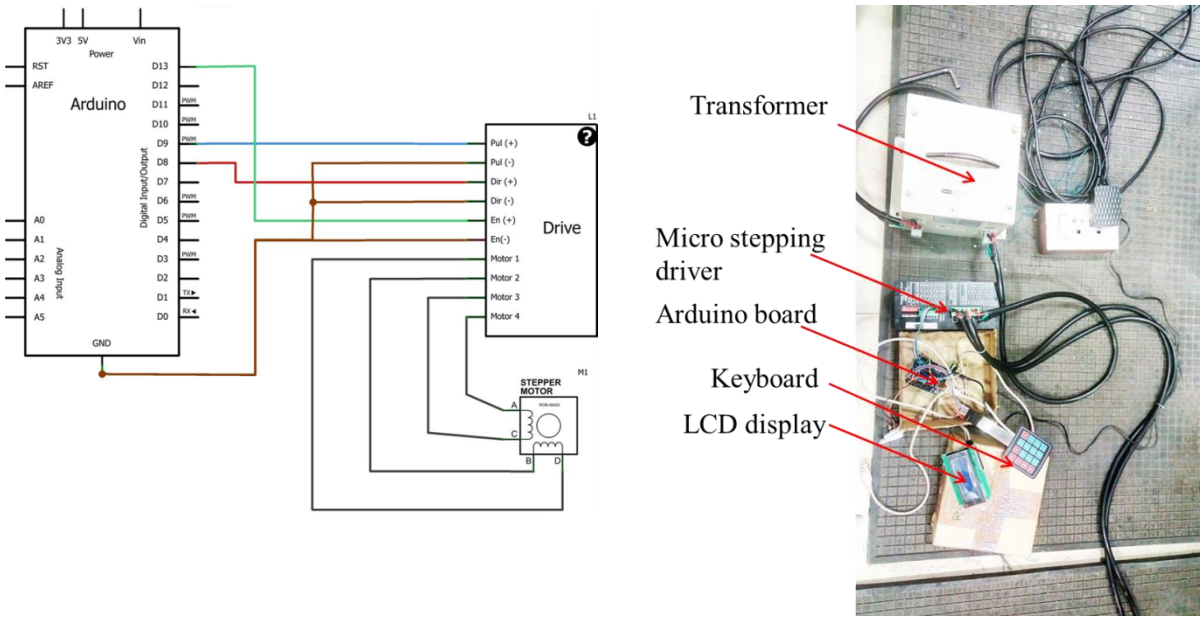

Figure 3.14.Layout of the control system

3.8 Parameter selection

3.8.1 End effector rotation speed

In single stage incremental forming without a manipulator,to get surface finish,process parameters have been optimised and validated through experiments.Out of all the process parameters,wall angle,step depth and feed rate have significant effect on surface quality.Other parameters were kept constant which have negligible effect on surface finish.

In Figure 3.15, schematic diagram of SPIF without manipulator and with manipulator has been shown.In this figure,it can be seen,in SPIF when manipulator is not used,feed rate is given to CNC machine.But when a manipulator is used, feed rate can be converted to angular rotation of end effector as shown below.

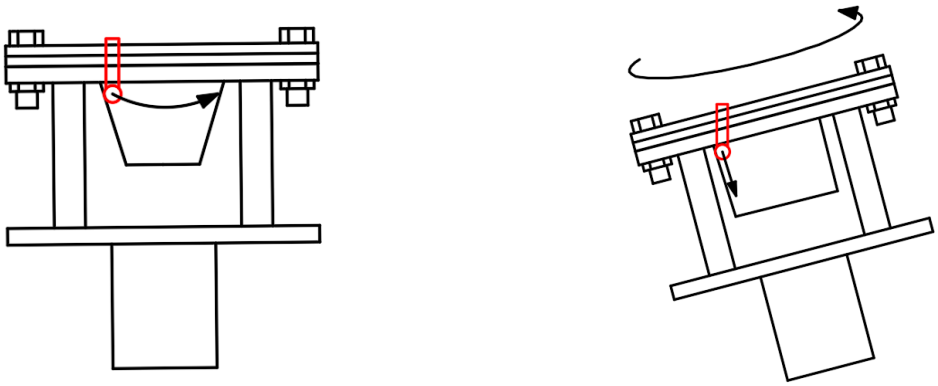

(a) (b)

Figure 3.15. Tool movement (a) without manipulator (b) With manipulator

In experiment,good surface finish can be achieved at forming angle α°,feed rate F mm/min and step depth of Zmm.End effector rotation speed can be obtained from optimised feed rate value.

θ_2 = Angular rotation of end effector which varies from 0° to 360°.

Let N is revolution per minute of the end effector.

$$N = \frac{F}{\pi * d} \tag{3.31}$$

where *d*= Top diameter of the cup.

3.8.2 Optimal Tilting and lead angle

To incline the sheet metal with respect to NC tool,maximum inclination angle needs to be calculated to avoid interference between tool shank and sheet metal part. In Figure 3.16 schematic diagram of a formed cup of 90º forming angle is shown.Where

H= Total depth to be formed

R_s=Radius of the cup

$\theta = \theta_1$ =Inclination angle

ϕ= Cup half angle or forming angle

$$\frac{2R_s}{\sin(\theta-\phi)} = \frac{H/\cos\phi}{\sin(90-\theta)}$$

$$\frac{2R_s}{H} = \tan\theta - \tan\phi$$

$$\theta = \tan^{-1}\left(\frac{2R_s}{H} + \tan\phi\right) \tag{3.32}$$

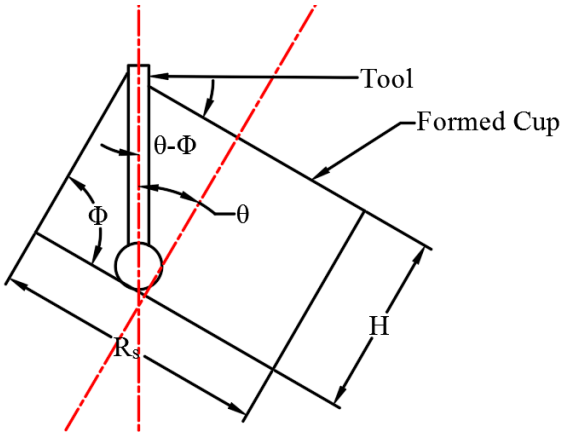

Figure 3.16. Inclination angle

Inclination angle can be calculated from above formula. But inclination angle will be calculated from optimised forming angle taken from experiments. At certain forming angle,surface quality is adequate. So the end effector will be inclined to 90º- forming angle to maintain the surface quality.

3.8.3 Scallop Height

Scallop height is one of the parameters to measure the surface quality in incremental forming operation.It depends on step depth and radius of the forming tool when forming operation is done on a 3 axis milling machine.But when two rotational degree of freedom

manipulator is added to 3 axis CNC machine,scallop height may also get affected by tilting angle while rotation of end effector about its own axis has no effect on scallop height.If the step depth d is lower than $2R_t\cos\theta$(Figure 3.17(a)), the tool will deform the same deformed portion as in preceding tool path resulting in more thinning of the sheet metal.On the other hand,if d is more than $2R_t\cos\theta$ (Figure 3.17(b)), there will be undeformed regions on the sheet in between two successive tool paths.When the inclination angle changes, to maintain same surface finish, scallop height should be same.In the second case,step depth value will be higher as compared to case-(a),which will reduce forming time.

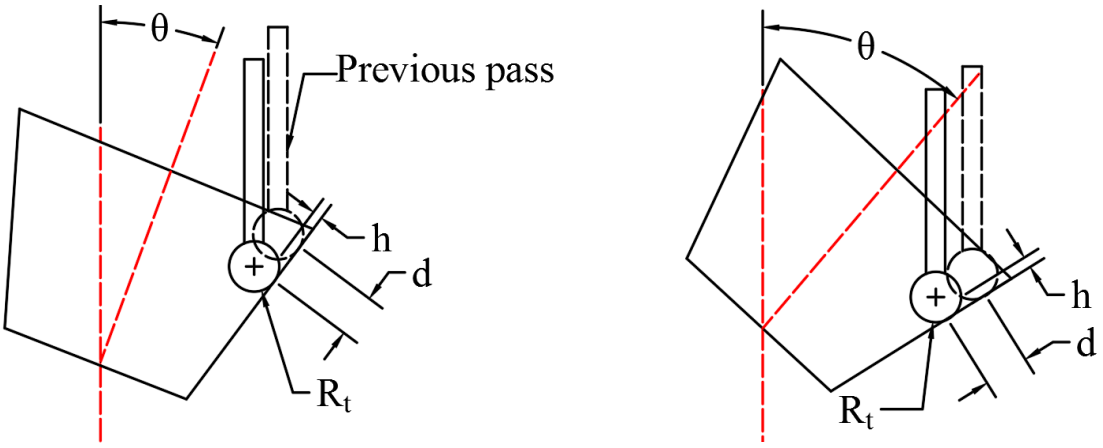

(a) (b)

Figure 3.17.Scallop Heights at (a) $d<2R_t\cos\theta$ (b) $d>2R_t\cos\theta$

3.9 Summery

This chapter presents the design of the manipulator for incremental forming. Modeling of the manipulator mainly involves kinematic analysis, dynamic analysis, and selection of joints, links and mechanism design. Depending on the tool path design, inverse kinematics has been implemented. The contribution also investigates the dynamic analysis of a robotic manipulator aimed to be used for incremental sheet metal forming. Analysis of the dynamic behavior of 2-DOF manipulator to be used for incremental sheet metal forming has been carried out using two methods, first the EL formulation and then using finite element multibody dynamic simulation using COMSOL Multiphysics. The link lengths of the manipulator are chosen as generalized coordinates and the velocity has been expressed in terms of the generalized coordinates. Linear and angular velocity of each joint and link have been calculated. The influence of tool force on the manipulator joint torques has been analyzed. Multibody dynamic analysis has been done by considering Aluminum alloy as the forming material, for which the average forming force was estimated from separate ISF experiments. Under the action of this force and the inertia force, the dynamic analysis helped estimate the displacement, velocity and accelerations for the range of rotational degrees of

freedom of the manipulator to be used in the incremental forming, helping in the design of the manipulator link material, dimensions that would withstand both the static and dynamic loads and would not impair the work piece geometric and surface accuracy. Selection of proper mechanism to control the torque and speed at the end effector which holds the sheet to be deformed has been designed. Control system has been designed to control the speed and torque at the output. Selection of proper parameters to avoid tool damage, improved surface quality and deformation has also been discussed in this chapter. However, theoretical selection of parameters should be investigated before starting actual forming operation. The next chapter will discuss numerical simulation of incremental forming process using the designed manipulator to investigate the sheet deformation, forming force, sheet thinning and formability.

CHAPTER 4
DEVELOPMENTAL OF NUMERICAL SIMULATION MODEL FOR FORCE AND STRAIN PREDICTION

FEM simulation of SPIF is a very complex task due to complex tool path and long process. By adding 2-DOF manipulator to the existing ISF process, due to change in tool path and input parameters, process output may vary. Before conducting the experiments, it is necessary to simulate the process to reduce material as well as process cost. In this chapter FEA modeling was used to predict the forming force, strain and thickness distribution and impact of various input process parameters on these outputs by using additional 2-DOF manipulator. The main objective is to understand the mechanics of RAISF through process simulation. By which FEA analysis can be used confidently to predict ISF forming process and effect of additional process parameters on the responses.

4.1 Material

Al1100 is a commercially used aluminum sheet which is widely used in chemical, food processing industries, hollowware, and heat exchangers due to its excellent resistance to corrosion. It is also used in applications where intrinsic formability and high corrosion resistance is needed but not high strength. In this work sheet of 250mmX250mmX1.2mm has been used for experiments. Chemical composition of the sheet has been shown in the Table 4.1. Sheet has been attached to a fixture and both are mounted on CNC machine table as shown in Figure-1.Sheet has been clamped on the fixture with locating pin and baking plate. EN36 hemispherical tool of 15mm diameter has been used for this operation. Tool was heat treated to 60HRC. Tool was polished with fine grade abrasive paper.

Table 4.1 Alloy Composition

	Aluminium	Copper	Iron	Manganese	Silicon	Zinc	Residuals
%age	99.0-99.95%	0.05-0.20%	0.95% max	0.05% max	0.95% max	0.1% max	0.15% max

4.2 Simulation of ISF

As ISF process involves localized plastic deformation, high nonlinearity should be considered in simulation. LS-DYNA v971 explicit dynamic module is capable of simulating highly nonlinear problems and solves dynamic problem using explicit time integration. To check the evolution of the forming force and to compare them with experimental work, with same working condition as experiments, LS-DYNA was adopted for numerical simulation. Blank and tool were modeled as shell element of type 2. Element edge of 1mm was used in

fine meshing of blank. Al-1100 sheet of 200×200×1.2 mm was selected as blank material and modeled using power law plasticity (MAT18 in LS-DYNA). Material was considered to be isotropic as difference in stress-strain behavior in three directions (rolling, diagonal and transverse) is small. Therefore, material was modeled using swift's isotropic strain hardening law. Tool of diameter 15 mm was modeled as rigid body (MAT20). The forming ONE_WAY_SURFACE_TO_SURFACE contact model was used to define contact pair between tool and blank. Due to application of sufficient lubricating oil, friction coefficient of 0.01 was used for simulation. To avoid convergence problem between tool element and sheet element, tool elements were bigger than sheet element. Due to longer tool path, to reduce computational time, the standard mass scaling and time scaling technique was used [92]. Mass scaling and time scaling parameters were chosen such that kinetic energy will be very less compared to internal energy which in turn reduces dynamic effect keeping the process as quasi-static. A scaling ratio of 0.0416 mm/sec to 0.4 mm/sec was arrived at using this method. For accurate result, adaptive meshing technique was used in simulation. The number of nodes per edge is also tested for different values and the result obtained was analyzed to verify their influence on accuracy and CPU time.

Baking plate hole was of 110mm diameter. So in finite element simulation (FEM) all nodes except 110mm diameter area were fixed in all direction. Most of the simulation in literature has been performed using simplified tool path rather than actual tool path. But here in this work, tool path was given as displacement verses time in three directions. The procedure to convert manufacturing code to time position data for FEM simulation has been reported in literature [94]. Using CAD model of the desired part in CAM software, tool path was generated. X, Y, Z coordinate of the tool path was imported from CAM file and converted to position verses time coordinates. These coordinates were given as input directly to FEM simulation in order to get result similar to experiment. As we are using actual tool path data, the length of the tool path is very long for simulation. Incremental forming is regarded as quasi-static process. So to shorten the time, tool velocity was artificially increased below a critical value and ratio of the kinetic and deformation energy was checked continuously which has to be maintained below 10% in order to avoid critical inertia effect on the effectiveness of the numerical results. Mass scaling was also done to reduce computational time. Adaptive meshing technique was used to get accurate results. In this analysis following three assumptions were made. (i) Material was assumed to be

homogeneous and isotropic, (ii) Material is assumed to be rigid except in the deformation zone, (iii) frictionless interface.

In this process, effect of additional process parameters like inclination angle and sheet rotational speed has to be investigated numerically before conducting experiments. Following process parameters has been considered for the numerical analysis.

Table 4.2. Process Parameters	
Process parameters	Parameter value settings investigated in the present work
Wall angle (°)	70, 72.5, 75, 77.5, 80, 82.5, 85
Inclination angle (°)	5, 10, 15, 20, 25
Rotational speed ($\dot{\theta}_2$) (RPM)	3, 4, 5, 6, 7, 8

4.2.1 Results and discussion

4.2.1.1 Effect of nodes per edge in adaptive meshing

The current section presents the effect of nodes per edge in adaptive meshing on accuracy and computational time in RAISF. The comparison of numerical results with different nodes per edge in adaptive meshing is compared with the experimental results for checking the accuracy. Strain distribution and thinning are the three outputs which are compared in this analysis.

a) Strain distribution

Slope of the fracture forming limit line (m) in principal strain space can be determined using the following equation [28]:

$$m = -\frac{5\left(\frac{r_{tool}}{t}\right) - 2}{3\left(\frac{r_{tool}}{t}\right) + 6} \tag{4.1}$$

Sheet thickness considered in the simulation and experiment is 1.2mm and tool diameter is 7.5mm. Putting these two values in equation (4.1), slope of the forming limit line in principal strain plane will be -1.18.

The thickness strain at the fracture (point q in Figure 4.1) in plain strain condition is $\varepsilon_1 + \varepsilon_2$. For a given material many empirical equations have been proposed to define fracture forming limit diagram (FFLD). In this work, following equation has been used to define FFLC proposed by Fratini et al. [95].

$$\mathbf{FLD_0 = 8.64 - 36.2n - 0.00798K + 0.373R_n - 0.104A\% + 0.0301K.n + 0.607n.A\%} \quad (4.2)$$

where K is the strength coefficient, n is the strain hardening exponent, R_n is the normal anisotropy and A% is the percentage reduction in area.

The FFLC for Al1100 was calculated using equation (4.2). The safety margin is 20% of the FLD. The FFLC was given as the input to numerical simulation to find out the formability of Al1100 in RASIF.

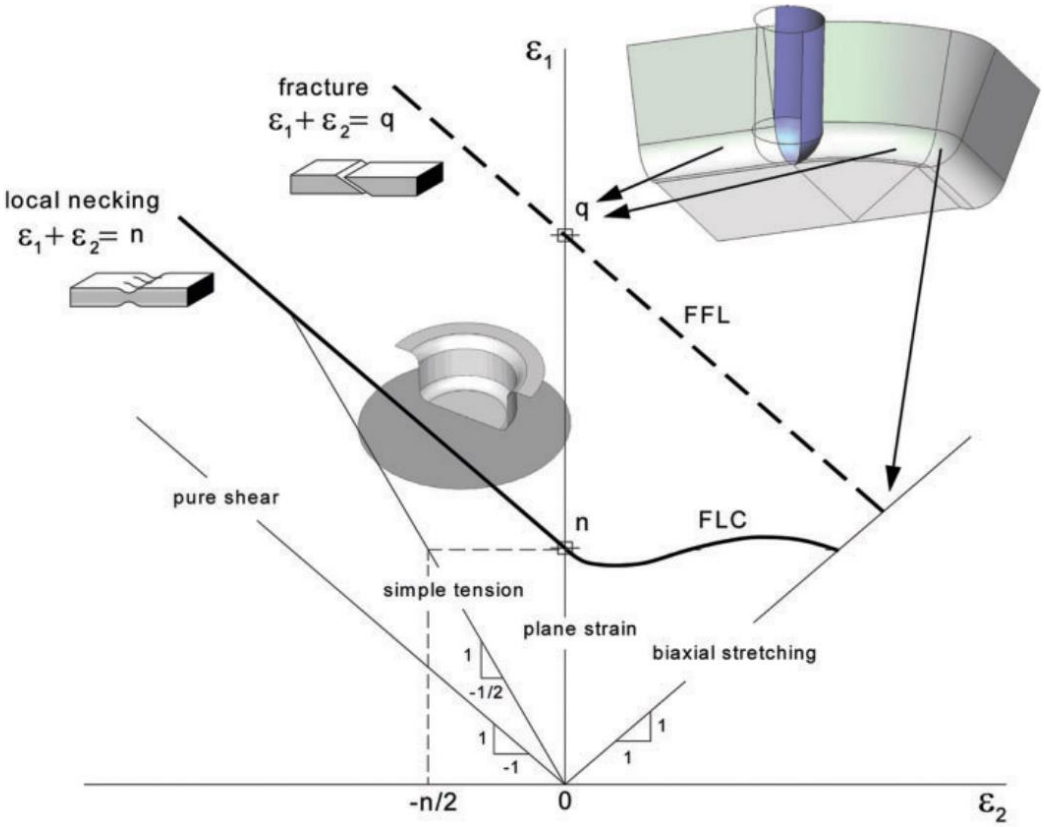

Figure 4.1. Representation of forming limits against conventional forming processes [28]

Major and minor strain have been predicted and compared with the experimental results in this work.

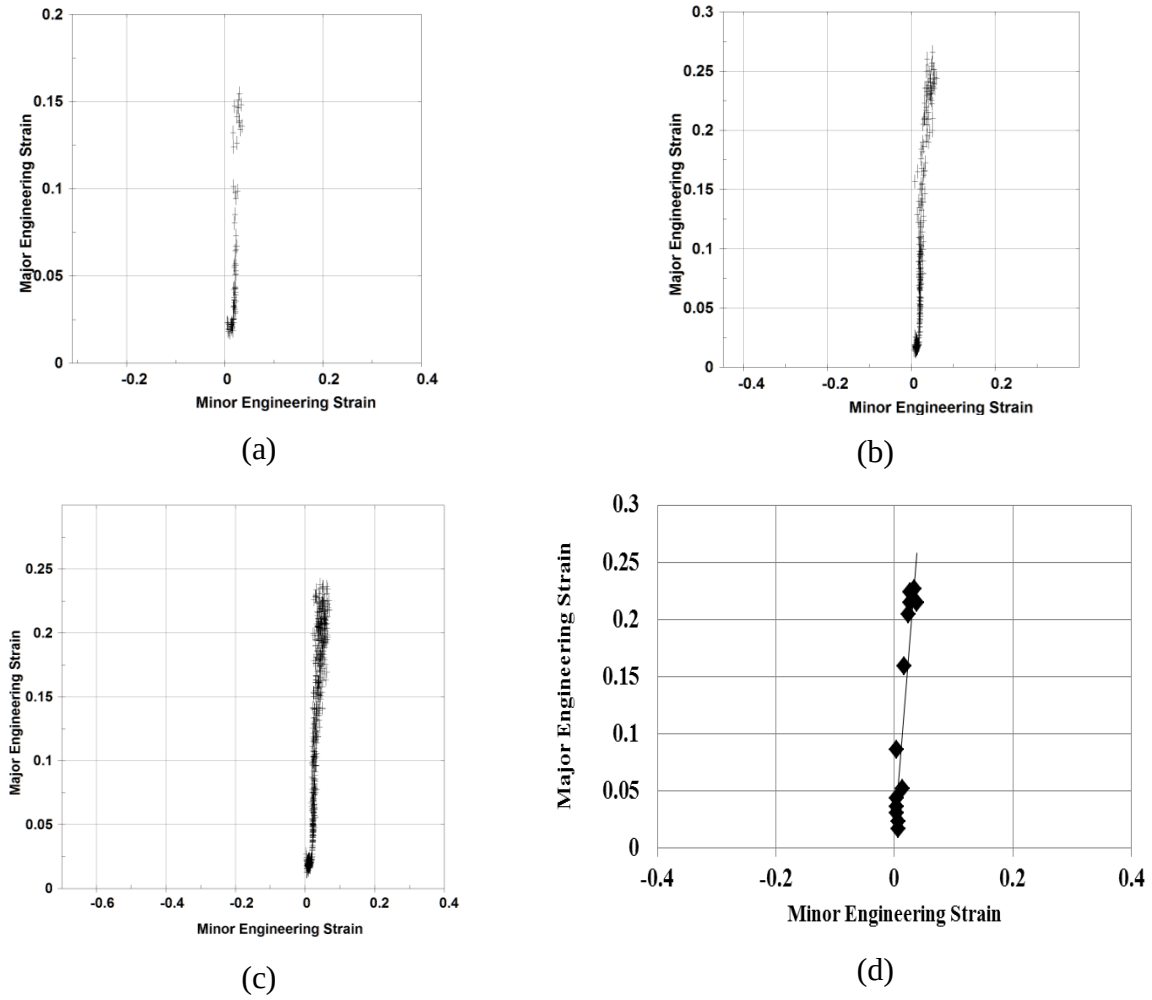

Figure 4.2 Strain distribution at refinement level (a) 1, (b) 2, (c) 3 and (d) experiment

Both the strains are measured along the wall and the depth of the formed part. The strain history in the Figure 4.2 combined with the maximum thinning strains in the cup reveals that material is undergoing plain strain deformation. The strains below the fracture forming limit curve remain in the safe region. The fracture depth could be found from the forming limit diagram and the depth found from the simulation has been compared with the experimental results for different refinement levels. Refinement level-3 was found to be closer to the experimental results.

b) Thinning

Thinning is the one of the indicators for the process robustness. As the material thinning in the ISF process follows a complex behavior, simple approach in predicting the thickness distribution of the formed part using "Sine law" is not a correct practice. Sine law predicts constant thickness distribution as it considers volume constancy.

As per sine law the thickness after forming should be

$$t_f = t_i \sin(90 - \alpha) \quad (4.3)$$

where t_f is the final thickness after deformation, t_i is the initial sheet thickness and α is the wall angle.

Sheet of thickness 1.2mm and 75° wall angle part has been considered for the simulation. Here parts has been simulated for three different nodes per edge and has been compared with the experimental results. The final part thickness has been measured along the part symmetry plane at each 5mm depth. As per sine law the final thickness should be 0.31mm. In Figure 4.3, curve A denotes thickness distribution at refinement level 1, similarly curve B and C represents thinning at refinement level 2 and 3. From Figure 4.3, it can be observed that, neither of the simulation results matches the sine law results. Since the sheet is fully clamped at the edges, the deformation due to tool motion is due to bending and stretching. It also shows that experimental observation for thickness distribution is closer to the results obtained in numerical simulation using refinement level 3. Mesh refinement level 1 and 2 shows deviation in thinning at the intersection zone of the forming wall and the base of the formed cup.

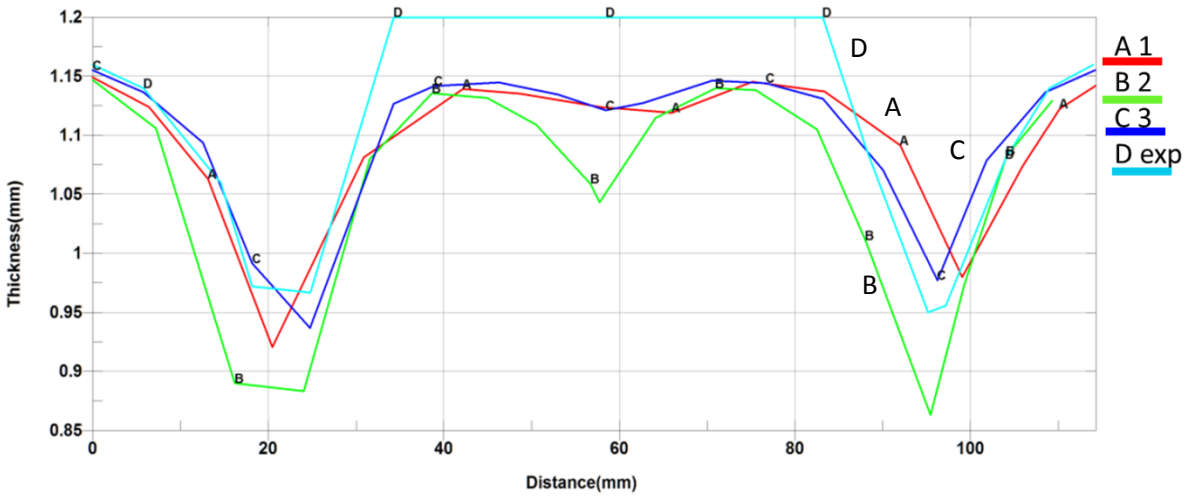

Figure 4.3 Comparison of thickness distribution in different refinement level

From both strain analysis and thickness distribution, it can be concluded that, results obtained using refinement level of 3 was closer to the experimental results.

4.2.1.2 Effect of Wall angle

a) Forming force

This section presents the numerical prediction of forming forces in RAISF by forming truncated cone of different wall angles. To simplify the comparison, the moving average

results of forming forces have been plotted. Wall angle of 65° was formed successfully till 60mm depth using different process parameters. To compare the forming forces, wall angle more than 65° wall angle has been chosen for numerical simulation. Forces have been measured at constant inclination angle of 15° with constant spindle speed, end effector rotation speed as well as step depth.

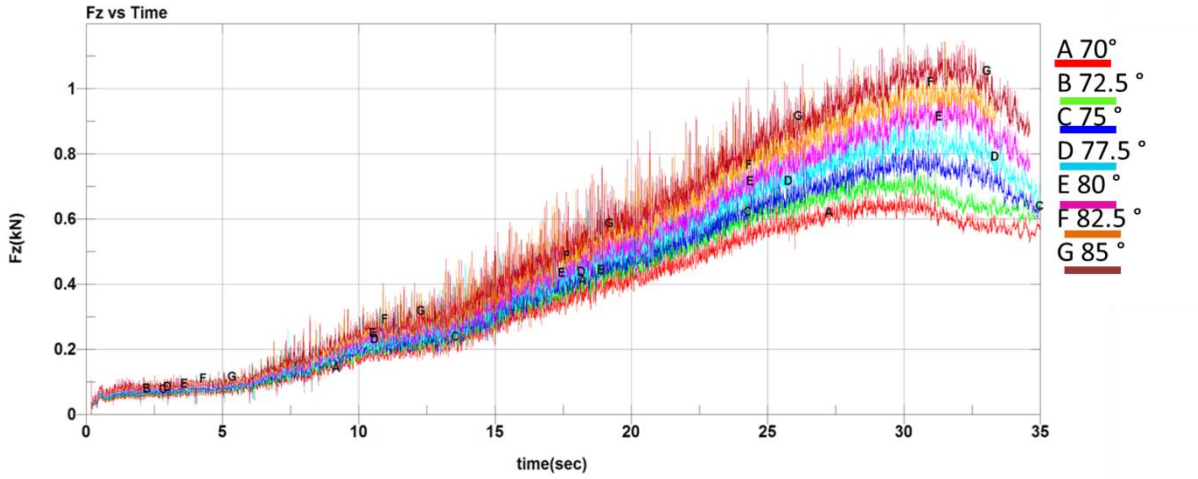

Figure 4.4 Axial force (F_z) at different wall angle

Figure 4.4 shows the evolution of the forming force in vertical Z direction at different wall angles. It can be observed in the force trend that, the force curve starts at zero once the forming initiates. As the tool pushes deeper in to the material, the force quickly increases up to a certain depth. From the plot it can also be observed that as the part wall angle becomes steeper, the magnitude of the peak force in vertical Z direction gradually increases.

b) Strain distribution

Strain distribution can be measured using fracture forming limit diagram as explained in the previous section. In this section, effect of wall angle on the strain distribution has been measured in the form of FLD as shown in the Figure 4.6. Inclination angle, rotation speed of the end effector and step depth has been kept constant at 15°, 0.5mm and 5RPM respectively for the whole process. However the wall angle has been varied from 70°-85° with an interval of 2.5°. Strain has been measured at constant forming depth at different wall angle in simulation. The extreme point in the plot in Figure 4.5 shows that with increasing wall angle the strain increases. As the strain in higher wall angle is higher, chances of fracture at early stage in higher wall angle parts are higher.

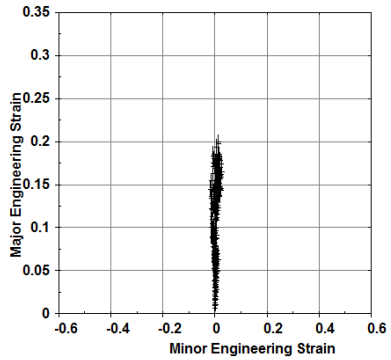

(a)

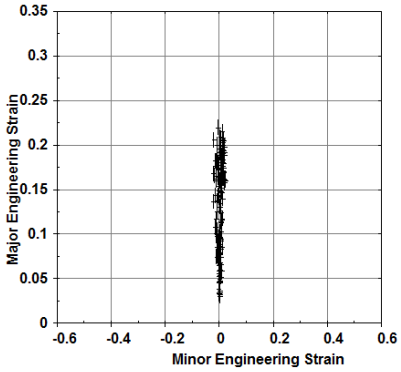

(b)

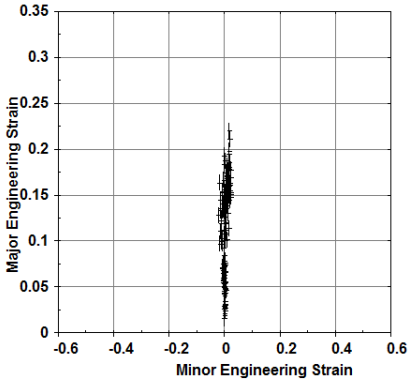

(c)

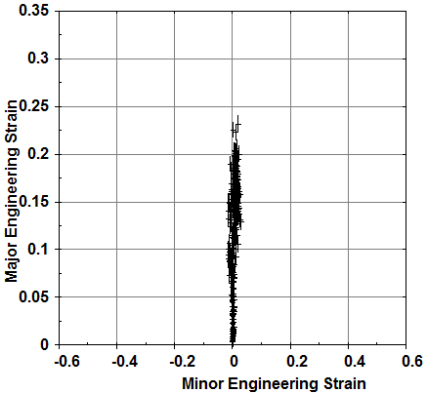

(d)

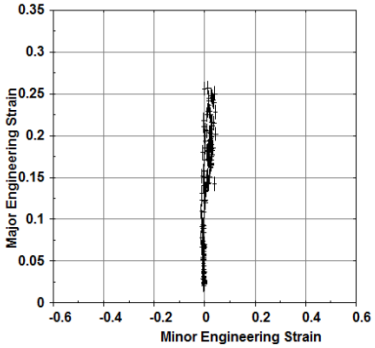

(e)

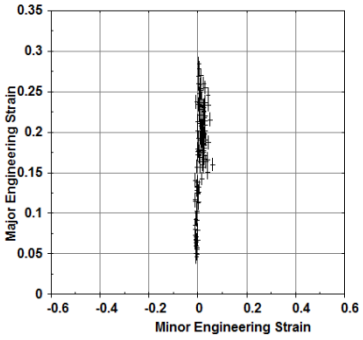

(f)

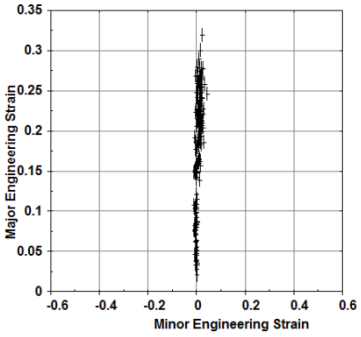

(g)

Figure 4.5 Strain distribution at wall different wall angles, (a) 70° (b) 72.5° (c) 75° (d) 77.5° (e) 80° (f) 82.5° (g) 85°

c) Thinning

According to Sine law which is based on constancy of volume, as wall angle increases the sheet thickness after deformation decreases. Local thinning determines the formability in incremental forming process. Therefore, at a particular forming depth, formability is lower for a higher wall angle part.

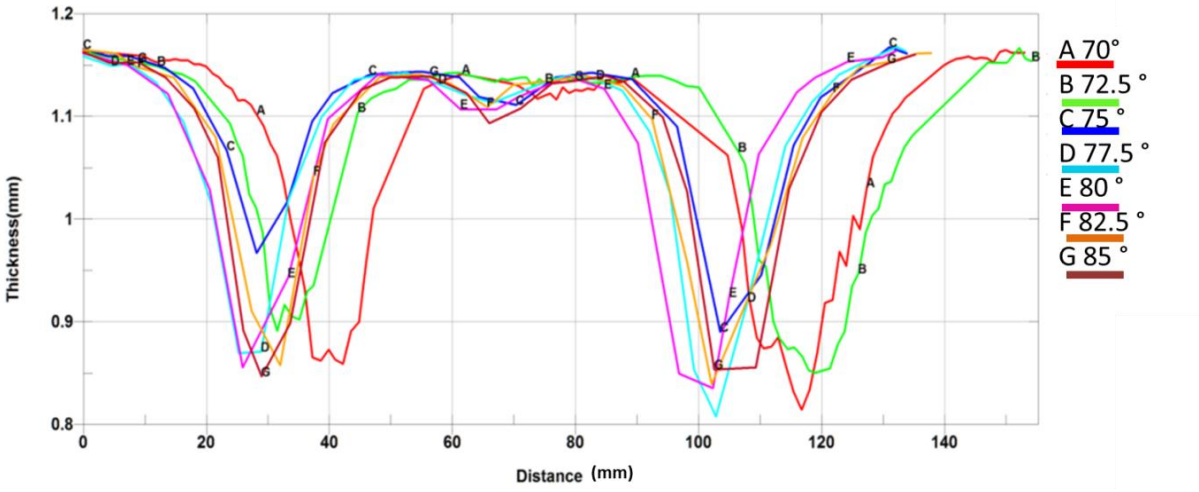

Figure 4.6 Comparison of thickness distribution along the section of the cup at different wall angles

Sheet of different wall angle has been simulated keeping other parameters constant to investigate the thickness distribution in the formed part. Figure 4.6 shows the simulation result for the formed part. It can be observed in the plot that variation in thickness distribution is observed only on wall region but at the base of the formed cup, thinning is nearly similar. At constant interval of time, thinning has been measured for all the parts. It can be observed in the plot that with increase in wall angle, thinning increases. However till wall angle of 75°. Thinning decreases with increasing wall angle. To confirm these results, experimental validation is necessary.

4.2.1.3 Effect of Inclination angle

a) Forming force

In the Figure 4.7, in the first half of the forming process, the amplitude of forces shows an increasing trend and becomes steady after achieving the peak force. This initial increase in the forming force is caused by the bending mechanism[96]. Then after the contact between the tool surface and sheet, force required to deform the sheet increases. The rise in force is

due to continuous stretching of the sheet after bending. During stretching operation, increase in force is caused by strain hardening process however subsequent thinning of the sheet reduces the forming force. Therefore after achieving peak force, due to combined effect of strain hardening and thinning force becomes steady. In Figure 4.7, it can also be observed that the achievement of steady state conditions is delayed with increase in inclination angle. This is because for a constant wall angle, with increase in inclination angle relative wall angle with respect to vertical forming tool decreases. With a decreasing relative wall angle, the sheet undergoes a longer bending mechanism before the strain hardening.

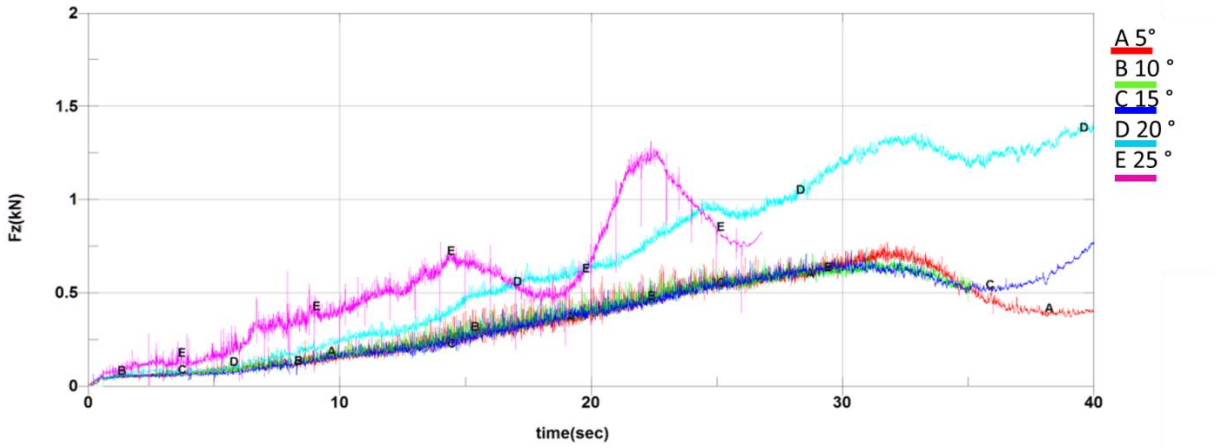

Figure 4.7 Axial force at different inclination angles

b) Strain distribution

Sheet has been tilted to different inclination angle to investigate the effect of inclination of the sheet on strain distribution. Major and minor strains obtained by inclination the sheet have been plotted in Figure 4.8. Form the plot it can be observed that, with increasing the inclination angle, major strain decreases. Strain is lower at higher inclination angle, which means the element tends to strain more at lower inclination angle which leads to early fracture of the sheet. However minor strain is nearly similar for all the tilted parts.

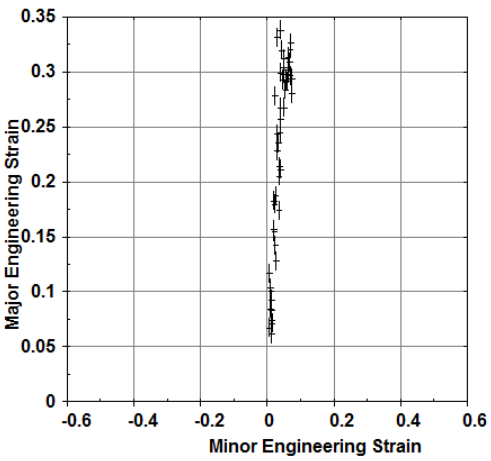

(a)

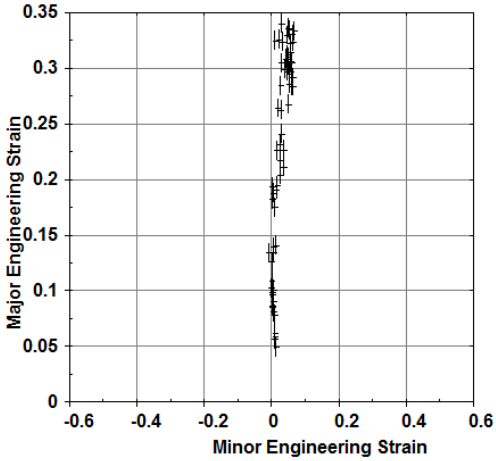

(b)

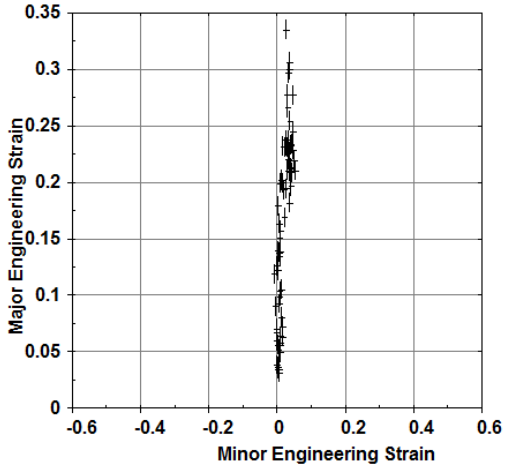

(c)

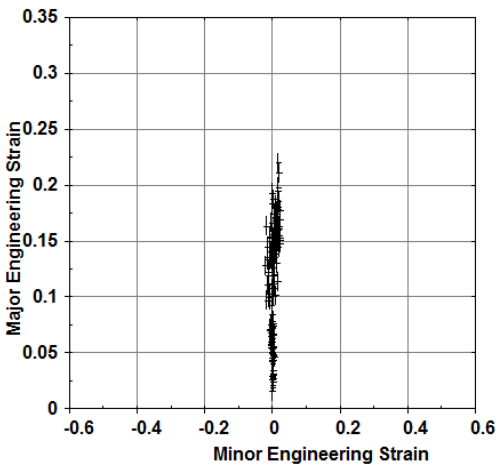

(d)

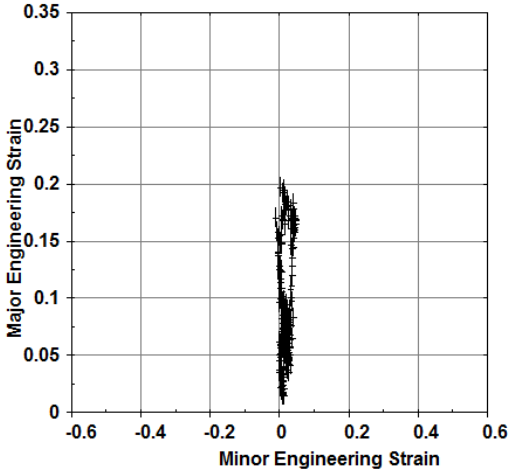

(e)

Figure 4.8 Strain distribution at inclination angles (a) 5° (b) 10° (c) 15° (d) 20° (e) 25°

c) Thinning

It is evident from the previous section that wall angle influences the final part thickness. The lower the wall angle, the lower the minimum thickness. The sheet can undergo a more severe thinning before failure, since its formability is improved. By inclination the sheet metal, due to decrease in relative wall angle between sheet and tool, contact area between sheet and tool changes. Figure 4.9 shows the thickness distribution of the sheet at different inclination angle. From the plot it can be concluded that thinning is higher at lower tiling angle till 20°. However simulation result showed that at 25° thickness is lesser than 20° which is a deviation from the other inclination angle. To confirm the simulation results and to study the exact behavior of the sheet at different inclination angle, experiments have been conducted and compared with the simulation results in the succeeding chapters.

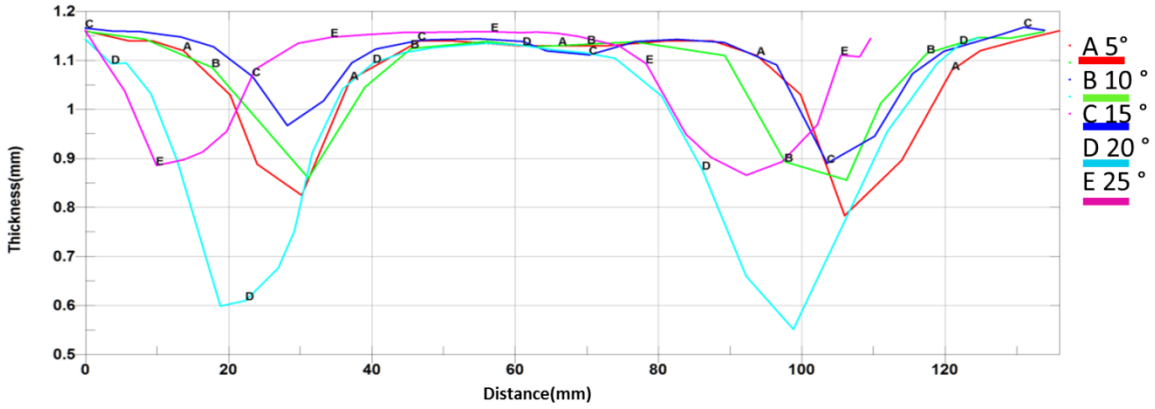

Figure 4.9 Comparison of thickness distribution along the section of the cup at different inclination angles

4.2.1.4 Effect of Sheet rotation

a) Forming force

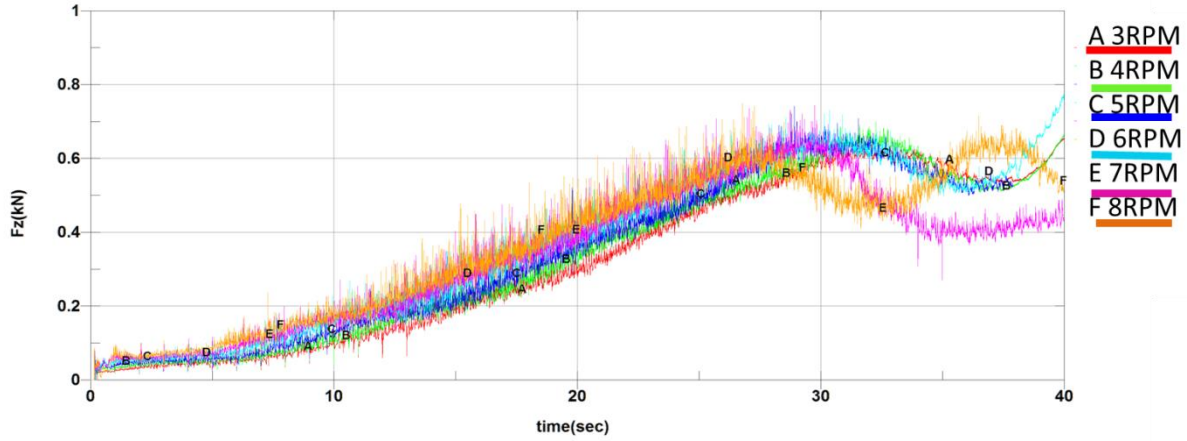

Figure 4.10 Axial force at different rotational speeds ($\dot{\theta}_2$) of the workpiece

The distribution of the forming force on the forming tool in vertical Z direction has been shown in the Figure 4.10. The results reveal that peak forming force is not getting affected by sheet rotation. Peak force is nearly same for all the rotational velocity, however a slight delay in peak force has been observed as the sheet rotational velocity decreases. Higher sheet rotation.

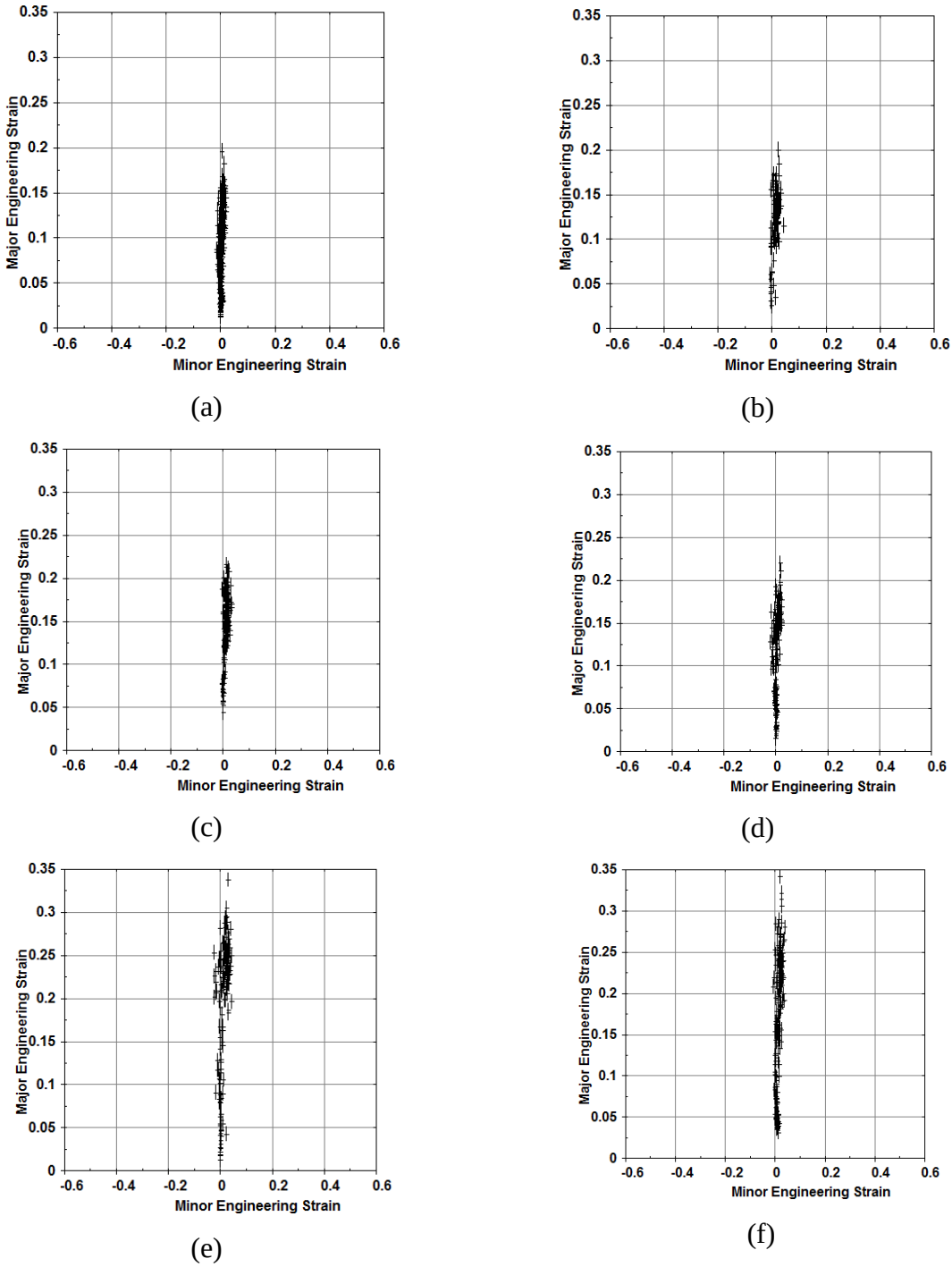

Figure 4.11 Strain distribution at different rotational speeds ($\dot{\theta}_2$) of the workpiece, (a) 3RPM (b) 4RPM (c) 5RPM (d) 6RPM (e) 7RPM (f) 8RPM

b) Strain distribution

Similarly, strain distribution for different sheet rotation has been measured in simulation using FLD plot. Here all other parameters have been kept constant. Figure 4.11 shows the FLD plot for different sheet rotational speed. In the plot it can be observed that with increasing sheet rotation, fracture major strain increases. At 8RPM the strain at fracture is higher but at 3 RPM the strain is the lowest among all. With increasing rotational speed if the step depth and feed rate are constant, then the forming tool overlaps the already formed zone in the sheet which leads to higher strain at the contact zone. Higher strain leads to early fracture in the sheet at higher rotational speed.

c) Thinning

Sheet has been rotated at varying rotational velocity to investigate its effect on thickness distribution. Figure 4.12 shows the thickness distribution of the formed cup at different sheet rotational velocity. Increasing end effector rotational velocity leads to non-uniform thickness distribution however at smaller rotational velocity, thickness distribution was nearly uniform. Base of the formed cup for higher rotational velocity shows more deviation in thinning than at lower RPM. However, lowering the rotational velocity below a critical value leads to overlapping of tool path. Overlapping of the tool path shows early fracture in the formed sheet. Increasing the rotational speed of the sheet above a critical value may lead to undeformed region which will result in formed parts with higher surface roughness.

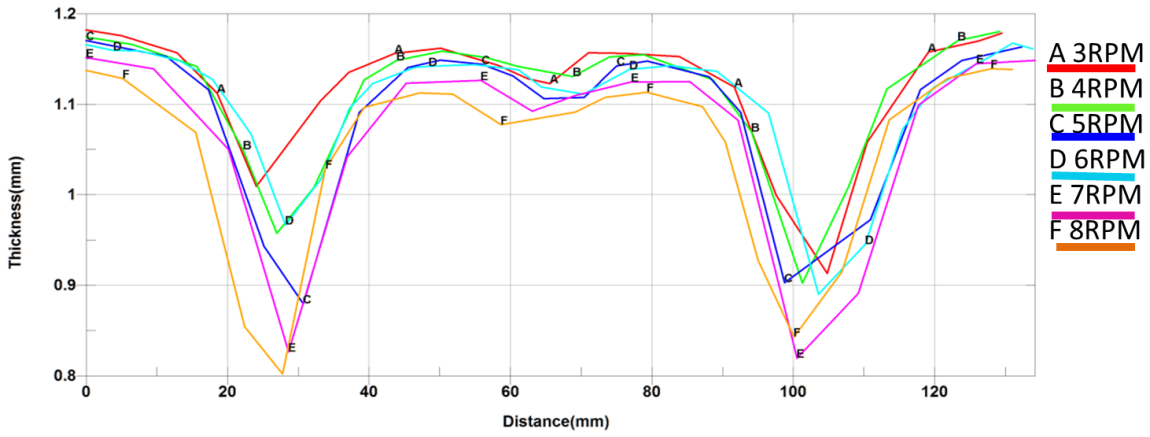

Figure 4.12 Comparison of thickness distribution at different sheet rotation

4.3 Summary

This chapter describes the process mechanics of RAISF using numerical simulation in LS-Dyna. Effect of additional process parameters on forming force, thinning and formability

has been investigated in this chapter. Results obtained in various mesh refinement levels have been checked and has been compared with the experimental results. Using the optimum refinement level which matches with the experimental results, parts have been simulated to investigate the effect of wall angle, inclination angle and rotational velocity on the forming force, thinning and formability of the sheet. The collected data on forming forces, sheet thinning and formability allowed concluding that when significant force reduction and geometrical accuracy improvement are the main objectives, ISF with additional inclination and rotation of the sheet should be adopted. Higher inclination results in delay in bending and sheet fracture. However rotational velocity has less significant effect than other process parameters. With increasing wall angle the formability was reduced and peak forming force was higher at higher wall angle. Low $\Delta\theta$ increments increase the material formability in terms of membrane deformation. In particular, the material formability improvement was verified measuring the part final thickness and the maximum thinning the material can undergo before rupture. As a consequence, maximum depth and wall slope before rupture increase. This chapter provides a basic understanding of the effect of process parameters on material forming behavior in the RAISF process by preliminary simulations. Validation of these results is necessary to investigate the exact impact of process parameters. Effect of these parameters on surface quality couldn't be analyzed using numerical simulation. In the subsequent chapters, surface quality, forming force and formability have been verified by experimental analysis.

CHAPTER 5

ANALYSIS AND MEASUREMNET OF PARAMETRIC DEPENDENCE OF FORMING FORCE

In this chapter forming force has been predicted for single stage forming with and without using the robotic manipulator. Prediction of forces helps to protect the forming tool and sheet metal clamp. Therefore, this chapter mainly focuses on forming force obtained in single stage ISF and RAISF. Effect of sheet inclination and sheet rotation with respect to vertical forming tool on forming force in RAISF has also been discussed. To study the forces, experiments were conducted by forming cone shapes and forming force data was collected using a data acquisition system.

5.1 Forming force in Single stage ISF

Forming force has an impact on fracture and accuracy of the part. Prediction of force helps in protecting the forming tool as well as the material blank. Direct relationship between forming force and stress in the sheet helps in investigating impact of forming force analytically. Stress is the evolution of plastic strain. State of stress and strain in ISF has been discussed below. The contact zone between tool and sheet undergoes normal and shear forces and also bending moment.

5.1.1 Theoretical analysis of forming force

Bending is most relevant till peak force, after the peak stretching mechanics begins. In this stretching zone force trend shows different behavior due to thinning (which reduces force) and material strain hardening (results in force increase). After peak is reached, forming force remains constant because material thinning is compensated by strain hardening and this compensation is more visible when wall angle is small. This constant force is called steady state force (SS). But in some material, after the peak force, the curve shows negative gradient due to large thinning in former stage or due to lower scallop height. In SPIF, if step depth is very less, tool forms same portion of the sheet several times. So material thinning happens due to override of the tool on the sheet. In low strength materials, after some depth, equilibrium between thinning and hardening is achieved from which a steady state force can be measured. This type of curves is called polynomial curves (PC).

Due to certain process parameters, material thinning dominates strain hardening. In this case strain hardening can’t be able to compensate material thinning for equilibrium

condition. Force decreases monotonically which results in material failure. These curves are called monotonically decreasing curves (MD).

Forming force in ISF can be mainly divided into three types, tangential force(F_t),radial force(F_r) and axial forming force(F_z).But dynamometer attached to manipulator can measure forming force in three linear directions(F_x, F_y, F_z). F_t and F_r can be calculated from linear forces as mentioned below[50]. Direction of forces has been shown in Figure 5.1.

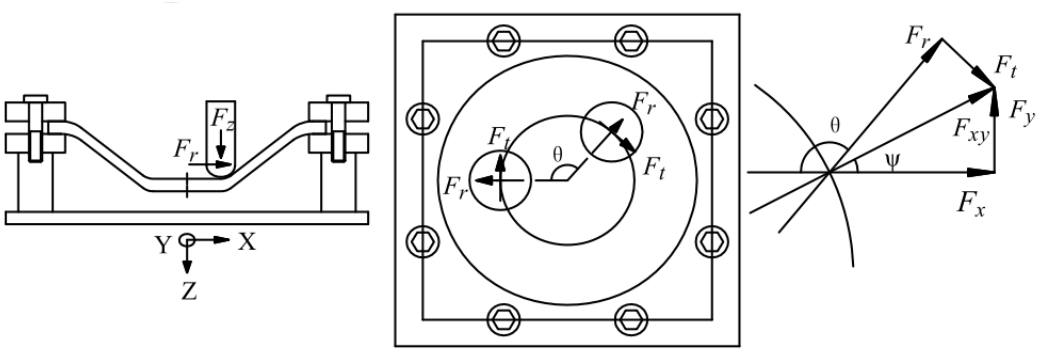

Figure 5.1.Direction of forces

$$F_{xy} = \sqrt{F_x{}^2 + F_y{}^2} \tag{5.1}$$

$$F_r = -\text{sign}(F_x)F_{xy} \times \cos(\pi - \theta - \varphi) \tag{5.2}$$

$$F_t = \text{sign}(F_x)F_{xy} \times \sin(\pi - \theta - \varphi) \tag{5.3}$$

where θ is the moving path angle of the tool and ψ the angle between F_x and F_y. The magnitude of F_x and F_y are smaller as compared to vertical force and impact on sheet is also very small. So here in this process only vertical force which is dominant has been considered. Axial component of the force F_z reaches a peak value at the step down and finally reaches a stable value. But F_x and F_y follows a sinusoidal trend and magnitude of these forces are very small as compared to F_z. In this process, change in magnitude of axial force is small due to continuous contact between tool and sheet. Steady state forming force can be predicted using tensile strength of a material [36], [38]. Tangential force can also be predicted by theory of energy method [34]. Strain components with minimum dissipated power are the best approximation for actual deformation. To analyze the deformation process, side and top view of deformed surface has been shown in Figure 5.2. Total dissipated power can be calculated

using combination of shear, bending and stretching on the curved surface. Tangential force and information about deformed zone can be calculated using calculated dissipated power. Dissipated power has been calculated in zones affected due to shear, bending zone with stretching zone. Tangential force was calculated from dissipated power.

Tangential force due to shear is expressed as follows

$$F_{Shear} = \frac{r_i w_{shear}}{f(r_i + r_o)/2} \quad \textbf{(5.4)}$$

where

r_i = tool path radius

r_o = outer radius of the deformed zone

w_{shear} = Total dissipated power due to shear

Tangential force due to bending with stretching is expressed as follows

$$F_{bs} = \frac{r_i w_{bs}}{f(r_i + r_o)/2} \quad \textbf{(5.5)}$$

However, in theoretical analysis force due to friction has not been considered. Therefore, numerical analysis and experimental validation is necessary for force prediction.

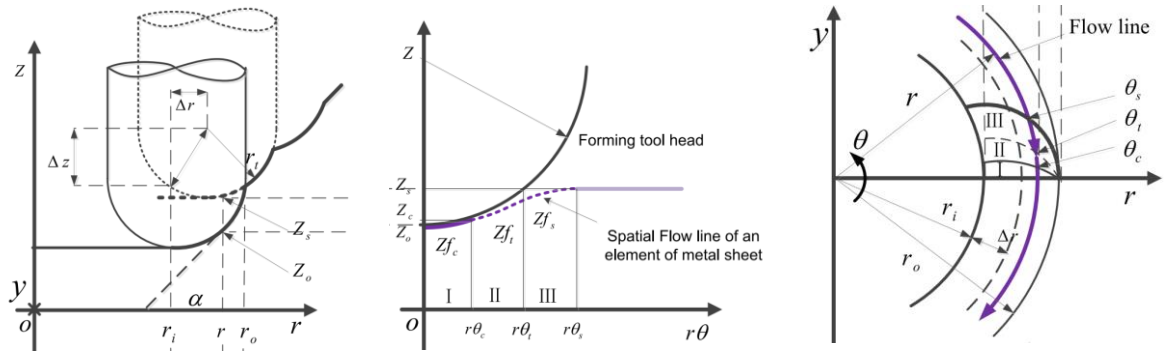

Figure 5.2. Deformation zone in cone forming process [34]

5.1.2 Experimental setup

The FE model was validated by conducting experiment on 3 axis CNC milling machine. Three forces F_x, F_y, F_z were measured using a table mount dynamometer on the FANUC three-axis vertical CNC milling machine as shown in Figure 5.3. A hemispherical forming tool of 15mm diameter has been attached to CNC milling machine. Data acquisitioning system includes a table mount dynamometer, an amplifier and an analogue to digital converter. Output of the amplifier is connected to input of analogue to digital converter.

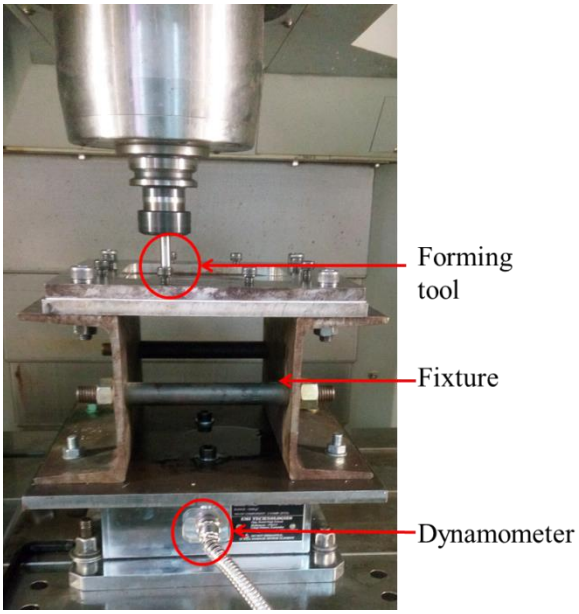

Figure 5.3.Dynamometer and fixture

As F_x and F_y are very small as compared to F_z, these two forces are neglected in this research. Peak value and steady state value of F_z have been measured in these experiments. Initially when tool pushes the sheet in downward direction, elastic deformation is more than plastic deformation which results in low force on the tool. But as the tool passes to consecutive stages, sheet undergoes plastic deformation and elastic deformation reduces which lead to higher force on the tool. This increase in force is called peak force. But after some pass, stiffness of the part doesn't increase more which leads to steady state force.

5.2 Forming force in RASIF

Material deformation mode in ISF is nearly under plane strain condition because the material largely deforms along meridional direction and circumferential strain is negligible. Previously researchers investigated strain and concluded that strain in tangential direction is smaller as compared to strain in radial direction [97] and tangential strain was found to be nearly zero [83]. Circumferential strain was very small which can be neglected [98]. This is true for high wall angle curvature but when circumferential curvature increases strain in circumferential direction also increases [99]. Increase in through thickness shear, normal and through thickness strain enhances the forming limit in plane strain condition and advances the formability [100].

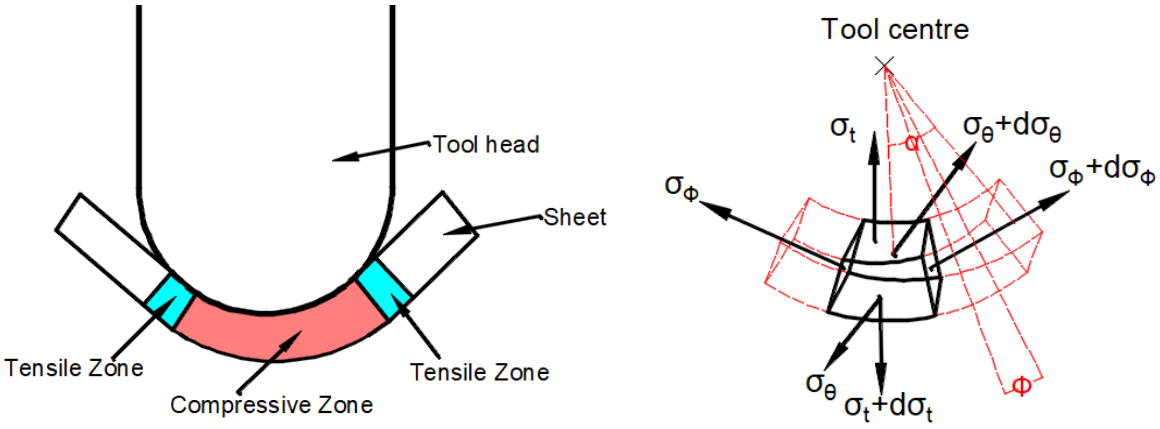

(a) (b)

Figure 5.4 (a) Contact zone in ISF (b) Deformation zone in RAISF

In robot assisted incremental sheet metal forming (RAISF), compressive zone deformation behavior is same as ISF. But deformation behavior in tensile zone will change due to part inclination. In the present analysis, material anisotropic effect is ignored. Figure 5.4 shows the deformation zone in RAISF. Sheet thinning as per sine law can be expressed as

$$t = t_0 \cos(\alpha) \tag{5.6}$$

where t_0 is initial thickness of the sheet, t is final thickness of the sheet and α is wall angle of the formed cup.

By considering volume constant condition

$$\varepsilon_\theta + \varepsilon_\phi + \varepsilon_t = 0$$

Where ε_θ is the tangential strain, ε_Φ is the meridional strain and ε_t is the thickness strain.

Considering plain strain condition,

$$\varepsilon_\theta = 0$$

$$\varepsilon_\phi + \varepsilon_t = 0$$

$$\varepsilon_\phi = -\varepsilon_t = -\ln(\cos(\alpha)) \tag{5.7}$$

In tensile region, there is no direct contact between tool and sheet, so there is no normal contact stress in this region. In this region, stretching of sheet happens in meridional direction. Therefore, stress can be described as

$$\sigma = \frac{1}{\sqrt{2}}\sqrt{(\sigma_\phi - \sigma_\theta)^2 + (\sigma_\phi - \sigma_t)^2 + (\sigma_\theta - \sigma_t)^2} = \frac{\sqrt{3}}{2}\sigma_\phi \tag{5.8}$$

where σ_Φ is the meridional tensile stress, σ_θ is the tangential stress and σ_t is the stress in thickness direction. σ is equivalent stress.

As per power hardening law

$$\sigma = k\varepsilon^n \tag{5.9}$$

where k is strength coefficient and n is strain hardening exponent.

Under plane strain condition

$$\varepsilon = \sqrt{\frac{2}{3}(\varepsilon_t{}^2 + \varepsilon_\theta{}^2 + \varepsilon_\phi{}^2)} = \frac{2}{\sqrt{3}}\varepsilon_\phi \tag{5.10}$$

Combining equation (5.9) and (5.10)

$$\sigma = k\left(\frac{2}{\sqrt{3}}\varepsilon_\phi\right)^n \tag{5.11}$$

Putting equation (5.7) in (5.11)

$$\sigma = k\left(-\frac{2}{\sqrt{3}}\ln(\cos(\alpha))\right)^n \tag{5.12}$$

The stretching force at tensile region can be obtained as follows

$$F = \sigma \times A = k\left(-\frac{2}{\sqrt{3}}\ln(\cos(\alpha))\right)^n t_0 r_{tool}\phi \tag{5.13}$$

From equation (5.13) it can be observed that with increase in wall angle, force along the wall increases, but by inclination the part, value of α (angle between wall and horizontal axis) will reduce. By reducing α, force along the wall will reduce which will lead to lesser thinning of the sheet.

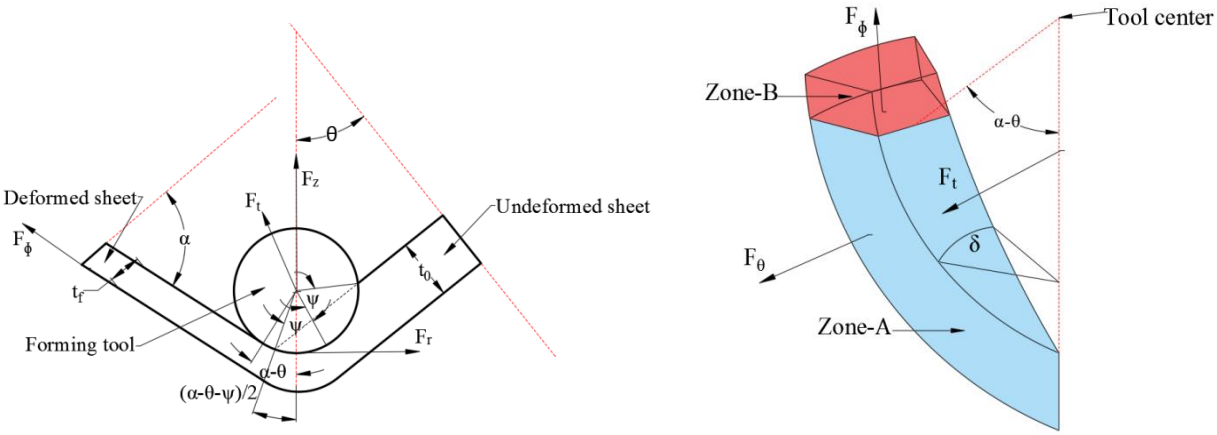

Figure 5.5.Schematic representation of the detailed view of RAISF

Study of forming forces in ISF provides insights into deformation mechanics. It is difficult to form steeper wall angle parts in single stage incremental sheet metal forming (SSIF). From literature survey, it is learnt that deformation variation changes due to induced forming forces by tool on the sheet. Forming force in Z-direction (Vertical direction) is higher in single stage forming and Z-force is responsible for straining in the sheet in meridional direction. Inclination of sheet has also influence on forming force. Surface inclination has influence on cutting forces. With increase in surface inclination, cutting force decreases and surface inclination between 0° to 15° has more influence on force [101], [102]. In Figure 5.5, Zone-A is the contact area between tool and sheet while Zone-B represents the neighboring area of the formed zone. Deformation occurs at the tool contact zone (Zone-A) and non-contact zone (Zone-B) of the sheet and mainly occurs in meridional direction. Fracture occurs at the outer side of the wall in the transition area between contact and non-contact area [103]. Force in tangential, circumferential and radial direction for ISF without inclination was predicted and experimentally validated[104]. Same force model has been used to predict all three forces for inclined sheet in this work. Assuming F_t is acting at the mid of the tool contact length, vertical Z force can be expressed as follows

$$F_z = f(F_\phi, F_\theta, F_t)$$

$$F_z = F_\phi \cdot \sin(\alpha - \theta) + F_\theta \cdot \sin\psi + F_t \cdot \cos\left(\frac{\alpha - \theta - \psi}{2}\right) \tag{5.14}$$

Shear deformation can be neglected compared to bending and stretching [105], [106], therefore value of F_θ is assumed to be equal in circumferential direction. To analyze the

effect of bending and stretching component of the force due to inclination of the part, F_Φ and F_t can be expressed as follows.

From Figure 5.5 Equilibrium equation in meridional direction for ISF can be expressed as[33]

$$F_\phi = F_t \sin\left(\frac{\alpha}{2}\right) + 2F_\theta \cdot \sin\frac{\delta}{2} \cdot \cos(\alpha) \tag{5.15}$$

Similarly force equilibrium equation in circumferential direction can be expressed as

$$F_t \cos\frac{\alpha}{2} = 2F_\theta \cdot \sin\frac{\delta}{2} \cdot \sin\alpha \tag{5.16}$$

Combining above two equations

$$F_\phi = F_t \cdot \left(\sin\frac{\alpha}{2} + \frac{\cos\alpha \cdot \cos\frac{\alpha}{2}}{\sin\alpha} \right) \tag{5.17}$$

But when the sheet is inclined at θ° inclination angle equation (5.17) can be expressed as

$$F_\phi = F_t \cdot \left(\sin\left(\frac{\alpha-\theta}{2}\right) + \frac{\cos(\alpha-\theta) \cdot \cos\left(\frac{\alpha-\theta}{2}\right)}{\sin(\alpha-\theta)} \right) \tag{5.18}$$

From equation (5.17) and (5.18), it can be observed that force component in meridional direction is less in tilted sheet as compared to fixed sheet. Lesser force in meridional direction will delay the peak force and bending component of the force will be higher as compared to fixed ISF. The developed analytical model gives a correlation between forming force, wall angle and inclination angle. However due to friction between tool and sheet, forming force will vary. Reducing friction resistance helps in improving formability, surface quality and reduced forming load.[105]. Numerical simulation for RAISF has been the part of the forming force and formability analysis which includes the friction coefficient between tool and sheet.

5.3 Numerical simulation for forming force

As ISF process involves localized plastic deformation, high nonlinearity should be considered in simulation. LS-DYNA v971 explicit dynamic module is capable of simulating highly nonlinear problems and solves dynamic problem using explicit time integration. To

check the evolution of the forming force and to compare them with experimental work, with same working condition as experiments LS-DYNA was adopted for numerical simulation. Blank and tool were modeled as shell element of type 2. Element edge of 1mm was used in fine meshing of blank. Al-1100 sheet of 200×200×1.2 mm was selected as blank material and modeled using power law plasticity (MAT18 in LS-DYNA). Material was considered to be isotropic as difference in stress-strain behavior in three directions (rolling, diagonal and transverse) is small. Therefore, material was modeled using swift's isotropic strain hardening law. Tool of diameter 15mm was modeled as rigid body (MAT20). Forming one way surface to surface model was used to define contact pair between tool and blank. Due to application of sufficient lubricating oil, friction coefficient of 0.01 was used for simulation. To avoid convergence problem between tool element and sheet element, tool elements were bigger than sheet element. Due to longer tool path, to reduce computational time, mass scaling and time scaling technique were used. Mass scaling and time scaling parameters were chosen such that kinetic energy will be very less compared to internal energy which in turn reduces dynamic effect keeping process as quasi-static. For accurate result adaptive meshing technique was adopted in simulation. Following process parameters have been considered for simulation.

Table 5.1.RAISF Process parameters

Parameter	Value
Wall angle (°)	75, 80
Inclination angle (°)	15, 20
Sheet rotational velocity (RPM)	6, 7, 8
Step depth (mm)	0.5

Baking plate hole was of 100mm diameter. So in finite element simulation (FEM) all nodes except 100mm diameter area were fixed in all direction. Most of the simulation in literature has been performed using simplified tool path rather than actual tool path. But here in this work, tool path was given as displacement verses time in three directions. Using CAD model of the desired part in CAM software, tool path was generated. X, Y, Z coordinate of the tool path was imported from CAM file and converted to position verses time coordinates. These coordinates were given as input directly to FEM simulation in order to get result similar to experiment. As we are using actual tool path data, the length of the tool path is very long for simulation. Incremental forming is regarded as quasi-static process. So to shorten the time, tool velocity was artificially increased. Mass scaling was also done to reduce computational time. Adaptive meshing technique was used to get accurate results. In this

analysis following three assumptions were made. (i) Material was assumed to be homogeneous and isotropic, (ii) Except Deformation zone, material is rigid, (iii) frictionless interface. Simulation was carried out to predict forming force in ISF and RAISF.

The influence of each process parameter on forming force is investigated for both ISF and RAISF. Influence of step depth and spindle speed has been discussed in literature so these two parameters were kept constant. Though influence of wall angle on forming force was already investigated in literature but to compare forming force results of RAISF and ISF, wall angle was also considered as a testing process parameter. In RAISF simulations, mainly influence of inclination angle, sheet rotational velocity and wall angle was investigated but for ISF only as inclination angle is 0°, keeping all other parameters constant, effect of wall angle on forming force was checked.

5.4 Results and discussion

Forming of the steeper wall angle part is the main focus in this research work. Forming force for steeper wall angle part has been numerically and experimentally measured. Table 5.2 shows the forming force obtained in ISF experiments as well as in simulation for 75° and 80° wall angle conical parts. The F_{z_p} is the peak force and the F_{z_s} is the steady-state force. This shows that as the forming angle increases the peak force as well as steady state forces increases. Numerical force values have been compared with the experimental forming forces. Peak force variation error in simulation and experiments is more as can be observed in the table. However steady state force is seen to be closer to the experimental value with less error. The forming forces at different inclination angle and rotational speed has been measured and compared with the ISF results. Effect of inclination and sheet rotation on forming force in RAISF has been discussed below.

Table 5.2.Simulated and experimental peak force and steady state force value in ISF

α (deg)	F_{z_p} (Simulation)	F_{z_p} (experiment)	Error (%)	F_{z_s} (Simulation)	F_{z_s} (experiment)	Error (%)
75	960.79 N	1305.94N	26.42	784.26N	798.654N	1.72
80	1226.12 N	1436.397N	14.6	984N	1002.03N	1.82

5.4.1 Influence of part rotation

Influence of sheet rotation on forming force, forming depth and strain distribution has been discussed in this section. Experiments as well as numerical simulation are carried out by varying the sheet rotation speed from 4RPM to 6RPM. At inclination angle of 15°, parts of wall angle of 75° and 80° parts have been investigated.

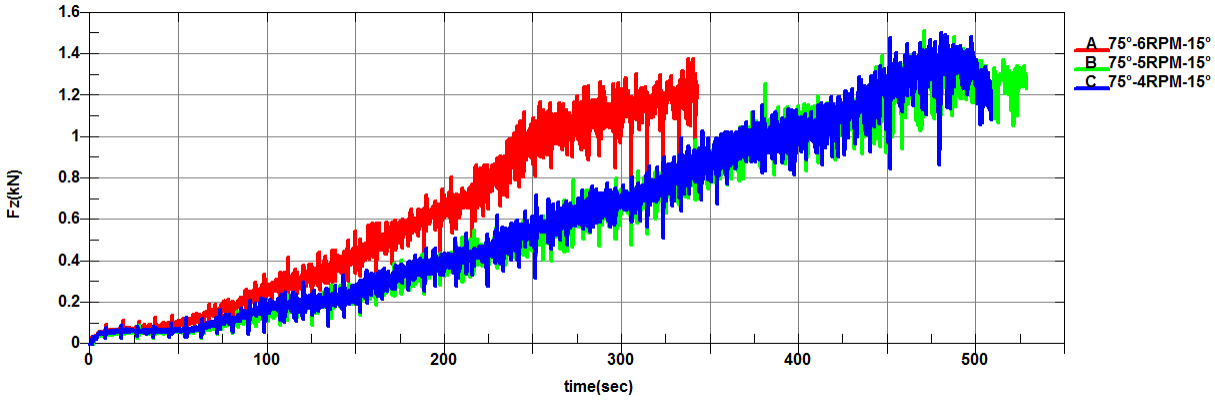

(a)

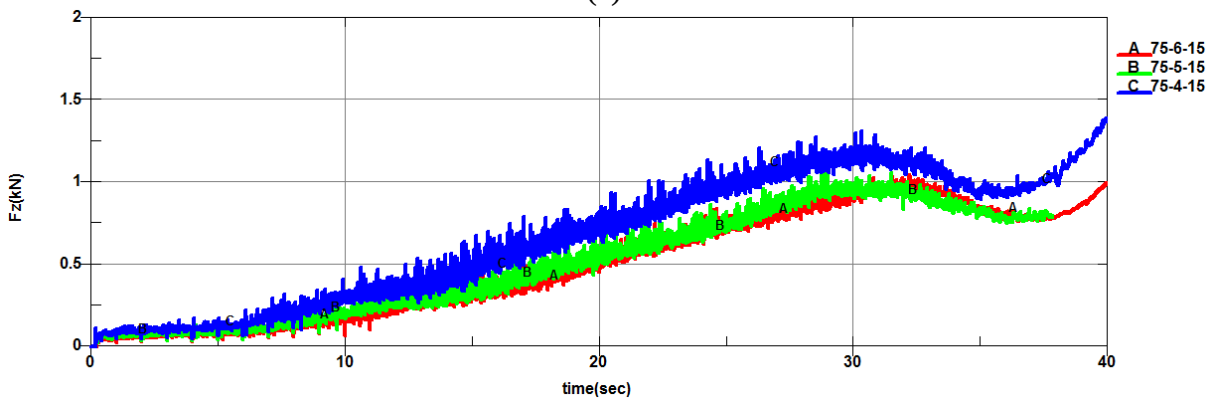

(b)

Figure 5.6 Forming force variation with increasing workpiece rotational speed, (a) experimental and (b) FEM simulation

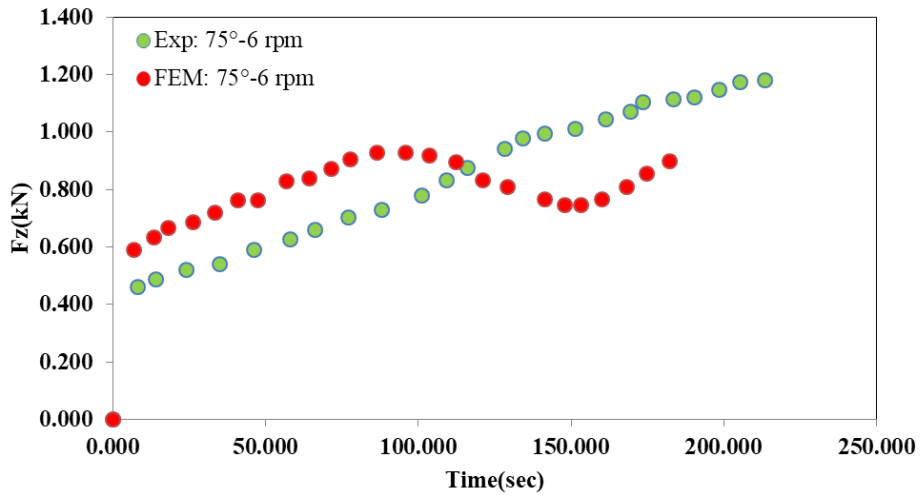

(a)

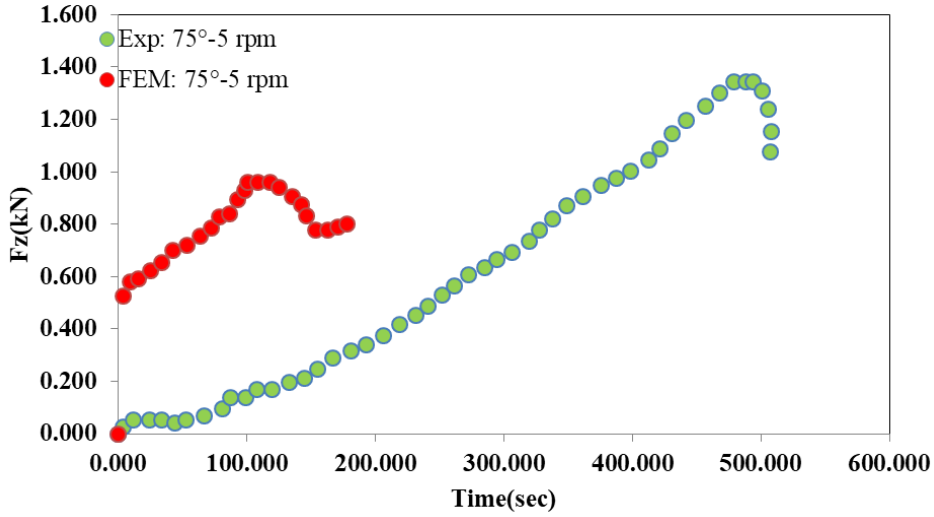

(b)

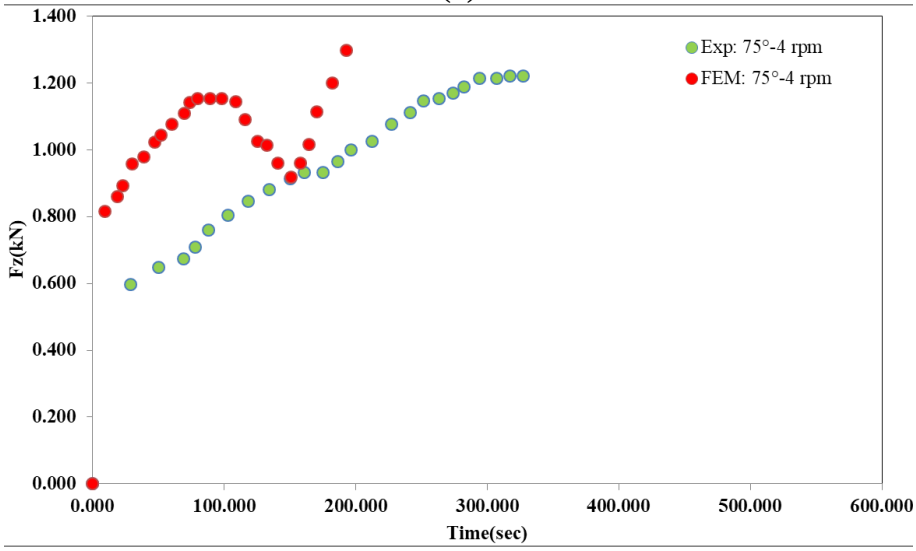

(c)

Figure 5.7 Comparison of experimental and FEM simulation results for forming force at 75° wall angle and at different workpiece rotational speeds, (a) 6 rpm (b) 5 rpm (c) 4 rpm

In Figure 5.6 and Figure 5.7, forming force has been plotted at specific wall angle-sheet rotational speed-Inclination angle. Figure 5.6(a) shows parts with wall angle of 75° formed at titling angle of 15° and this shows increase in rotational speed doesn't affect the peak force however at lower rotational speed F_z is higher. Due to time scaling, the range of time is smaller as compared to experimental time in Figure 5.6 (b) but the trend in both simulation and experiment are similar. Figure 5.7 shows the comparison of experimental and simulation plot without mass scaling and it reveals that the difference in peak force in the plots attributed to the friction conditions between the tool and work piece which can exactly be estimated from the experimental results. Similarly for 80° wall angle parts at 15° inclination angle, Figure 5.8 shows with increase in sheet rotational speed, stretching force has been delayed and peak force increases. Figure 5.9 shows the comparison of FEM and experimental results without time scaling.

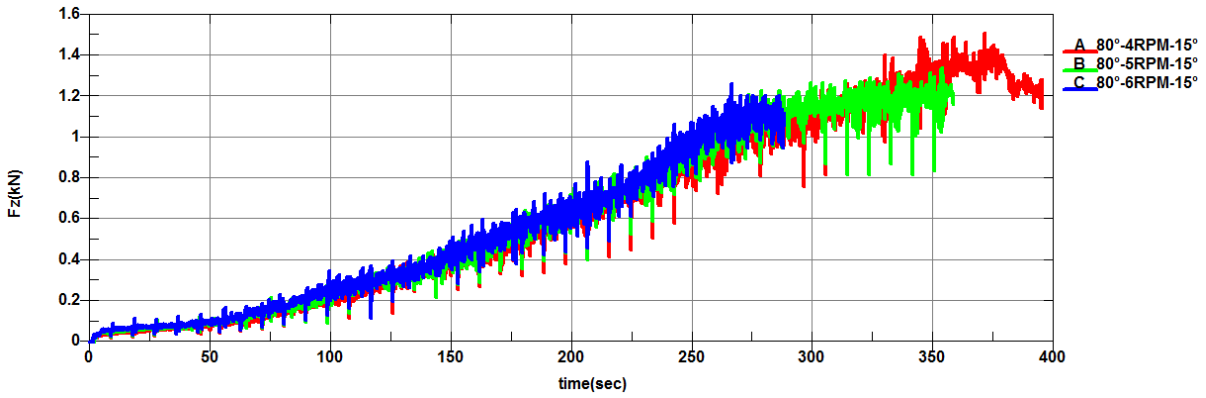

(a)

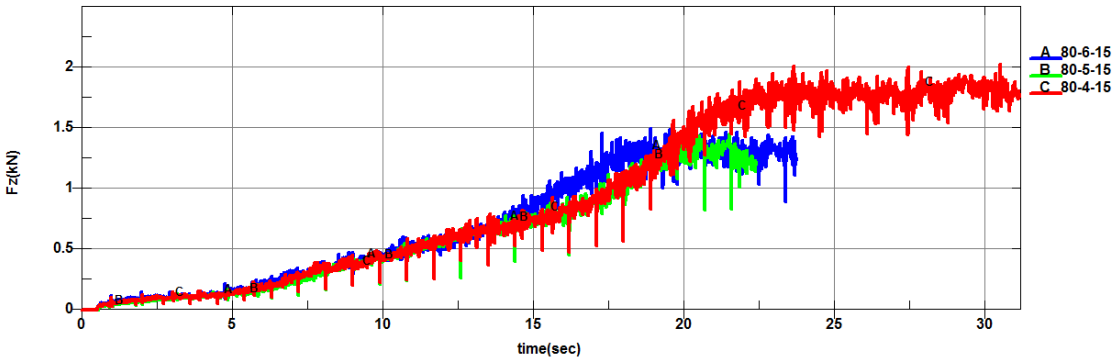

(b)

Figure 5.8 Forming force variation with increasing workpiece rotational speed, (a) experimental and (b) FEM simulation

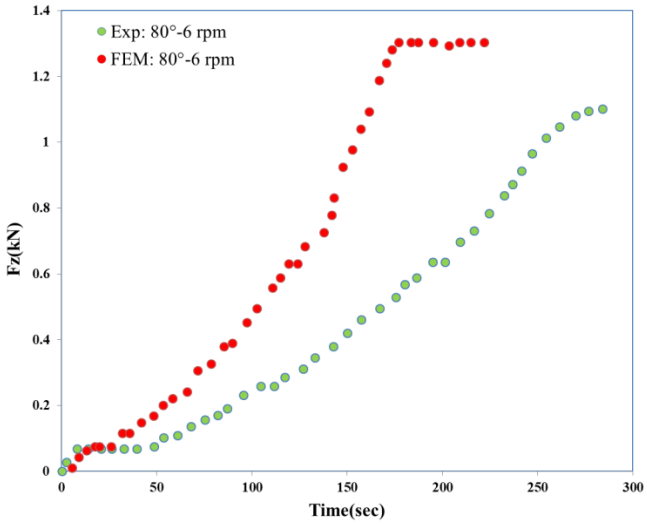

(a)

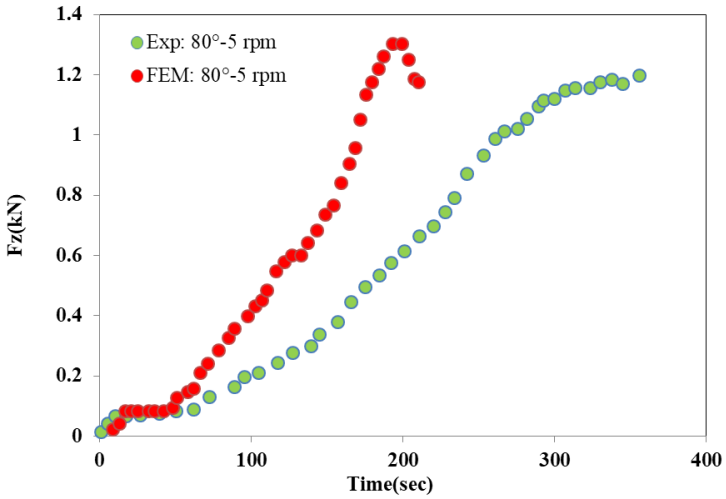

(b)

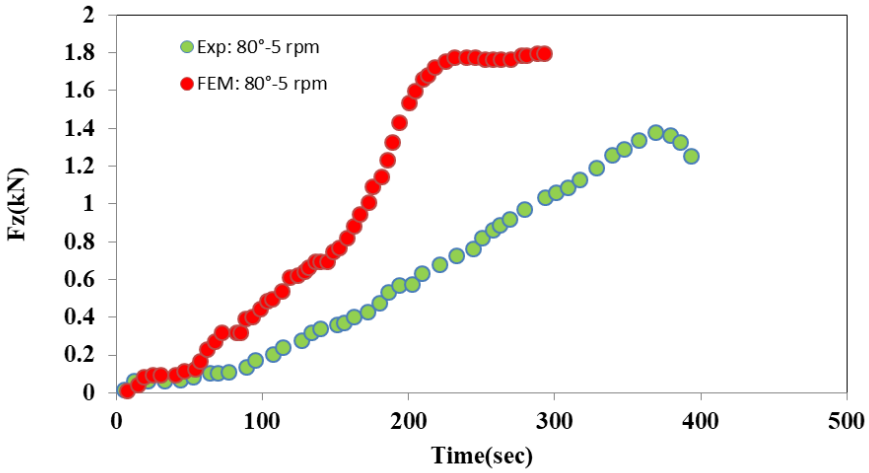

(c)

Figure 5.9 Comparison of experimental and FEM simulation results for forming force at 80° wall angle and at different workpiece rotational speeds, (a) 6 rpm (b) 5 rpm (c) 4 rpm

5.4.2 Influence of inclination angle

Effect of inclination on forming force has been examined for steeper wall angle parts keeping other process parameters constant. It can be observed in Figure 5.10(a,b) that stretching of the sheet can be delayed by inclining the sheet. However peak force increases as the sheet inclination angle increases. Though the behavior of the sheet for 75° and 80° wall angle was similar at fixed base and 15° inclination angle Figure 5.10(a) and Figure 5.12(a), but for 75° wall angle at 20° inclination angle peak force was observed way later than 80° wall angle at same inclination base. By delaying stretching component of the force, formability of the sheet was increased. Figure 5.11 and Figure 5.13 shows the comparison of the forming force without time scaling and it reveals that experimental peak forming force was nearly same as predicted force in FEM analysis. However, the delay in FEM forming force was observed than experimental results.

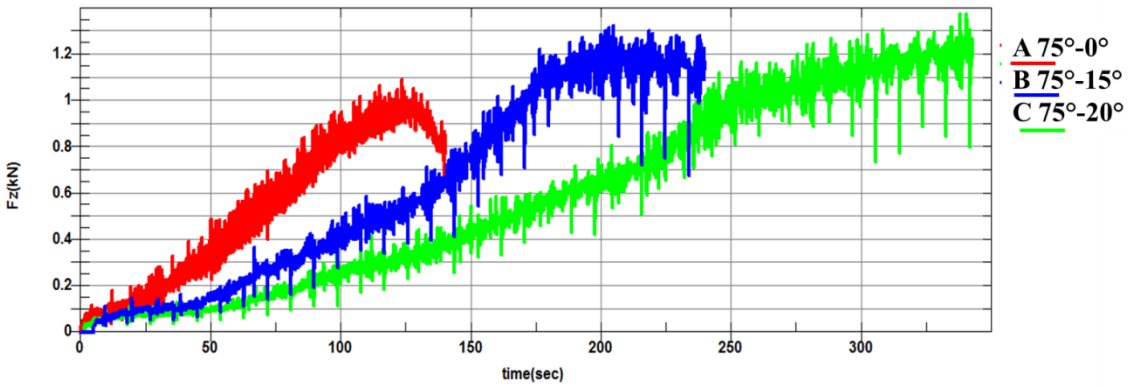

(a)

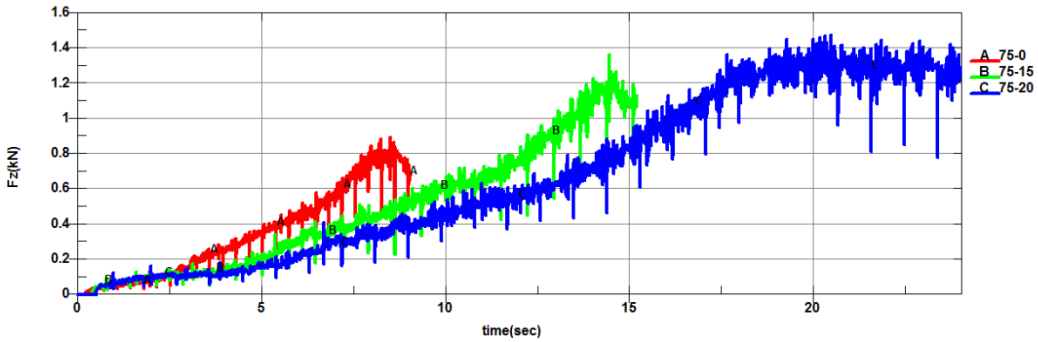

(b)

Figure 5.10 Forming force variation with increasing workpiece inclination angle for 75°, (a) experimental and (b) FEM simulation

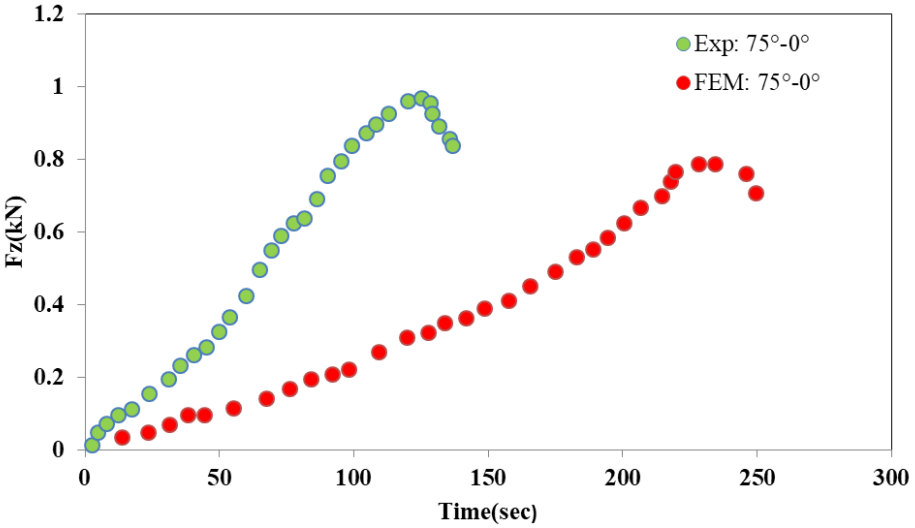

(a)

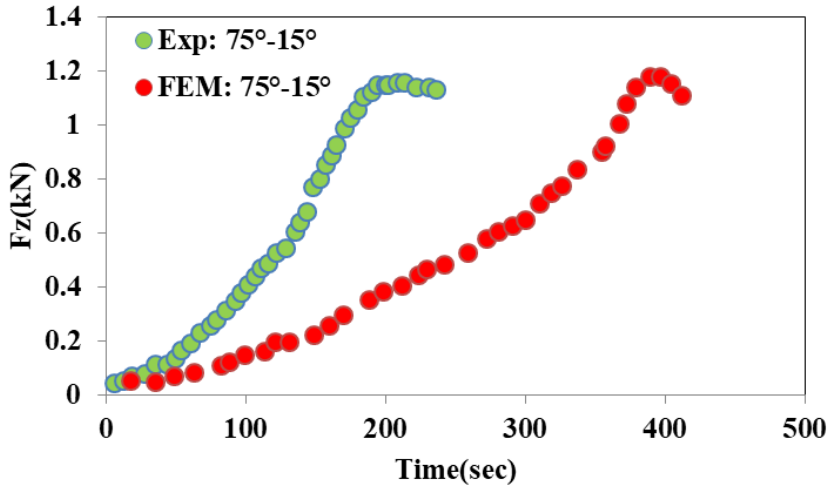

(b)

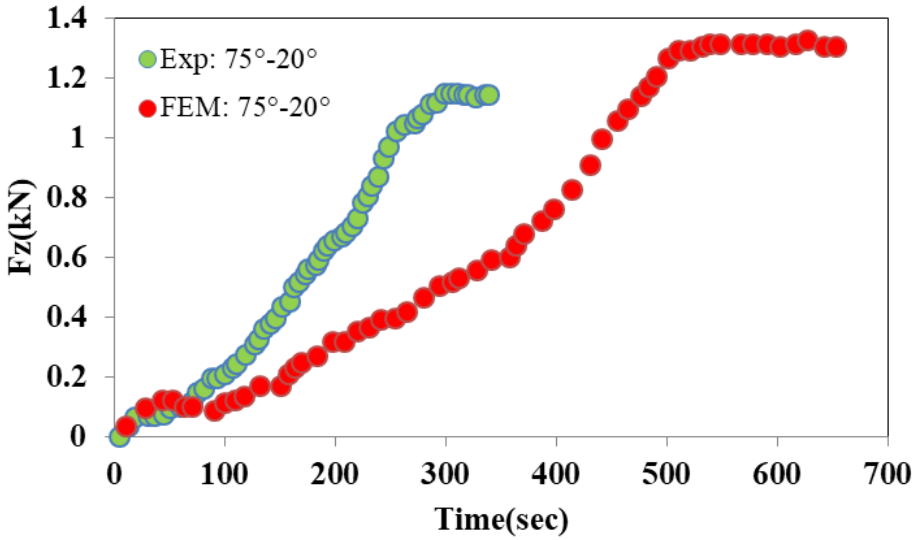

(c)

Figure 5.11 Comparison of experimental and FEM simulation results for forming force at 75° wall angle and at different workpiece rotational speeds, (a) 0° (b) 15° (c) 20°

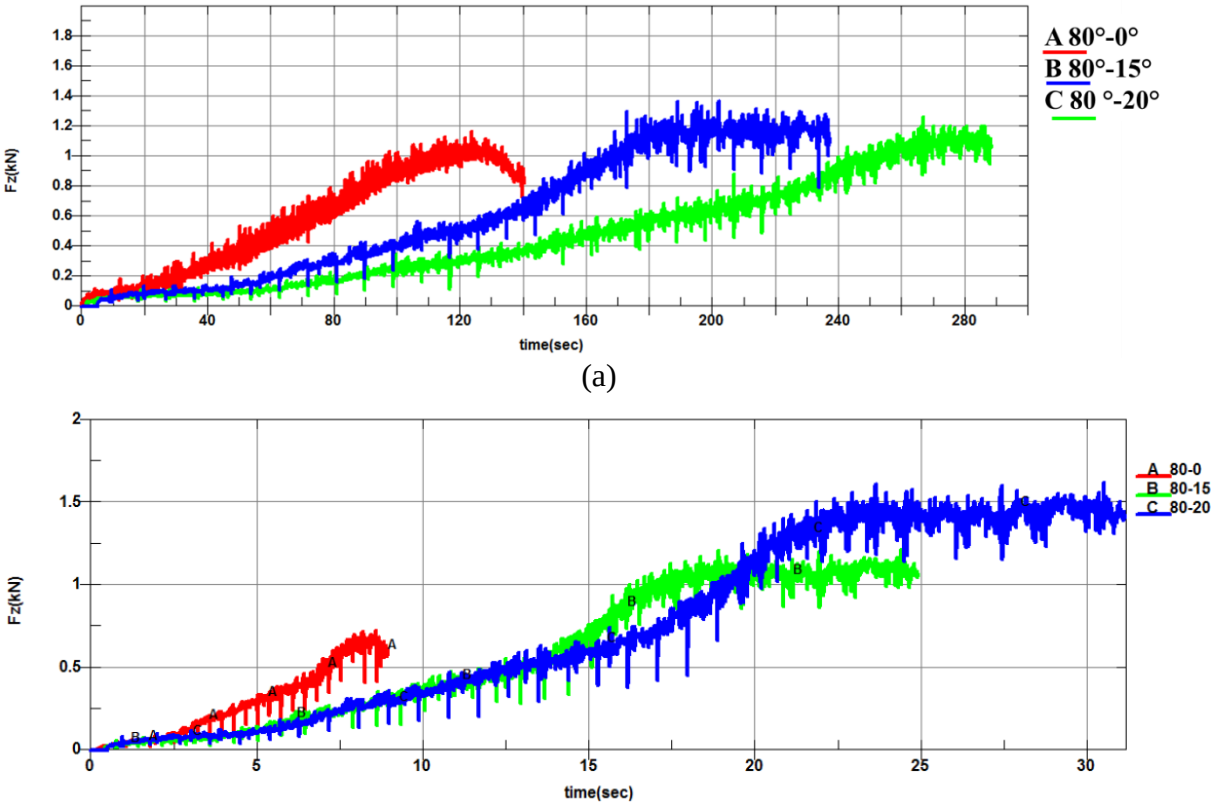

(a)

(b)

Figure 5.12 Forming force variation with increasing workpiece inclination angle for 80°, (a) experimental and (b) FEM simulation

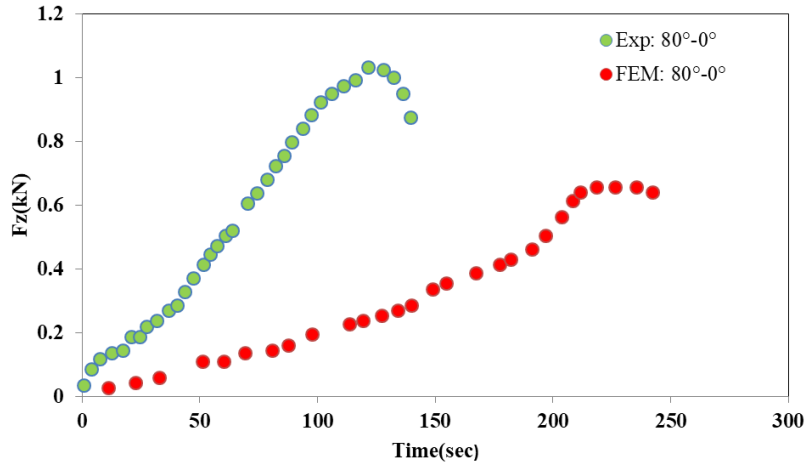

(a)

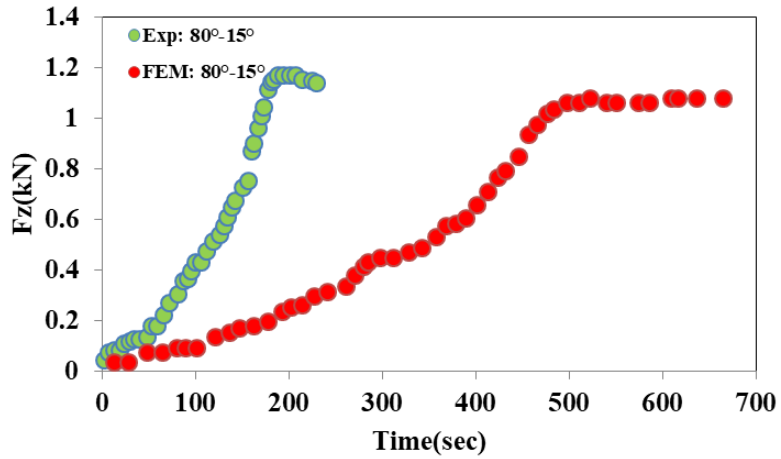

(b)

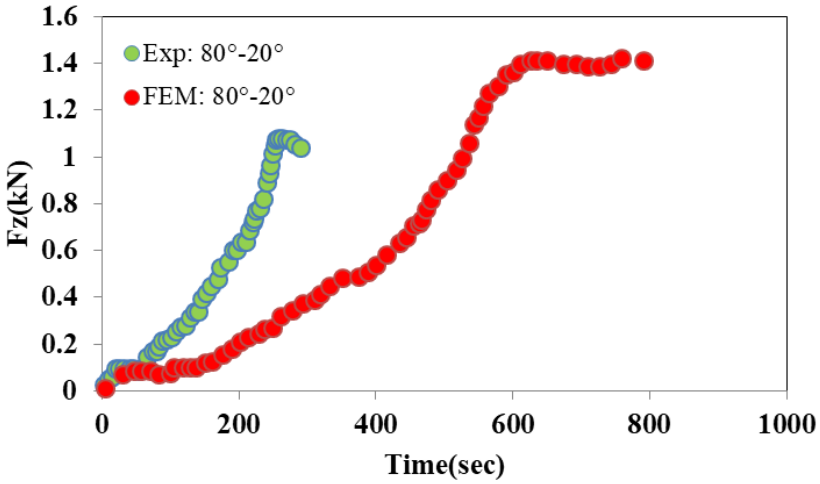

(c)

Figure 5.13 Comparison of experimental and FEM simulation results for forming force at 80° wall angle and at different workpiece rotational speeds, (a) 0° (b) 15° (c) 20°

5.5 Summary

In the present work, a new technology has been added to the existing ISF process to form the steeper wall angle parts in single stage. An additional two DOF manipulator has

been added to the vertical CNC milling machine to improve the formability as well as process flexibility. Effect of additional process parameters has been analyzed to investigate the forming force, at steeper wall angle. Inclination of the part, rotation of the part are the main parameters considered in the analysis.

Forming force in ISF process can be divided in to three stages, stretching, bending and shearing. However shearing effect has been ignored in this analysis. By inclining the sheet, net wall angle between tool vertical axis and sheet horizontal axis could be reduced. From analytical solution it was observed that by increasing the inclination angle, meridional force decreases. Stretching component of force could be delayed and bending became slower which can be observed in numerical simulation. However peak force has been increased by increasing inclination angle. Due to faster bending in ISF, steeper part fails on fixed base. By increasing inclination angle, relative wall angle could be reduced with respect to tool. With increases in inclination angle due to reduced stretching force along slanted wall of the formed cup, fracture depth was higher than zero inclination angles. At constant inclination angle and part rotation, when wall angle of the part was increases, fracture limit was reduced.

The numerical analysis also shows the effect of sheet rotational velocity on forming force. It reveals that increase in rotational velocity will not have major effect on peak forming force. Peak force increases as the sheet rotational velocity increases but by lesser amount. However, bending force will be slower as the sheet rotation increases. Forming force has major impact on formability of the sheet. Due to inclination and rotation of the sheet, forming force changes. This variation in forming force may change the formability of the sheet. This has been discussed in the subsequent chapter.

CHAPTER 6

EXPERIMENTAL STUDY OF SURFACE ROUGHNESS

In this chapter the effect of process parameters on surface roughness in RAISF has been discussed. In RAISF, sheet has been inclined and rotated with respect to vertical tool. Therefore, along with existing process parameters, effect of inclination angle and rotational velocity has also been investigated in this chapter. ISF experiments are also conducted to compare the results with RAISF experiments. The main aim of this process is to minimize surface roughness and to maximize the formability by incorporating proper combination of process parameters.

6.1 ISF surface roughness

The surface finish in single stage incremental forming is affected by various process parameters. To achieve certain surface quality, effect of process parameters should be known. The other parameter in ISF is long forming time. Therefore the objective of this section is to understand the effect of various process parameters on surface quality as well as forming time. For this analysis, experiments were conducted. Design of experiments was carried out using L9 orthogonal array method. These nine experiments were conducted on a CNC vertical milling machine. The results were analysed using ANOVA and response surface method to obtain optimum process parameter settings.

6.1.1 Theoretical Analysis

6.1.1.1 Tool Path Planning

The tool path planning for conical spiral of the work piece for a given wall angle α was derived as follows:

$$0 \leq u \leq 1 \begin{cases} z = \Delta z[i-1+u] \\ x = (R - z\cot\alpha)\cos 2\pi u \\ y = (R - z\cot\alpha)\sin 2\pi u \end{cases} \quad (6.1)$$

6.1.1.2 Scallop Height

The dependence of the scallop height, h, on the process parameters of tool radius (r_t), step depth (z) and the wall angle (α) is given by the equation (6.2) as per the configuration given in Figure 6.1.

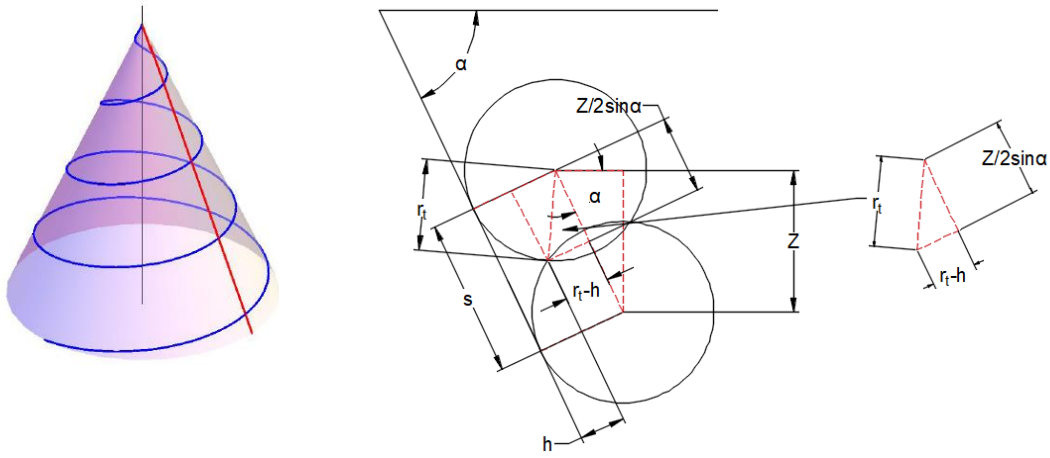

(a) (b)

Figure 6.1.(a) The spiral tool path for the conical cup part, (b) the scallop height

From Figure 6.1, relation between tool radius, scallop, and step depth and wall angle can be expresses as

$$r_t^2 = (r_t - h)^2 + \left(\frac{z}{2 \cdot \sin\alpha}\right)^2$$

$$h = r_t - \sqrt{r_t^2 - \left(\frac{z}{(2 \times \sin\alpha)}\right)^2} \qquad (6.2)$$

where h is scallop height, r_t is tool radius, z is step depth and α is wall angle.

From equation (6.2), it can be observed that, with increases in step depth, scallop height increases but with increase in wall angle, scallop height decreases if step depth is constant. But increase in step depth, reduces overall forming time. Similarly, if step depth has to be maintained constant throughout the sheet, scallop height will decrease with increase in wall angle. Decrease in scallop height, will increase surface quality.

Similarly increment in step depth will increase the undeformed area on the formed sheet but will reduce the overall forming time. Feed rate will vary surface quality along the tool path contour but will not affect roughness value along the wall if other process parameters are constant. From Figure 6.1(b), relation between step depth, tool centre distance and wall angle can be represented as follows.

$$z = s \times \sin\alpha \qquad (6.3)$$

where s is distance between centres of the tool in two consecutive passes.

Combining equation (6.2) and (6.3), scallop height can be represented as follows.

$$h = r_t - \sqrt{r_t^2 - \left(\frac{s}{2}\right)^2} \tag{6.4}$$

In the above relation, it can be observed that,

$$h_{(s<r_t)} < h_{(s=r_t)} < h_{(s>r_t)}$$

With increase in distance between the tools, step depth increases which in result increases scallop height. Increases in scallop height leads to reduced surface finish.

Increment of feed rate will not affect the surface roughness in vertical direction but forming time can be greatly reduced by increasing feed rate due to larger tool travel in shorter time interval. However, combined effect of all the parameters is difficult to analyse theoretically. Therefore, experiments were conducted to verify the combined effect of all parameters on surface quality.

6.1.2 Experimental Setup

Experiments were conducted using Fanuc-I series GX600 three axes vertical CNC milling machine. Al-1100 is a commercially used aluminium sheet which is widely used in chemical, food processing industries, hollowware, and heat exchangers due to its excellent resistance to corrosion. It is also used in applications where intrinsic formability and high corrosion resistance is needed but not high strength. In this work, sheet of 200mm×200mm×1.2mm has been used for experiments. Sheet has been clamped on the fixture with locating pin and baking plate and both are mounted on CNC machine table as shown in Figure 6.2. Larger tools are suitable for SPIF to avoid pillow effect as contact zone between tool and sheet increases [107]. It also helps in improving formability [108]. EN36 hemispherical tool of 15mm diameter has been used for this operation. Tool was heat treated to 60HRC and was polished with fine grade abrasive paper. Forming tool and fixture has been shown in Figure 6.2. Tool and sheet surface friction was reduced by using SAE40 lubricant. Forming angle, step depth and feed rate has been varied in each operation with constant spindle speed of 1300rpm.

Thickness, surface quality and dimensional accuracy can be affected by tool path. So a proper tool path is an essential input in ISF to get desired output. Various tool path generation techniques have been used previously but out of all tool paths, profile tool path and spiral tool path (Helical tool path) have given significant output till date. To reduce uneven scar mark in profile tool path, helical tool path was proposed [109]. Spiral tool path was found to be more effective in strain distribution, Relative thinning, surface quality and

forces [110]. So to investigate surface roughness, spiral tool path was used in this study. 3D model has been generated using Pro E software. Spiral tool path has been generated in the form of G code and M code using CAM software. G-codes and M-codes were directly given as input to CNC machine for experiments.

After Single stage ISF experiments, the surface roughness measurement was done by using Taylor Hobson surface roughness tester shown in Figure 6.2. In this tester a diamond tip stylus moves across the peaks and valleys of the surface and measures roughness. Surface roughness at 4 points along the perpendicular direction to the tool direction on a single sheet has been measured for all the sheets as shown in Figure 6.2. Samples were cut by EDM wire cut machine from each part. For circular geometry, samples were cut from 4 regions located at 90º relative to each other. Four measurements were recorded from each part and average of these four measurements was calculated.

6.1.3 Design of Experiment

Planning and execution of experiments affects result to a great extent. Selection of parameters, no. of experiments also affects the same. In most of the cases full factorial experiments are conducted, but considering time and cost it cannot be implemented when number of input parameters is more. The design of experiment is the one of the effective tools to reduce the number of experiments. It can collect all the statistically significant data with less number of repetitions. This process has been successful for improving the product quality and the process. Taguchi orthogonal array (OA) is one of the widely used design of experiments (DOE) techniques. It helps in selecting the interaction which can influence the quality of the product and based on this it calculates number of experiments. As in this study, the number of influencing parameters is three which is called three-level factors in OA, so as per OA-3^2 experiments were conducted. Forming tool diameter and spindle speed was kept constant throughout the experiment. All the 9 experiments have been conducted using vertical CNC milling machine (specifications shown above). Forming angle, step depth and feed rate were the input in these and value and level of these controlled parameters are shown in Table 6.1. The L9 orthogonal array experimental combinations between all parameters have been shown in the Table 6.2. All the factors have been coded as A, B and C. All the three values for each factor have been coded as 1, 2 and 3. Combination of interaction of all the levels for each factor has been tabulated in Table 6.2.

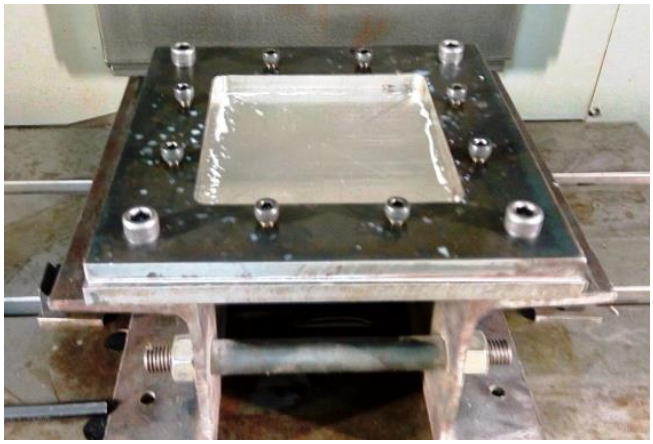

(a)

(b)

(c)

(d)

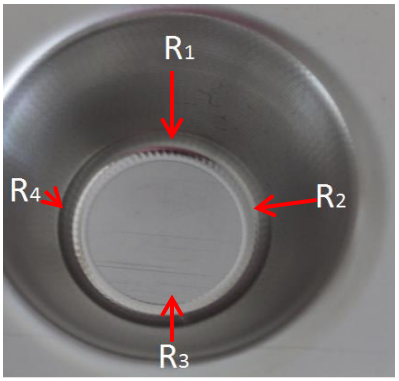

(e)

Figure 6.2.The (a) forming fixture, (b) the experimental setup and (c) forming tool mounted on the 3-axis vertical CNC milling machine used for the experiments, (d) Profilometer (e) direction of surface roughness measurement

Table 6.1.Level of selected control parameters.

			Original values			Coded values		
Factors	Units	Notations	Level-1	Level-2	Level-3	Level-1	Level-2	Level-3
Forming Angle	º (deg)	A	60	65	70	1	2	3
Step depth	mm	B	0.5	1	1.5	1	2	3
Feed rate	mm/min	C	1000	1500	2000	1	2	3

To analyse the result S/N (Signal to Noise) ratio is calculated which shows both average and variation in experimental results. In this study, low forming time and better surface finish are our main objective. So smaller the S/N value better is the result. S/N ratio is given by equation given below.

$$\frac{S}{N} = -10\log\left[\frac{1}{n}\sum_{1}^{n} y_i^{\,2}\right] \tag{6.5}$$

where n is the number of observations per row which is 4 for surface roughness and 1 for time in our study and y_i is the i^{th} measured roughness and time in the row.

Table 6.2. Experimental results (Forming Time).

	A	B	C	Time taken(min)	S/N ratio
1	1	1	1	24.39	-27.74
2	1	2	2	8.59	-18.67
3	1	3	3	4.54	-13.14
4	2	1	2	18.15	-25.17
5	2	2	3	7.27	-17.23
6	2	3	1	9.22	-19.29
7	3	1	3	15.05	-23.55
8	3	2	1	15.21	-23.64
9	3	3	2	7.15	-17.08

The parameter interaction and effect of the same on surface texture was uncertain in Figure 6.4. So to check significance of all parameters, Analysis of variance technique was chosen.

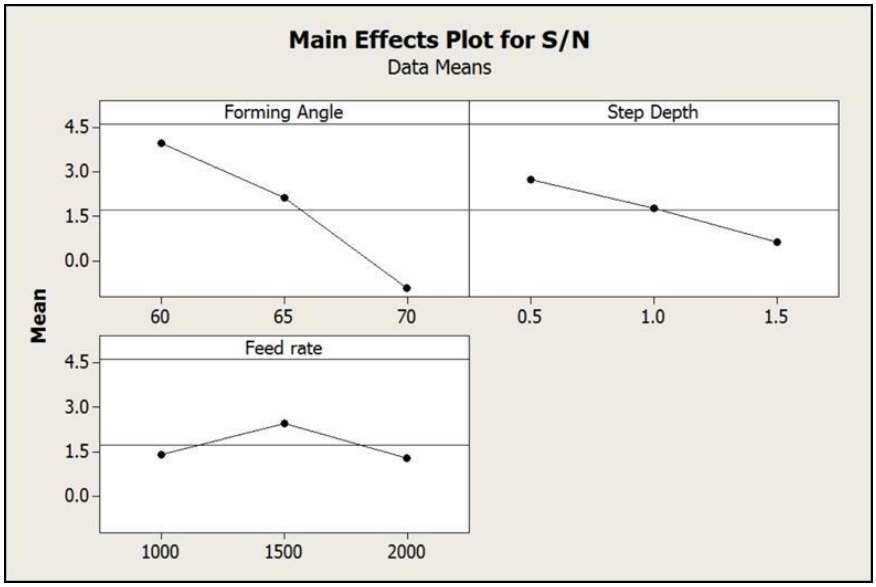

(a)

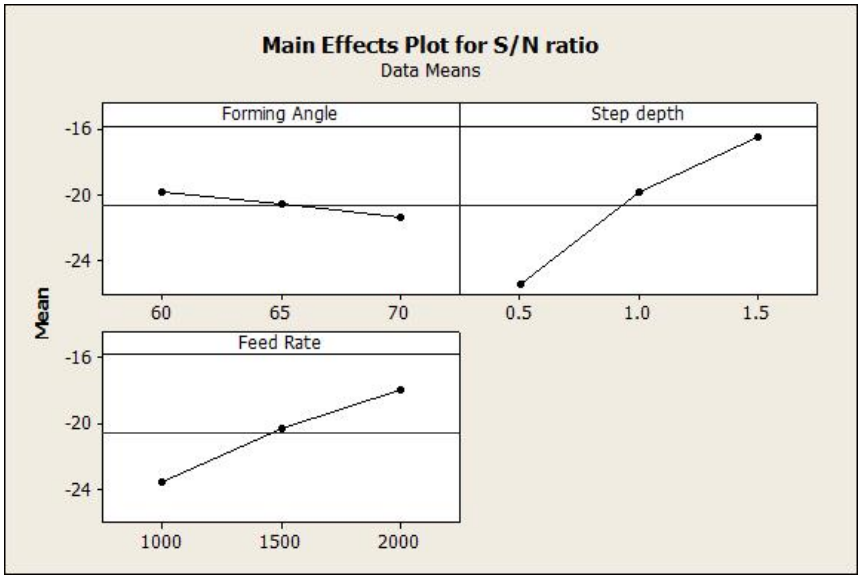

(b)

Figure 6.3.Response graph for (a) Surface roughness and (b) forming time

Table 6.3. Experimental results (Surface roughness).

	A	B	C	R_1(µm)	R_2(µm)	R_3(µm)	R_4(µm)	S/N ratio	Mean
1	1	1	1	0.545	0.544	0.476	0.593	5.334341	0.5395
2	1	2	2	0.543	0.502	0.507	0.656	5.106611	0.552
3	1	3	3	0.889	0.814	0.938	0.733	1.441705	0.8435
4	2	1	2	0.501	0.492	1.06	0.662	2.892674	0.67875
5	2	2	3	0.656	0.669	0.834	0.851	2.407754	0.7525
6	2	3	1	0.888	1.37	0.407	0.549	1.061697	0.8035

7	3	1	3	1.07	1.54	0.434	0.533	0.012019	0.89425
8	3	2	1	0.715	1.48	1.66	1.07	-2.17624	1.23125
9	3	3	2	1.28	1.34	0.755	0.770	-0.60407	1.03625

Table 6.3 shows all roughness values measured. Forming time has been measured during forming operation which is shown in Table 6.2. From this table it can be observed that forming time is more for first experiment with less step depth and lower wall angle. S/N ratio has been calculated using equation (6.5) shown above and mean of all 4 roughness values shown in Table were calculated to get the approximate roughness value.

The variables affecting surface roughness can be determined by analysis of variance (ANOVA) technique. A cut-off criterion is used to categorise the significant factors from insignificant factors. Here in ANOVA F-test has been used as cut-off criterion. Table 6.4 shows the S/N ratios for surface roughness and forming time.

Analysis of experimental results can be done by using response table and response graph which will investigate the effect of each process parameter on output rank wise. From response graph, effect of each level of each parameter on output can be obtained graphically. Response table shows rank of each parameter on both the responses. S/N and mean response table has been analysed here. Both these tables and graphs help in summarising the effect of each process parameter on surface roughness as well as forming time. As per the response Table 6.5, rank of forming angle, step depth and federate are 1, 2, 3 respectively for surface roughness. Factor ranking is the difference between response extremes. Higher the factor response, higher is the rank. The higher the S/N ratio, smaller is the variance in the quality of the result. From response graph A1, B1, C2 are the highest for surface roughness and A1, B3, C3 are highest for forming time in main effect plot.

Optimisation of response influenced by input variables is the objective in Response surface methodology (RSM). RSM is a widely used technique to measure surface roughness using mathematical models. Changes are made in input variables in experimental runs to test the response on output. The response can be represented in three dimensional spaces either as contour plot or as surface. In this work, surface roughness and forming time are the response and forming angle, feed rate and step depth are input parameters. From response table and graph, it was observed that feed rate has less effect on forming angle as compared to other two parameters. So keeping feed rate constant, the response surface has been plotted and compared with experimental result in Figure 6.4.

Table 6.4.ANOVA For Surface Roughness.							
Surface Roughness	Source	DF	Seq SS	Adj SS	Adj MS	F	P
	Forming Angle(º)	2	36.499	36.499	18.250	7.84	0.113
	Step depth(mm)	2	6.715	6.715	3.357	1.44	0.409
	Feed Rate(mm/min)	2	2.522	2.522	1.261	0.54	0.649
	Error	2	4.655	4.655	2.327		
	Total	8	50.391				
Forming Time	Source	DF	Seq SS	Adj SS	Adj MS	F	P
	Forming Angle(º)	2	1.775	1.775	0.888	0.26	0.794
	Step depth(mm)	2	239.106	239.106	119.553	34.92	0.028
	Feed Rate(mm/min)	2	83.841	83.841	41.920	12.24	0.076
	Error	2	6.848	6.848	3.424		
	Total	8	331.571				
DF=Degree Of Freedom, SS=Sum of squares, MS=variance (Mean of squares), F=Ratio of two mean square values, P=Determined from F value and degree of freedom							

Table 6.5.Response table.				
Surface Roughness	Level	Forming Angle	Step Depth	Feed Rate
	1	3.96089	2.74634	1.40660
	2	2.12071	1.77937	2.46507
	3	-0.922764	0.633111	1.28716
	Factor	4.883654	2.113229	1.17791
	Rank	1	2	3
Forming time	1	-19.8551	-25.4908	-23.5605
	2	-20.5676	-19.8510	-20.3145
	3	-21.4265	-16.5073	-17.9742
	Factor	1.5714	8.9835	5.5863
	Rank	3	1	2

The second order response surface representing surface roughness is given by

$$R = 10.8390 - 0.412442 \times A - 0.9620 \times B + 0.003146 \times C + 0.00418 \times A^2 + 0.152 \times B \times + 4.060 \times 10^{-7} \times C^2 + 0.010466 \times A \times B - 6.7166 \times 10^{-5} \times A \times C$$

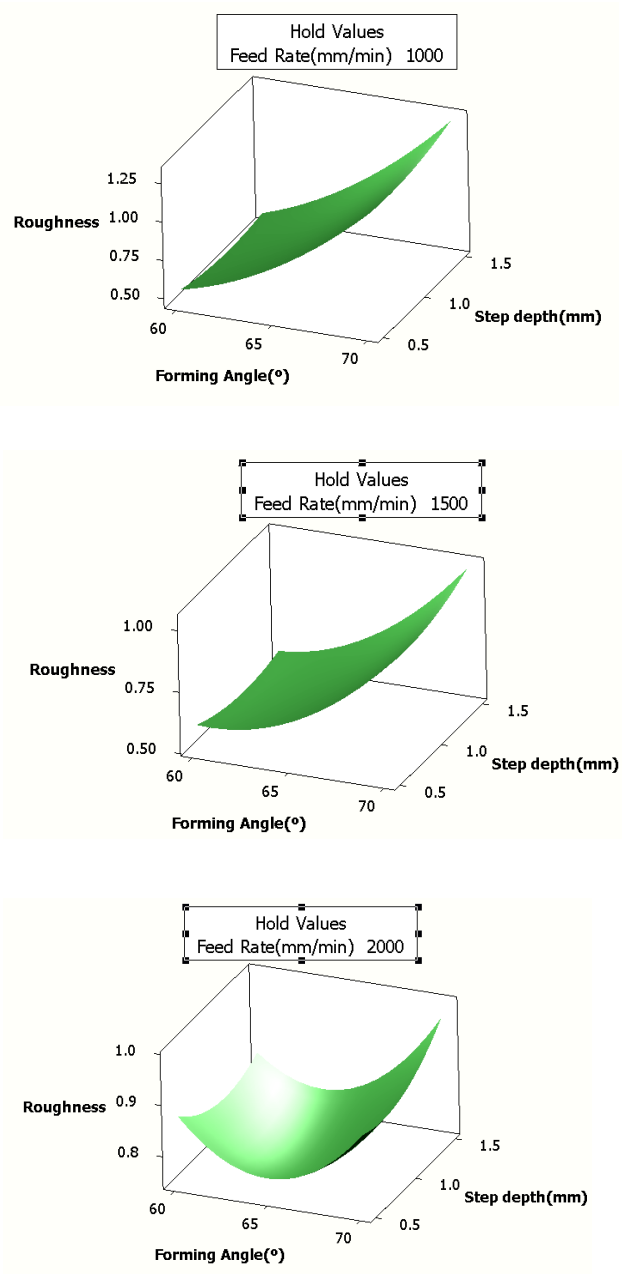

Figure 6.4.Texture of the formed sheet and RSM plot at constant feed rate

*Pictures are lebelled as per L9 orthogonal array sequence number

Similarly, from response graph and table, it was observed that wall angle has less effect on forming time as compared to other two parameters. So keeping wall angle constant, RSM has been plotted as shown in Figure 6.5.

The second order response surface representing forming time is given by

$$R = 210.010 - 4.68567 \times A - 94.0067 \times B + 0.0106433 \times C + 0.0376667 \times A^2 + 14.2667 \times B^2 + 9.23 \times 10^{-6} \times C^2 + 0.7933 \times A \times B - 6.7 \times 10^{-4} \times A \times C$$

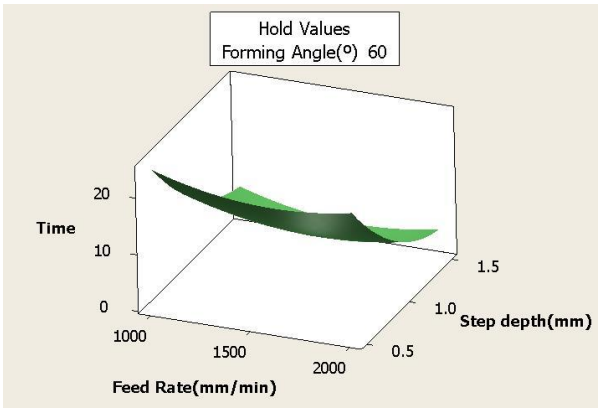

(a)

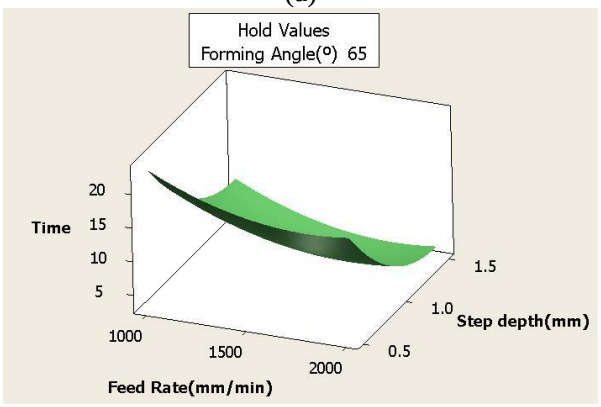

(b)

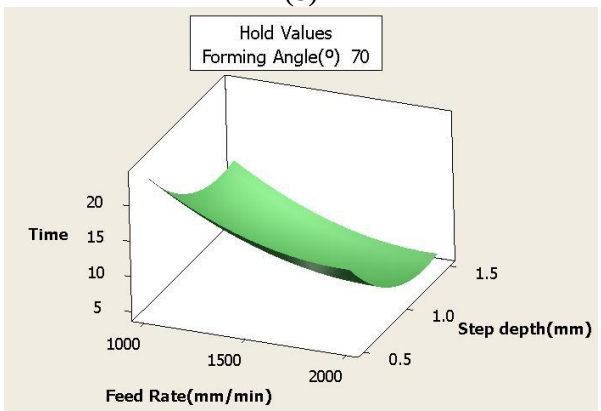

(c)

Figure 6.5.Response surface plot for forming time at constant wall angle from experiment (a) 1,2,3 (b) 4,5,6 (c) 7,8,9 in L9 orthogonal array table

6.1.4 Results and Discussion

Using L9 orthogonal array combinations 9 experiments have been performed. In Figure 6.4, texture of all the formed cups has been shown From the Table 6.1. It can be observed that F statistics is higher for forming angle. So, feed rate has negligible effect on roughness as compared to step depth and forming angle. Similarly, ANOVA Table 6.4 for

time reflects when F statistics is larger than P values small producing a statically significant result. Forming angle has negligible impact on forming time as compare to other parameters and P value < 0.05 shows step depth has significant effect on forming time. As per the response Table 6.5, rank of forming angle, step depth and feed rate are 1, 2, 3 respectively for surface roughness. Form Table 6.5, ranking of forming angle, step depth and feed rate are 3, 1, 2 respectively. Factor ranking is the difference between response extremes. Higher the factor response, higher is the rank. The higher the S/N ratio, smaller is the variance in the quality of the result. In main effect plot Figure 6.3, A_1, B_1, C_2 are the highest for surface roughness and A_1, B_3, C_3 are highest for forming time.

From Response table and ANOVA test it can be concluded that surface roughness is affected by forming angle the most and then step depth. Feed rate has least impact on surface quality. Similarly from response table for S/N ration of forming time, it is observed that step depth affects forming time the most out of all the three parameters. Forming angle has the least effect on forming time.

In Figure 6.4, it can be observed that, at constant feed rate, surface roughness increases with increase in feed rate and with increase in step depth. In photo-1, 6, 8 also, surface texture changed and seems to be more jagged in Photo-6 due to high step depth. In high step depth scallop height increases leaving visible undeformed lines on the part. But in 2nd RSM plot, it can be observed that at constant feed rate of 1500mm/min, surface roughness is nearly equal in photo-2,4 and rougher in Photo-9 due to higher step depth. In 3rd RSM plot, Surface quality in photo-3 is inferior to other two.

Table 6.6.Optimum Parameters.

Surface Roughness	Parameters	Forming Angle(°)	Step depth (mm)	Feed Rate (mm/min)	T1 (µm)	T2 (µm)	T3 (µm)	T4 (µm)
	Levels	1	1	2	0.108	0.0726	0.177	0.0748
	Values	60	0.5	1500				
Forming Time	Levels	1	3	3	4.54			
	Values	60	1.5	2000				

So in all the experiments it is observed that, higher step depth increases surface roughness due to increase in scallop height. Out of all the experiments, in experiment number-1 surface quality and texture of the surface has better visibility than others. But time

taken in experiment-1 is more than other experiments which is shown in Table 6.2.

Confirmation test has been conducted to confirm the quality of surface roughness and forming time. Using optimum parameters from response graph shown in Table 6.6, experiment has been conducted for forming time and time taken for forming was 4.54min. Also roughness was measured using above forming parameters and roughness value is shown in the Table 6.6. Mean of all four readings taken is 0.1081µm. Texture of the final formed cup was found to be smoother and surface quality was improved.

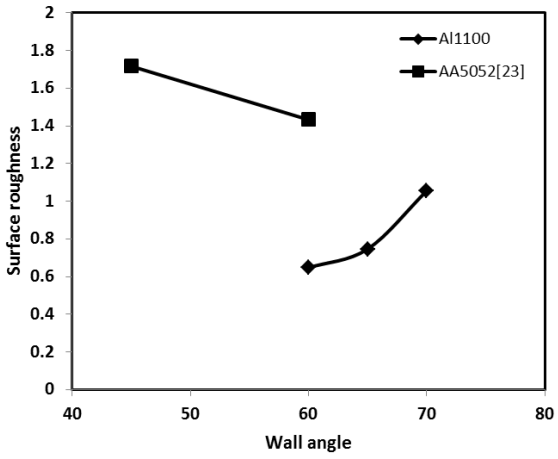

(a)

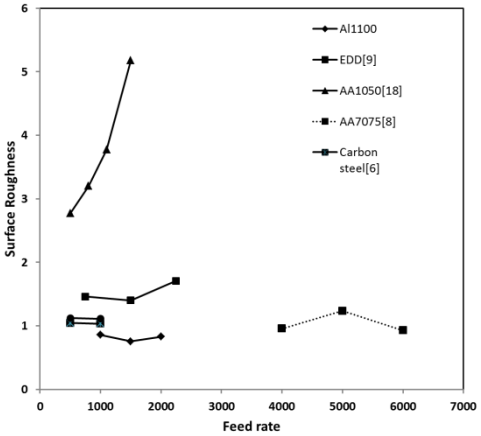

(b)

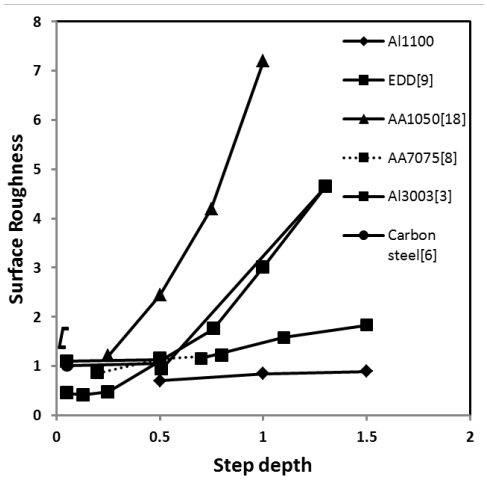

(c)

Figure 6.6.Effect of (a) Wall angle (b) Feed rate (c) Step depth on Surface roughness

Different materials have been used in ISF for investigating surface roughness by varying various process parameters in literature. As spindle speed has less effect on surface roughness, this parameter from literature has been ignored and effect of other process

parameters on surface roughness has been plotted in Figure 6.6. There was only limited literature available for investigating surface roughness variation due to wall angle change. Surface roughness variation due to wall angle in Figure 6.6(a) shows opposite trend for two materials. For AA5052 surface roughness decreases with increase in wall angle, but for Al1100, surface roughness increases with increase in wall angle. Figure 6.6(b) shows the surface roughness deviation due to change in tool feed rate for different materials. For almost all the materials, roughness trend is similar. Surface roughness increases with increase in tool feed rate. Only Al7075 shows a decreasing trend after 5000mm/min feed rate. Figure 6.6(c) shows the roughness trend for different materials when step depth varies. At lower step depth, nearly all the materials show lower surface roughness but at higher step depth, drastic variation in roughness has been observed.

6.2 RAISF surface roughness

Therefore, a process that can relatively reduce the stretching component may delay the fracture and hence enable obtaining larger wall angles than those possible by current ISF. Such a process also should change the friction processes at the tool-work piece interface so as to result in a better surface finish. With this null hypothesis, a novel variant of ISF, the robot-assisted incremental sheet metal forming (RAISF) has been investigated in the present work, in which the angle at which the sheet metal is presented to the tool is varied using a robotic manipulator providing two additional degrees of freedom. In addition, one of the degrees of freedom of the tool has been transferred to the robotic manipulator, thereby introducing a controllable sliding friction between the tool and sheet. This robotic manipulator was fitted on the table of the three-axis vertical machining center for presenting the sheet metal blank to the vertical tool at a desired angle. Table 6.7 shows the advantage of this retrofitted robotic manipulator fitted to 3-axis machine in comparison to a full-fledged 5-axis machine. The new experimental test arrangement and the tool path planning have been explained in the next section. The results obtained using this test setup in terms of the effect of part inclination, rotation and tool linear motion interval on depth of fracture and surface quality in this process have been discussed in the later sections.

Table 6.7.Comparative advantages of a retrofitted robotic manipulator fitted to 3-axis machine in comparison to a full-fledged 5-axis machine		
Attribute	5-axis CNC milling machine	3-axis CNC with robotic manipulator
Cost	Expensive	Cheaper
Ease of Programming	Complex	Simpler
Ease of operation	All five axis simultaneously	Axis motions can be decoupled
Possibility of material gouging	More	Less
Possibility of collision	More	Less

6.2.1 Process parameters

6.2.1.1 Optimal Inclination angle

To incline the sheet metal with respect to NC tool, maximum inclination angle needs to be calculated to avoid interference between tool shank and sheet metal part. In Figure 6.7 schematic diagram of a formed cup of 90º forming angle is shown. Where H is total depth to be formed, R_s is radius of the cup, θ is maximum Inclination angle and 90-ϕ is cup half angle or forming angle.

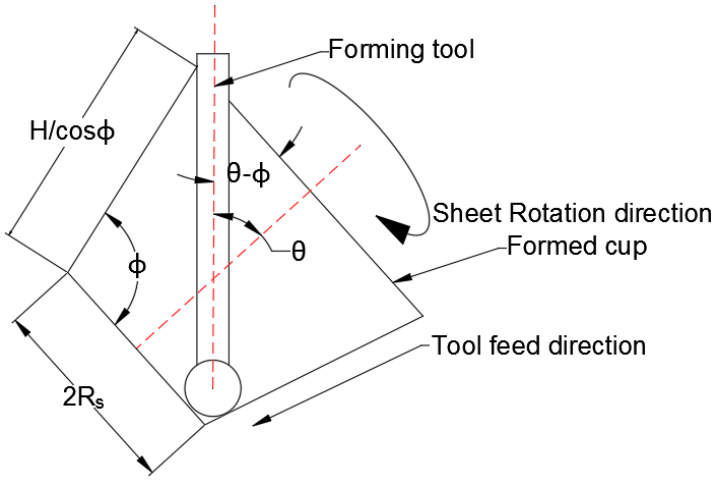

Figure 6.7.Inclination angle

Inclination angle can be calculated from optimized forming angle taken from ISF experiments. At wall angle of 60°, surface quality was better than other combinations. So the end effector will be tilted to 90º-θ forming angle to maintain the surface quality.

6.2.1.2 End effector rotation speed and tool feed rate

In single stage incremental forming without a manipulator, to get proper surface finish, process parameters have been optimized and validated through experiments. Out of all the process parameters, wall angle, step depth and feed rate have significant effect on surface quality. Other parameters were kept constant which have negligible effect on surface finish. But when a manipulator with two rotational DOF is used to manipulate sheet in ISF, end effector rotational speed and tool feed rate has to be synchronized to get proper surface finish. At wall angle α^{o}, inclination angle of $\theta°$, and end effector angular speed of N RPM, tool feed rate F mm/min can be obtained as mentioned below to maintain step depth of *Z* mm.

F (mm/min) = Z/(1/N)

a) If rotational speed is too high and tool feed rate is low, deformed portion of the sheet will deform multiple numbers of times depending on the tool feed rate as shown in Figure 6.8(a). This will lead to excessive thinning and fracture will be seen in early stage.

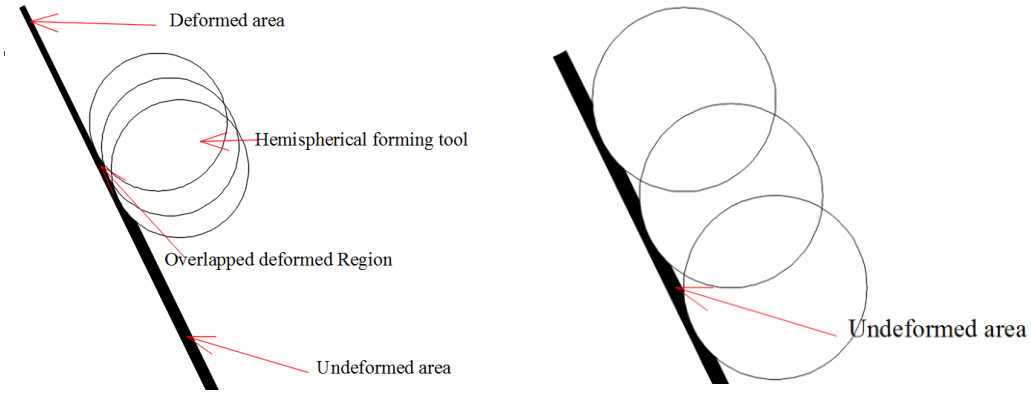

Figure 6.8.Deoformation zone at (a) high Rotational speed (b) Low rotational speed

b) If rotational speed is too low and tool velocity is high, sheet will not undergo complete rotation and part of the sheet will remain undeformed as shown in Figure 6.8(b). This will lead to varied thickness distribution and part accuracy will be disturbed. So the velocity of the tool should be synchronized with rotational speed of the end effector. So for the experiment, lower RPM were chosen and tool feed rates were calculated.

6.2.1.3 Scallop Height and distance

Scallop height and scallop distance are two parameters to maintain the surface quality in incremental forming operation. It depends on step depth and radius of the forming tool. By adding two rotational degrees of freedom manipulator to 3 axis CNC machine, part can be tilted to certain angle and scallop height will change by inclination the part. But rotation of

end effector about its own axis has the least effect on scallop height. In ISF by increasing wall angle, scallop height increases [36]. But when the sheet is inclined at the inclination angle of θ as shown in Figure 6.9 relative angle between actual wall angle and tool horizontal axis changes to α-θ as shown in figure. Scallop distance and Scallop height in inclined sheet will be as mentioned below

$$d_s = \frac{d}{\sin(\alpha - \theta)} \tag{6.6}$$

$$h = r_t - \sqrt{r_t^2 - \left(\frac{d}{2\sin(\alpha - \theta)}\right)^2} \tag{6.7}$$

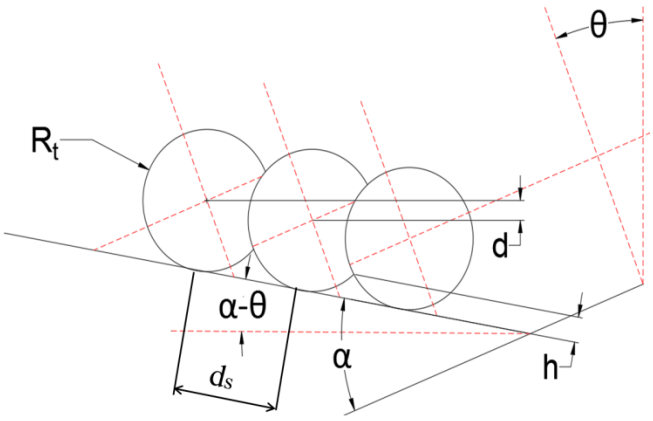

Figure 6.9.Scallop height and distance in (a) ISF

(b) RAISF

From the equation (6.6) and (6.7) it can be concluded that by increasing the inclination angle and wall angle of the part, scallop distance and height increase. Increase in scallop distance will have fewer scallop peaks for a particular height of the cup which in turn will reduce the surface roughness. Decrease in scallop height will lead to better surface quality due to lesser undeformed region.

6.2.2 Design of Experiments

DOE is an effective tool to optimize process parameters with minimum number of experiments. Out of various widely used DOE techniques, in this study Box-Behnken technique was used to plan number of experiments. This tool is widely used response surface designs for more than 3 factors. With 4 factors and each with 3 levels, this DOE tool gives 27 combinations to conduct experiment. The process parameters with all three levels have been shown in Table 6.8. Spindle speed of the tool was kept constant as spindle speed has less influence on surface roughness. Tool linear velocity depends on end effector rotation and step

interval. In one revolution of end effector, tool should move one step along the wall. So tool linear velocity can be calculated as follows.

V (mm/min) = s*N

So the combination of different rotational speed and step interval will give different tool linear velocity.

Table 6.8.Process parameters

Parameters	Notations	Notations in DOE	Values			Coded		
			Low	Middle	High	Low	Middle	High
Wall angle(°)	α	A	70	75	80	-1	0	1
Inclination angle(°)	θ	B	15	20	25	-1	0	1
Rotational speed(RPM)	N	C	4	5	6	-1	0	1
Interval(mm)	S	D	0.05	0.1	0.2	-1	0	1

6.2.3 Experimental procedure

Experimental setup for RAISF has been shown in the Figure 6.10. Two degree of freedom manipulator was attached on the bed of 3axis vertical CNC milling machine. An EN36 hemispherical headed tool of 15mm diameter was attached to CNC milling machine. Al1100 commercial aluminum sheet of 150*150*1.2mm was attached to manipulator. A frustum of cone with top diameter 100mm was considered for the experiment. The required tool trajectory was generated using MATLAB. Rotation direction of the tool has significant effect on surface finish and forces in ISF [111]. So tool rotation direction and end effector rotation direction was kept same in the experiment. Tool here moves in linearly downward direction along the wall of the cup and sheet attached to end effector rotates about inclination axis which maintains the circumferential contact between tool and sheet. To investigate the surface quality of the part, process parameters like inclination angle, wall angle, rotational speed of the end effector and stepping interval were varied. The measurement of surface roughness was done by using Taylor Hobson surface roughness tester shown in Figure 6.10. In this tester a diamond tip stylus moves across the peaks and valleys of the surface and measures roughness. Surface roughness was measured at four different locations which are 90° apart from each other. For the measurements evaluation length was taken as 4mm and cut-off length as 0.8mm. Average of all the four roughness value is reported in Table 6.8.

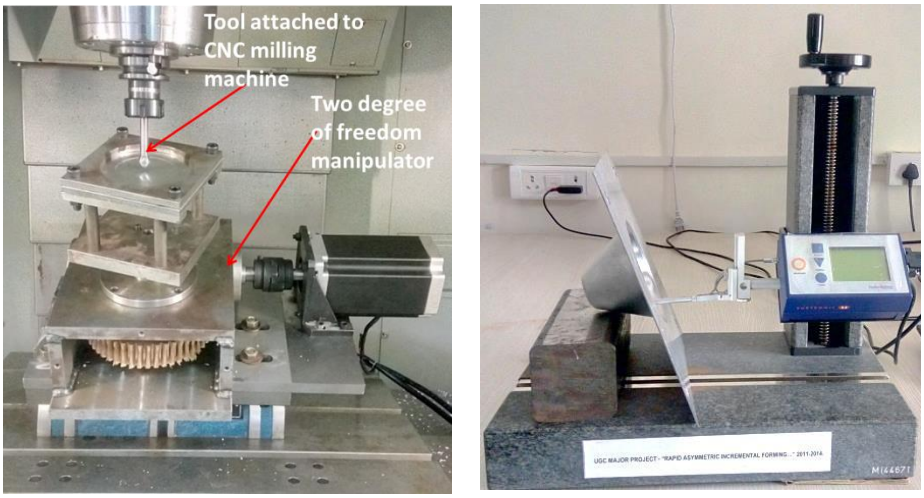

2DOF manipulator attached to CNC vertical milling machine

Profilometer

Figure 6.10.Experimental setup

6.2.4 Results and Discussion

To analyze the result S/N ratio is calculated which shows both average and variation in experimental results. In this study, better surface finish is our main objective. So smaller the S/N value better is the result. S/N ratio is given by equation (6.8) given below.

$$\frac{S}{N} = -10\log\left[\frac{1}{n}\sum_{1}^{n} y_i^{\,2}\right] \tag{6.8}$$

Where n= number of observations per row which is 4 for surface roughness in our study.

y_i= i^{th} measured roughness in the row

Table 6.9. Taguchi Orthogonal array

Run Order	A	B	C	D	α	θ	N	s	R(μm)	S/N ratio
1	-1	-1	0	0	70	15	5	0.1	0.32	9.897
2	0	0	0	0	75	20	5	0.1	0.0459	26.76375
3	-1	0	1	0	70	20	6	0.1	0.512	5.814601
4	0	1	1	0	75	25	6	0.1	0.721	2.841295
5	-1	0	0	-1	70	20	5	0.05	0.011	39.17215
6	1	0	0	1	80	20	5	0.2	0.0348	29.16842
7	0	-1	1	0	75	15	6	0.1	0.177	15.04053
8	1	-1	0	0	80	15	5	0.1	0.0772	22.24765
9	-1	1	0	0	70	25	5	0.1	0.367	8.706679

10	0	-1	-1	0	75	15	4	0.1	0.866	1.249642
11	1	1	0	0	80	25	5	0.1	0.383	8.336025
12	0	0	-1	-1	75	20	4	0.05	0.021	33.55561
13	-1	0	-1	0	70	20	4	0.1	0.022	33.15155
14	0	0	0	0	75	20	5	0.1	0.0459	26.76375
15	1	0	1	0	80	20	6	0.1	0.0351	29.09386
16	0	0	0	0	75	20	5	0.1	0.0459	26.76375
17	0	1	0	1	75	25	5	0.2	0.371	8.612522
18	0	1	0	-1	75	25	5	0.05	0.846	1.452593
19	1	0	0	-1	80	20	5	0.05	0.0562	25.00527
20	0	-1	0	1	75	15	5	0.2	0.512	5.814601
21	0	1	-1	0	75	25	4	0.1	0.113	18.93843
22	1	0	-1	0	80	20	4	0.1	0.063	24.01319
23	-1	0	0	1	70	20	5	0.2	0.641	3.862839
24	0	-1	0	-1	75	15	5	0.05	0.375	8.519375
25	0	0	-1	1	75	20	4	0.2	0.023	32.76544
26	0	0	1	1	75	20	6	0.2	0.718	2.877511
27	0	0	1	-1	75	20	6	0.05	0.661	3.595971

Significance of all the parameters was checked using analysis of variance technique (ANOVA). A cut-off criterion is used to categorize the significant factors from insignificant factors. Here in ANOVA F-test has been used as cut-off criterion.

Table 6.10.ANOVA analysis for surface roughness

Source	DF	Seq SS	Adj SS	Adj MS	F	P
Regression	14	1.76773	1.76773	0.126267	3.55	0.017
Linear	4	0.41337	0.47863	0.119658	3.37	0.046
α	1	0.01871	0.00123	0.001229	0.03	0.856
θ	1	0.12479	0.20172	0.201724	5.68	0.035
N	1	0.24542	0.26663	0.266626	7.50	0.018
s	1	0.02446	0.00905	0.009053	0.25	0.623
Square	4	0.64129	0.64129	0.160322	4.51	0.019
α*α	1	0.16331	0.00767	0.007671	0.22	0.651
θ*θ	1	0.28675	0.44179	0.441792	12.43	0.004

N*N	1	0.04195	0.10201	0.102010	2.87	0.116
s*s	1	0.14928	0.14928	0.149278	4.20	0.063
Interaction	6	0.71307	0.71307	0.118845	3.34	0.036
α*θ	1	0.01674	0.01674	0.016744	0.47	0.506
α*N	1	0.06706	0.06706	0.067055	1.89	0.195
α*s	1	0.11485	0.11485	0.114846	3.23	0.097
θ*N	1	0.42055	0.42055	0.420552	11.83	0.005
θ*s	1	0.07160	0.07160	0.071604	2.01	0.181
N*s	1	0.02227	0.02227	0.022270	0.63	0.444
Residual Error	12	0.42652	0.42652	0.035543		
Lack-of-Fit	10	0.42652	0.42652	0.042652		
Pure Error	2	0.0	0.0	0.0		
Total	26	2.19425				

The statistical significance of the effect depends on p-value. It can be observed from the ANOVA Table 6.10 that, F statistics is larger than P values producing a statically significant result. F statistics is higher for inclination angle and rotational speed as compared to other parameters and P<0.05 shows that inclination angle has significant effect on surface roughness. Significance level of interaction term should also be considered in statistical analysis. P value is higher than 0.05 for all interactions except θ-θ and θ-N interaction. So interactions with P>0.05 are statistically insignificant. As the interaction effect is statistically significant, main effects can't be interpreted without considering the interaction effect.

6.2.4.1 Response table and Response graph

Analysis of experimental results can be done by using response table and response graph which will investigate the effect of each process parameter on output rank wise. From response graph, effect of each level of each parameter on output can be obtained graphically. Both response table and graph help in summarizing the effect of each process parameter on surface roughness. Response table, Table 6.11 shows rank of each parameter on the responses. As per the responses, rank of inclination angle, rotational speed, wall angle and step increment are 1, 2, 3, 4 respectively for surface roughness. Factor ranking is the difference between response extremes. Higher the factor response, higher is the rank. Inclination angle has higher effect than other parameters on surface roughness. Higher S/N ratio leads to smaller variance in the quality of the result. From main effect plot θ_2, α_3, N_1 and

s_1 are the highest for surface roughness. As the stepping interval has lowest rank in response table, it can be kept constant while performing experiment.

Table 6.11.Response Table

Level	α (deg)	θ (deg)	$\dot{\theta}_2$ (rpm)	s (mm)
1	16.767	10.461	23.946	18.550
2	12.464	22.218	15.197	15.853
3	22.977	8.148	9.877	13.850
Delta	10.514	14.071	14.068	4.700
Rank	3	1	2	4

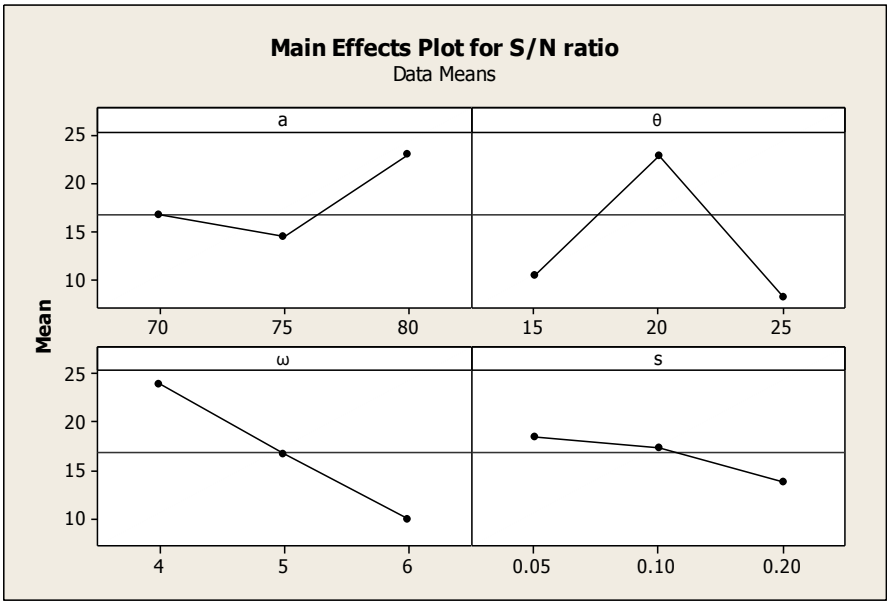

Figure 6.11. Main effect plot for means

In RSM, the objective is to optimize a response which is influenced by several input variables. Changes are made in input variables in experimental runs to test the response on output. The response can be represented in three dimensional spaces either as contour plot or as surface. In this work, surface roughness is the response and inclination angle, wall angle, stepping interval and angular rotation are input parameters. Response surface for interaction of parameters except stepping interval are plotted in Figure 6.12. At constant rotational speed, when wall angle and inclination angles are varied, surface roughness is the lowest at 20°

inclination angle and 80° wall angle. Similarly when wall angle was kept constant and inclination angle and rotational speed were varied, surface roughness was lowest at 20° inclination angle and at lowest RPM. When inclination angle was kept constant and other two parameters were varied, surface roughness was the lowest at smaller wall angle and rotational speed.

The second order response surface representing surface roughness is given by

$$R = -0.933658\theta + 0.332103\alpha - 0.698863\mathrm{N} + 26.5820\mathrm{s} + 0.0115125\theta^2 - 0.00151700\alpha^2 + 0.138300\mathrm{N}^2 + 34.2764\mathrm{s}^2 + 0.00258800\theta \times \alpha + 0.0648500\theta \times \mathrm{N} - 0.344262\theta \times \mathrm{s} - 0.0258950\alpha \times \mathrm{N} - 0.435993\alpha \times \mathrm{s} + 0.959966\mathrm{N} \times \mathrm{s}$$

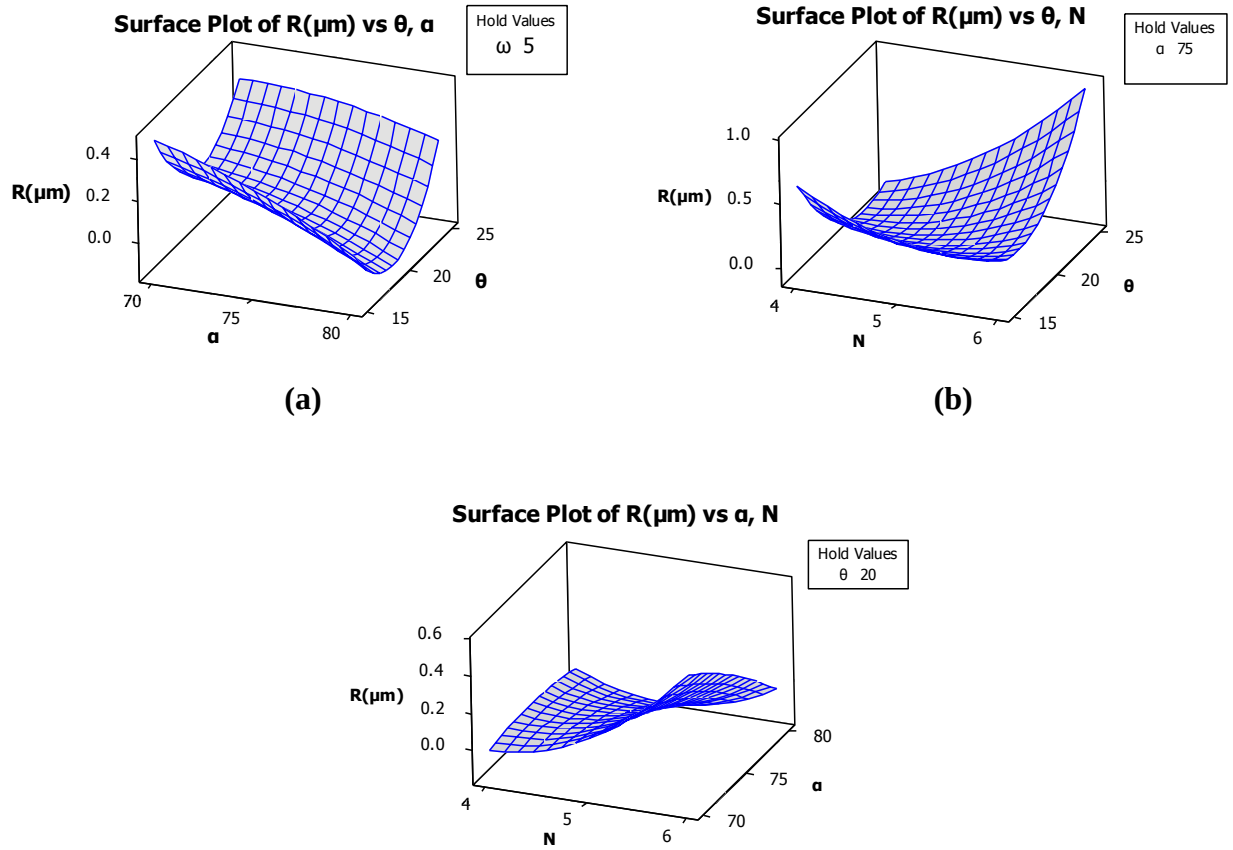

Figure 6.12.Response surface

6.2.5 Effect of process parameter on surface roughness

6.2.5.1 Effect of inclination angle

The individual plot in Figure 6.14(a), shows the variation of surface roughness with inclination angle which varies from 15° to 25°. It can be noted from this figure that, with increase in inclination angle, surface roughness increases. When only inclination angle was

varied keeping all other parameters constant, roughness increases with increase in inclination angle. With increase in inclination angle scallop height and scallop distance increase which leave undeformed marks on sheet. But when other parameters vary with inclination angle, roughness doesn't increase with inclination angle. From Figure 6.12(a), it can be noted that, with increase in wall angle as well as inclination angle, surface roughness decreases at 20° wall angle and increases again at 25° inclination angle. Combination of increase in wall angle and inclination angle compensate the effect on scallop height.

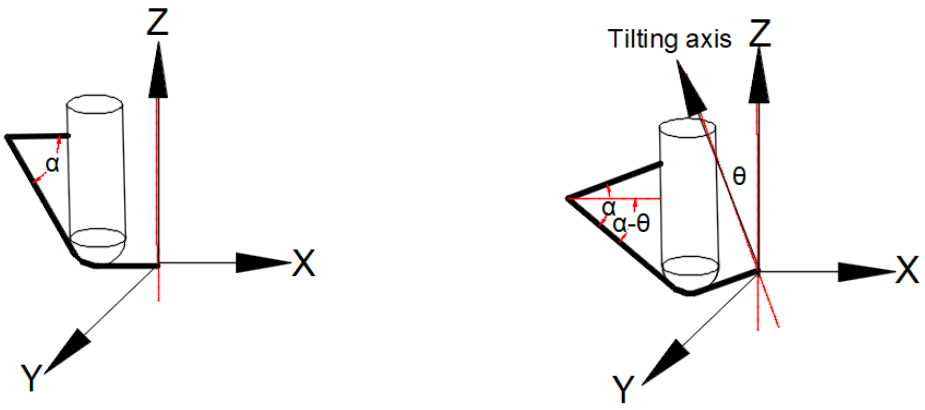

Figure 6.13.Relative wall angle between tool and sheet in ISF and RAISF

6.2.5.2 Effect of Wall angle

To study effect of wall angle on surface roughness, wall angle was varied from 70° to 80°. With increase in inclination angle, though the actual wall angle of the part remains same, but relative wall angle between tool and sheet decreases by θ as shown in the Figure 6.13. Figure 6.14(b) shows the variation of surface roughness with wall angle. It can be noted from the figure that with increase in wall angle, surface roughness increases. With increase in wall angle alone, keeping other process parameters constant, scallop distance increases. Due to increase in scallop distance for higher wall angle, surface roughness increases. But surface roughness changes when other process parameters vary along with wall angle. In Figure 6.12(a), when inclination angle varies, surface roughness decreases with increase in wall angle.

6.2.5.3 Effect of Sheet Rotation

Rotational speed of the end effector also affects roughness. Rotational speed was varied from 4 RPM to 6 RPM to investigate surface roughness variation. From Figure 6.14(c), it can be noted that, surface roughness increases with increase in rotational speed.

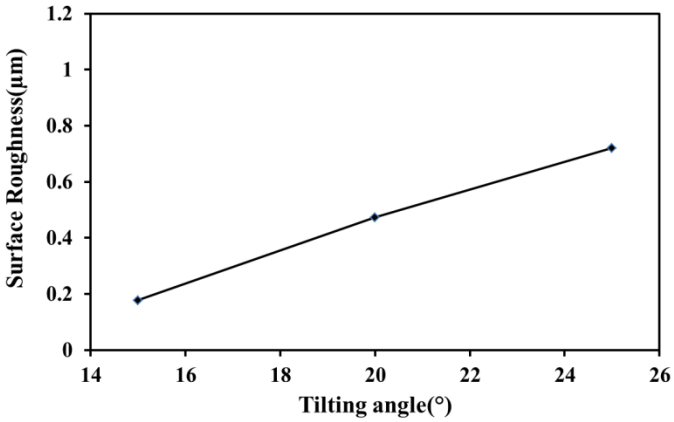

(a)

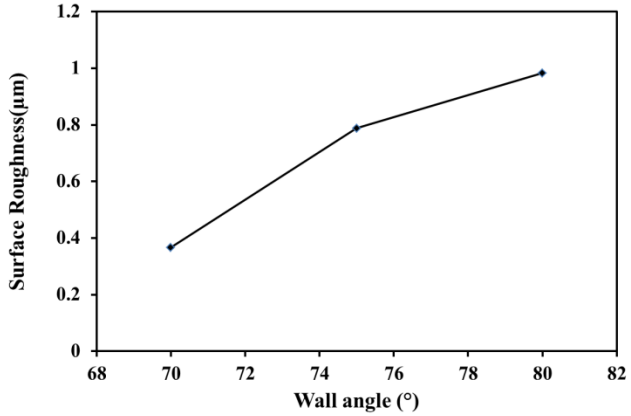

(b)

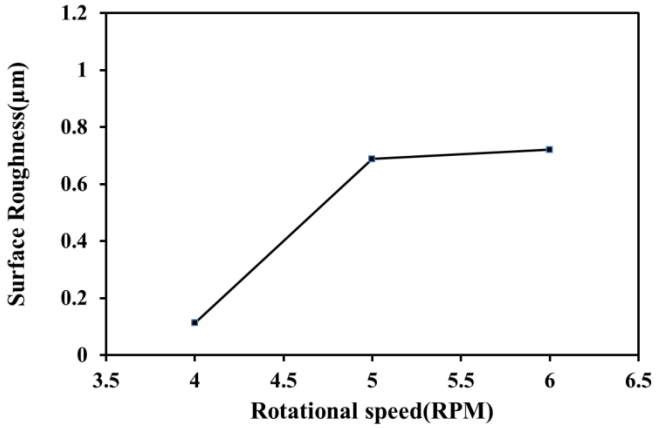

(c)

Figure 6.14.Effect of single parameter (a) inclination angle(°), (b)Wall angle(°), (c)Rotational speed (RPM)

In response surface plot in Figure 6.12, effect of other parameters variation along with rotational speed has been shown. Form Figure 6.12(b), it can be noted that, surface roughness increases with increase in angular rotation and inclination angle. If the tool feed rate is constant and rotational speed is increasing, at higher rotational speed thinning will be high and at very low rotational speed roughness will be high due to undeformed area left on the

sheet. Figure 6.15 shows the roughness profile obtained in ISF and RAISF experiments. From this profile it can be observed that scallop distance in RAISF (d_{si}) is more than ISF (d_{sf}) which is an approximate match with the results obtained from analytical calculation. Though the scallop height in both ISF and RAISF was found to be nearly same as shown in Figure 6.15, but roughness within the scallop distance on fixed base was 1.07µm and for inclined base roughness was 0.473µm.

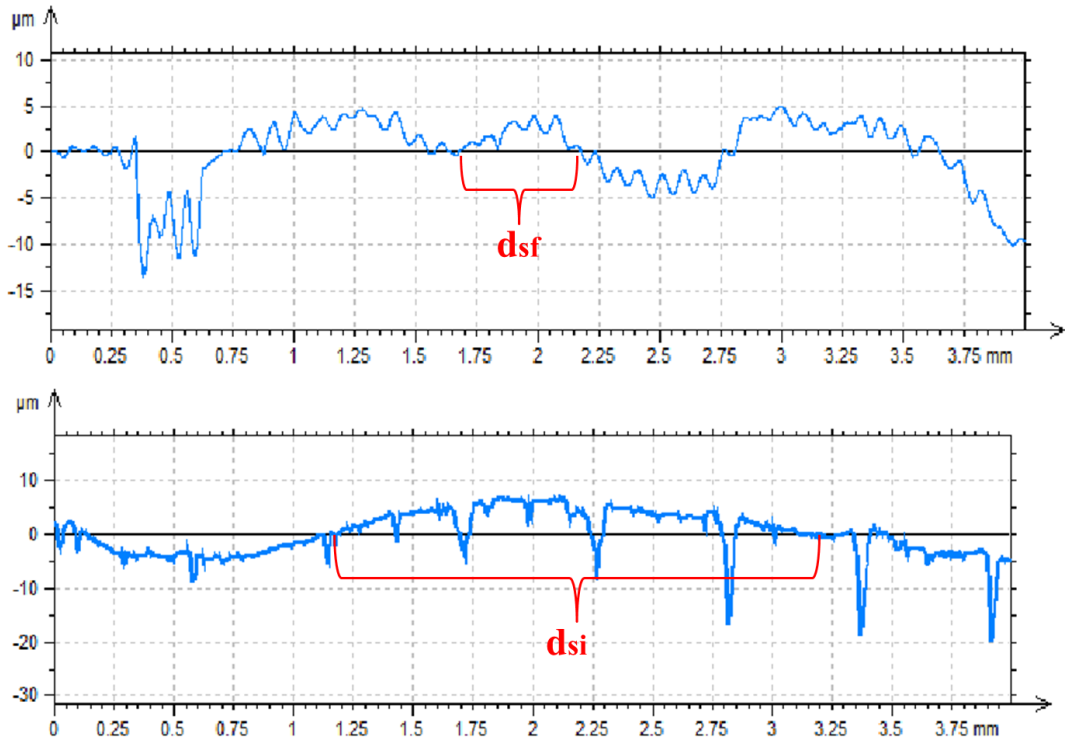

Figure 6.15.Scallop distance in (a) ISF and (b) RAISF

Without robotic manipulator experiments were conducted for different wall angle with minimum step depth of 0.5mm. Feed rate has negligible effect on surface roughness in ISF so feed rate was also kept constant at 700mm/min. Parts were also formed with different inclination angle and rotational speed to compare the surface quality. Comparisons of surface roughness in ISF and RAISF have been shown in Table 6.12, which shows for all three wall angles, better surface finish was achieved in RAISF.

Table 6.12.Compariosion of surface roughness (µm)

Wall angle	RAISF	ISF
70°	0.011	0.89425
75°	0.021	0.361
80°	0.0348	0.130

6.3 Summary

The surface quality of the sheet in ISF on three axis milling machine can be improved by adding distinct robot or manipulator which can manipulate the sheet with respect to tool. This paper presents a new technology for ISF and outline to evaluate process parameters for achieving good surface finish for robot assisted incremental sheet metal forming from the optimized parameters obtained from Single stage incremental forming without manipulator. It is shown that up to certain inclination angle, part can be tilted if tool length and formed part depth are known. By using 3 axes and additional 2 axes, trajectories for tool path has been plotted in MATLAB. Experiments with manipulator were conducted on vertical 3 axis CNC machine using hemispherical forming tool. Effect of various process parameters on surface quality in RAISF has been evaluated through experiment and Taguchi method. Rotational speed, inclination angle and wall angle were found to be more influential parameters on surface quality than step interval of the end effector. Keeping all parameters constant, with increase in inclination angle, surface roughness decreases due to increase in scallop distance. But along with inclination angle if wall angle is also varying, surface roughness first decreases and then increases after certain angle. Scallop height variation gets compensated by varying inclination angle and wall angle. When rotational speed of the end effector varies along with inclination angle, surface roughness increases.

Step interval has the least effect on surface roughness if all other parameters are varying. But if all process parameters are constant, with increase in step interval, surface roughness increases due to increase in scallop height. Surface roughness increases with increase in rotational speed. Surface roughness increases with increase in angular rotation and inclination angle due to the increase the scallop height. At high rotational speed, if tool feed rate and step interval are constant, then early thinning was observed due to overlapping of the tool path. But at low rotational speed, due to presence of undeformed area on the sheet, surface roughness increases. In ISF, surface roughness highly depends on wall angle and step depth but in RAISF, surface roughness depends on inclination angle. At certain inclination angle if wall angle is higher, roughness was found to be better than part formed with same wall angle in ISF due to compensation of angle between tool and sheet by sheet inclination in RAISF. With increase in wall angle alone, keeping other process parameters constant, due to increases in scallop distance, surface roughness decreases. This chapter gives a preliminary idea of improving surface quality in ISF process by adding two additional DOF to the existing system. However, along with improvement of surface quality, improvement of

formability is also a requirement in ISF process which needs to be addressed. Next chapter investigates the change in formability of the sheet by additional 2-DOF manipulator.

CHAPTER 7

FORMABILITY IN RAISF

This chapter presents the formability study of Al1100 sheet in RAISF. Maximum formable angle and depth is the key to investigate the formability of any material. In this chapter the deformation behaviour of the material due to part inclination and rotation has been analysed. In this chapter the effect of process parameters on the formability has been investigated in terms of thinning and the maximum forming depth achieved before tearing occurs in the specimen. Effect of various process parameters on forming depth as well as thinning has been explained numerically as well as experimentally.

7.1 Formability

It is commonly known that formability of SPIF is much higher than traditional sheet forming process[4]. This section focuses on formability and thickness distribution in RAISF in Al1100 sheet. Formability can be measured by maximum forming wall angle and thickness distribution. The angle which the side of the wall of the sheet makes with the horizontal xy plane is called as forming angle. Forming angle mainly depends on sheet thickness and material properties. Here formability and thinning of the sheet has been investigated in SPIF and it has been compared with the formability and thinning obtained in RAISF process. Formability has been investigated in terms of maximum formable depth achieved in the process. In order to get maximum allowable thinning the thickness has been measured at various locations on the deformed sheet along the forming depth. Theoretical thickness obtained from sine law, thickness distribution obtained from numerical simulation and experimental results has been compared. In ISF sheet thickness of the part varies as per sine law. If t_0 is the initial thickness of the sheet and t_f is the final thickness after sheet deformation. Wall angle of the formed cup is α. Then as per sine law

$$t_f = t_i \cos\alpha \tag{7.1}$$

From sine law it is clear that with increase in wall angle, sheet final thickness decreases and at 90° wall angle final thickness becomes zero which leads to fracture. Thus the maximum forming depth before fracture can be a parameter to measure formability of the sheet.

In the following section material is assumed to be isotropic and follows the Holloman expression for yield stress.

$$\sigma_{yield} = C\varepsilon^{n} \tag{7.2}$$

7.1.1 Forming Limit Curves in Single point incremental forming (SPIF)

Failure of the sheet can be predicted by understanding the limit of forming. In sheet metal forming, forming limit can be determined by forming limit curve (FLC) in forming limit diagram (FLD). FLC is measured after necking and these are the plots of major and minor principal strains which show a defined state of failure. Traditional FLC is used to predict the failure in metal forming but it lacks the ability to measure the failure in incremental sheet metal forming. Forming limit curve in SPIF is higher than the conventional FLC by an approximation of 2.7 times higher than stamping and deep drawing [25]. This increase in formability is due to large amount of through thickness shear or due to serrated strain path arising from cyclic deformation [53]. In SPIF, FLC is replaced by fracture forming limits (FFLD) because FLC gives local necking strains and in SPIF formability is limited by fracture without previous necking [26]. FFLD in SPIF can be characterized by ductile damage mechanics. The concept of FFL helps to characterize the material by checking the fracture strain location on the specific line.

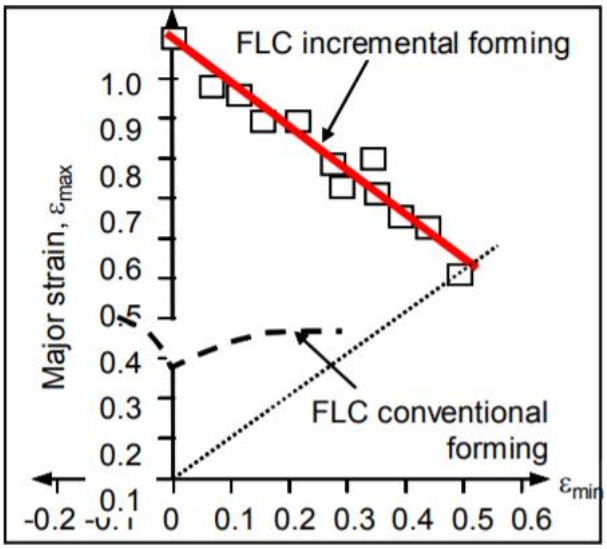

Figure 7.1 Formability Limit Diagram [112]

Formability in ISF can be defined in terms of maximum drawing angle and maximum forming depth. The FLC in ISF is quite different from the conventional forming FLC. The FLD in SPIF is determined in two steps. First one is in single point forming work piece and second one is by grid measuring system. Two deformation states are observed in ISF.

a. On straight surface the plane strain is originated on the sheet metal and material flow is mainly in tool direction.
b. On curved surfaces the longitudinal and biaxial deformation is observed in the deformed sheet metal.

7.2 Experimental Investigation

To verify the accuracy of FEM prediction, experiments were conducted using same condition and process parameter combinations. ISF experiments were conducted on Bridgeport hardinge 3-axis CNC milling machine and fixture fixed on the base of the CNC milling machine was used to clamp the sheet. For RAISF experiments, fixed fixture has been replaced by a two-DOF manipulator. Cylindrical tool made of EN36 and of 15mm diameter is attached to CNC milling machine. Al1100 sheet of 200X200X1.2 mm is attached to the manipulator. SAE-40 lubricating oil is applied to minimize the friction between the sheet and forming tool.

To measure the major and minor strain, circular grids of 3mm diameter was etched on the sheet before forming operation by electrochemical etching. After the occurrence of fracture, the machine tool stopped manually and the fracture depth was measured using Vernier height gauge. Major and minor diameters were measured and engineering strain was calculated in both the direction. Strain was measured form the top of the sheet to the bottom of the sheet along the deformed wall till the fracture. Both the strains for steeper wall angle parts are plotted in FLD.

In order to get thickness variation along the depth of the formed cup, the parts were cut at the middle for thickness measurement. On the formed part, sheet was marked at each 5mm depth from the top. The thickness at the cut sections were measured using the digital pointer anvil micrometer with least count of 0.01mm. Process variables considered for formability study are wall angle, rotational speed of the end effector, inclination angle and step depth. After the preliminary set of experiments, three levels were selected as input for each parameter. Table 7.1 shows the process parameters used to investigate the material formability in RAISF.

Table 7.1 Process Parameters				
Levels	**Wall angle(°)**	**Rotational speed(RPM)**	**Inclination angle(°)**	**Step depth(mm)**
-1	70	4(0.6)	15	0.05
0	75	5(0.7)	20	0.1
1	80	6(0.8)	25	0.2

To plan systematic set of experiments design of experiments (DOE) has been conducted. DOE is a statistical technique that provides an efficient method to analyze the effect of process parameters on the responses and their interaction using minimum number of experiments. It also evaluates all the independent parameters simultaneously. To carryout optimization study through mathematical modeling, study of RSM's Box-Behnken method was used to design the experiments. This method is applied to find the effect of each parameter on the responses and how they interact with each other. The behavior of the response by multiple parameters can be presented by response surface methodology (RSM). Table 7.2 shows the combination of factors for conducting experiment obtained using DOE method.

Table 7.2 Combination of factors				
Exp. No	Wall angle	Rotational speed	Inclination angle	Step depth
1	-1	-1	0	0
2	-1	0	0	1
3	0	-1	1	0
4	0	1	0	-1
5	0	0	0	0
6	0	0	-1	1
7	1	0	1	0
8	1	0	0	1
9	1	0	-1	0
10	0	1	0	1
11	-1	1	0	0
12	-1	0	1	0
13	0	0	0	0
14	0	1	1	0
15	0	-1	0	1
16	0	0	1	1
17	0	0	0	0
18	1	1	0	0

19	1	0	0	-1
20	-1	0	-1	0
21	0	0	-1	-1
22	1	-1	0	0
23	0	-1	0	-1
24	0	-1	-1	0
25	-1	0	0	-1
26	0	0	1	-1
27	0	1	-1	0

7.3 Finite element modeling

Before conducting experiments, to explore the effect of parameters on formability at both bending and stretching zone, a series of finite element analysis has been conducted. Combined effect of forming parameters on sheet thinning and formability has also been investigated using numerical simulation. The process parameters selected for numerical simulation is same as experimental investigation. The element size and boundary condition chosen in this simulation has been discussed in earlier chapters. The strain distribution in FE model has been compared with the experimental results. The distribution of major and minor true strains in the principal strain space obtained by finite element simulation analysis confirm that RAISF of conical shape is nearly under plane strain condition because all strain lie closer to the major strain.

7.4 Results and discussion

7.4.1 Thickness distribution

The experiments were planned as per above mentioned DOE and simulated results were compared with the experimental results. The thickness has been measured at equal depths for all the parts in simulation as well as experiments. The above mentioned experimental data was fed to software to identify the best fitting RSM for regression analysis. Significance of each process parameters on the response can be evaluated using ANOVA by the application of quadratic model. The results obtained in both simulation and experiments were analyzed using regression analysis. Using the fit model, ANOVA was carried out. As per ANOVA analysis titling angle, wall angle, rotational speed and their interaction have higher significance than step depth. Interaction of wall angle and rotational speed has higher significance than their individual effect. Inclination angle alone has the highest significance than other parameters and their interactions and step depth has the least significance on thickness distribution.

Interactive effect of ISF operating parameters on the sheet thinning can be estimated using interactive plots between the parameters. Here parameters in pair were investigated keeping other parameters constant at their mid-level. The minimum, middle and maximum level of the factors are referred as -1, 0, 1 respectively as shown in Table 7.1. In each of the two dimensional contour plot, thinning increases by moving from center to edges and remain constant in any layer. ANOVA for thinning test indicates that inclination angle and wall angle interaction have very significant effect compared to other parameters. Figure 7.2 shows the correlations between the variables of input, inclination angle, sheet rotation, and wall angle and step depth. It can be observed that at higher titling and lower sheet rotation, thinning is lower. In this plot it can also be observed that, sheet rotation-wall angle, sheet rotation-inclination angle and inclination angle-wall angle interactions are not parallel to each other. However, interaction of all the parameters with inclination angle has nearly parallel relation. In interaction plot, greater is the strength of the interaction if the lines are non-parallel. Except step depth, all other process parameters have higher interaction effect on thickness distribution. However, the amount of interaction effect can't be estimated from interaction plot alone. Therefore, contour plot is necessary to understand how the response is related to predictor variables.

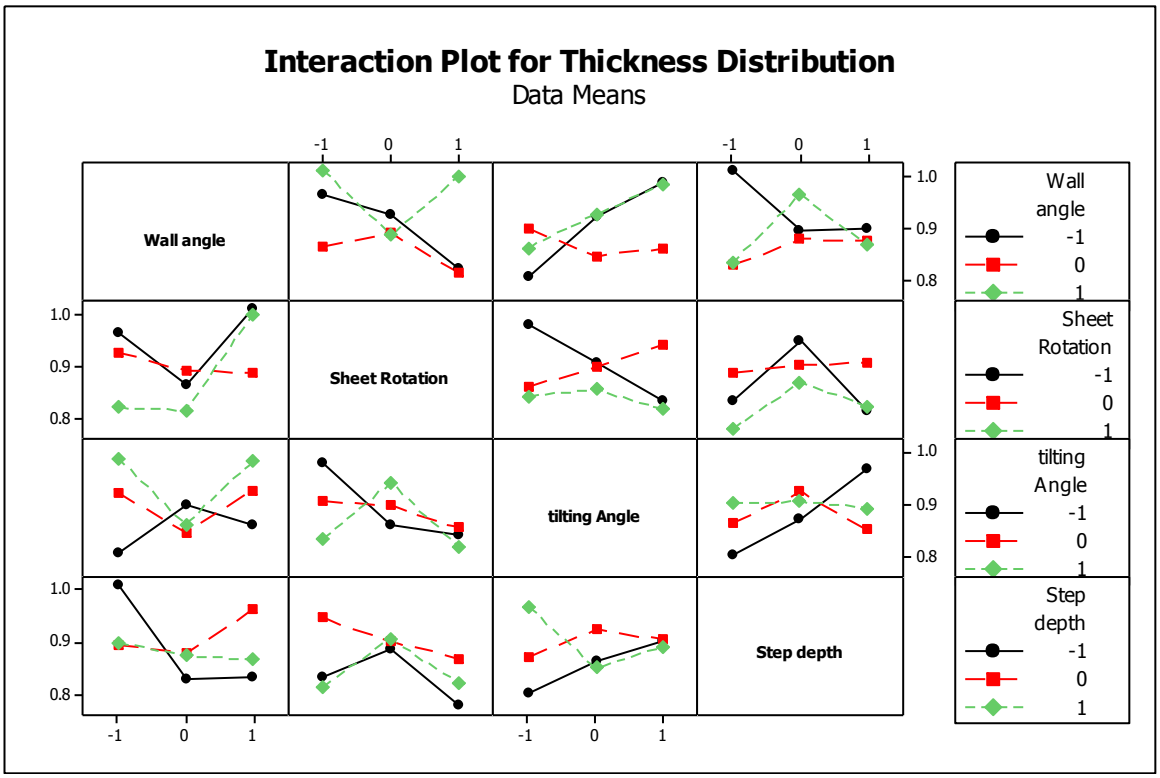

Figure 7.2 Interaction effect of process parameters on thickness distribution

Each of the two dimensional contour plot, in Figure **7.3** represents the combined effect of input parameters on sheet thinning. Here all the points which have same responses are connected to produce a contour line. As step depth has least significance on thickness distribution, the contour plot of step depth can be ignored for this parameter. Sheet rotation-wall angle and titling angle-wall angle contour plots show higher thickness area than other interaction contour plots. Titling angle and wall angle interaction contour plot has higher thickness area than rotation speed and wall angle interaction plots. Therefore, it can be concluded that inclination angle and wall angle has more effect on thickness distribution than sheet rotation and step depth respectively.

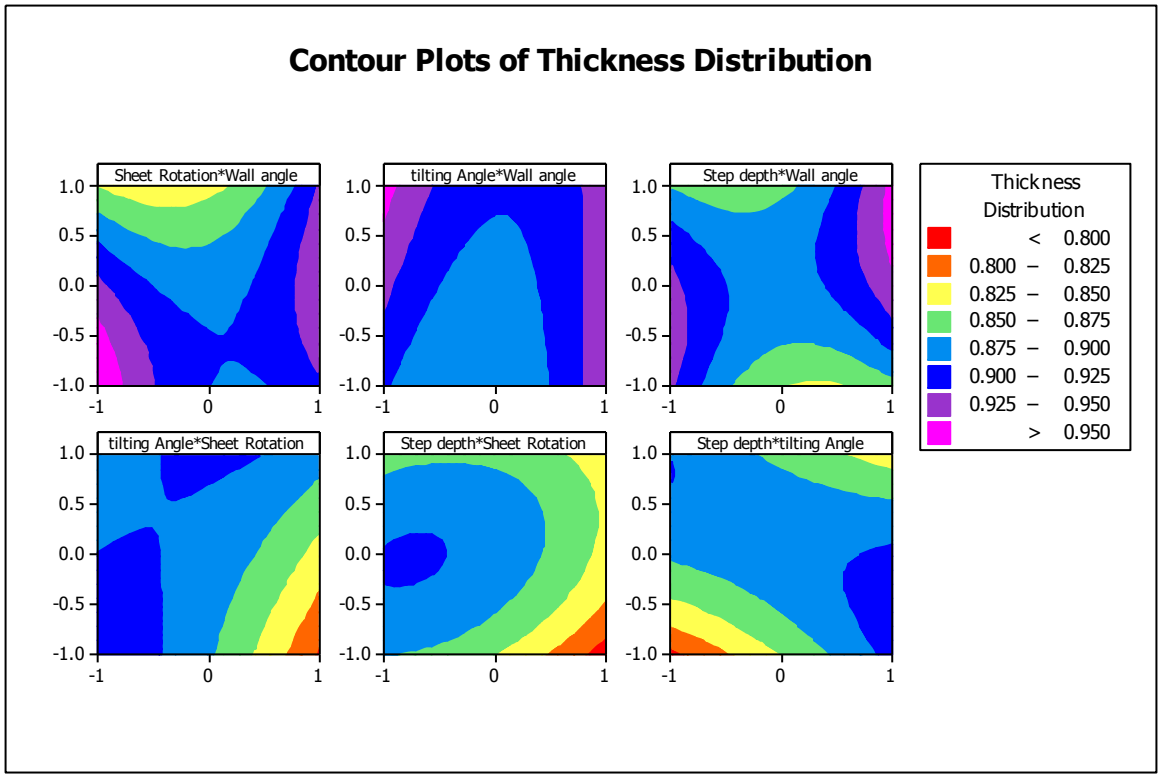

Figure 7.3 Contour plot/ interactive effect of effect of process parameters on sheet thickness distribution

7.4.2 Strain at fracture

Effective plastic strain has been measured for all the simulated as well as experimental parts. The experiments were first conducted by implementing the DOE plan. The simulation was then performed and FFLD was plotted for all the simulated results to find out the fracture strain. The depth of the fracture in formed part was measured experimentally. Effective plastic strain in simulation was measured exactly at the same depth as like experimental formed part.

ANOVA test was conducted similar to thinning test for fracture strain results to identify the most significant parameter and the interactions. ANOVA test indicates that wall angle-sheet rotation and wall angle–inclination angle interaction have very significant (P value is less than 0.05) effect compared to other parameters and their interactions. Individually inclination angle, wall angle and sheet rotation have significant effect on fracture strain compared to step depth. Inclination angle-step depth interaction has the least significance on fracture strain.

Figure 7.4 shows the interaction plot for the effect of process parameters on fracture strain. In this plot, it can be observed that none of the interactions have parallel lines which indicate that all the parameter interactions have significant effect on fracture strain. However the contour plot will give the exact relation between parameters interaction effect on output.

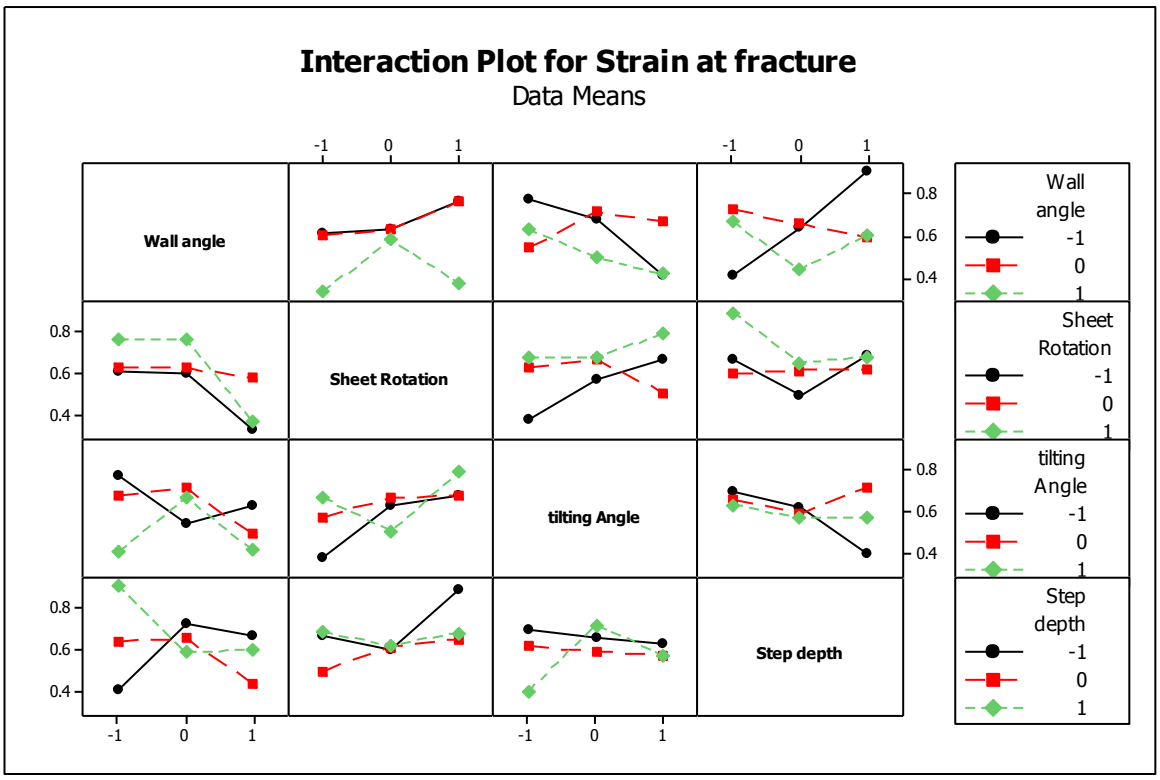

Figure 7.4 Interaction effect of process parameters on Fracture strain

Figure 7.5 indicates that strain for the step depth-wall angle, sheet rotation-wall angle, inclination angle-sheet rotation and step depth-sheet rotation is higher than other interactions. Therefore, it can be concluded that, effective plastic strain at fracture is highly affected by inclination angle, sheet rotation and wall angle and their interaction.

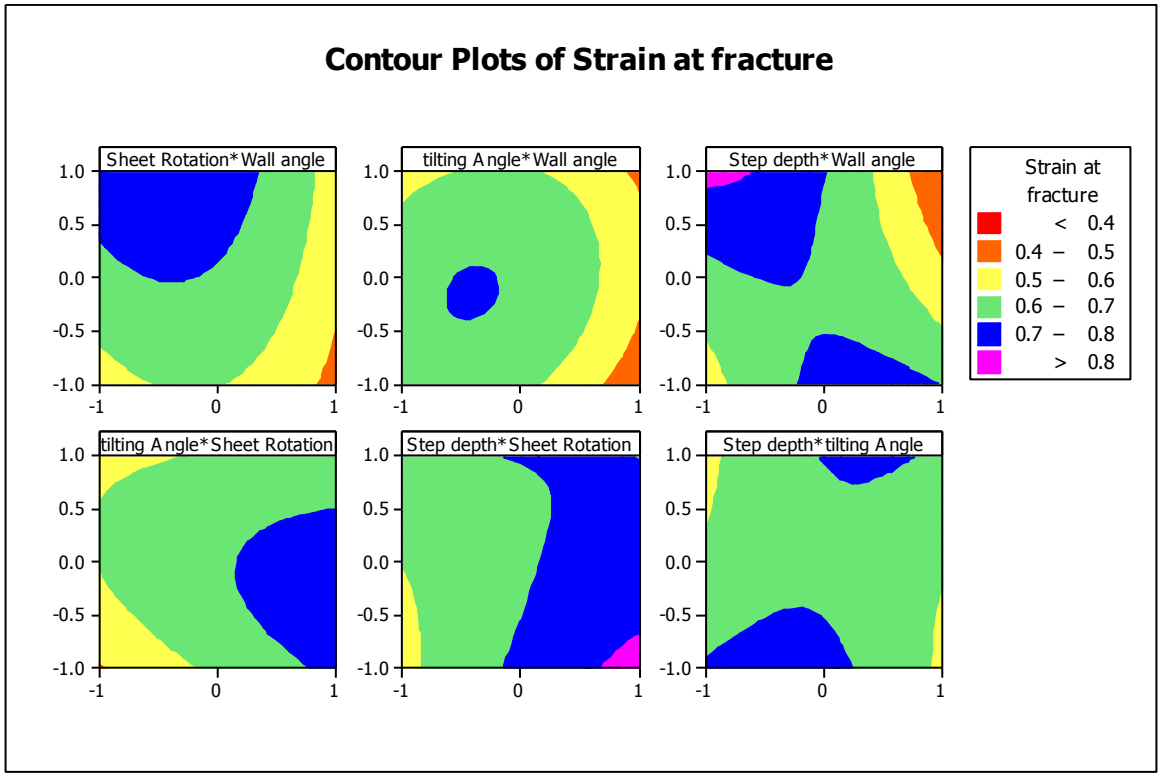

Figure 7.5 Contour plot for effect of process parameters on fracture strain

Forming limit has also been investigated for steeper wall angle parts. Unlike 70° wall angle, both RAISF and ISF have sheet failed at different forming depth for 75° and 80° wall angle parts. For 70° wall angle part, in both the process forming depth of 60mm was successful. Therefore, formability for 75° and 80° wall angle parts have been investigated at different sheet rotation speed. Sheet was marked with grids to measure the major and minor strain. After RAISF experiments at different rotational speed, due to sheet deformation major and minor strain changed. Figure 7.6 (a, b, c) shows the forming limit plot for 75° wall angle parts and it shows that, with decrease in sheet rotation, fracture limit increases due to increases in meridional strain at contact zone. Similarly Figure 7.6 (d, e, f) shows the similar results for 80° wall angle parts. It also reveals that forming limit decreases with increase in forming angle.

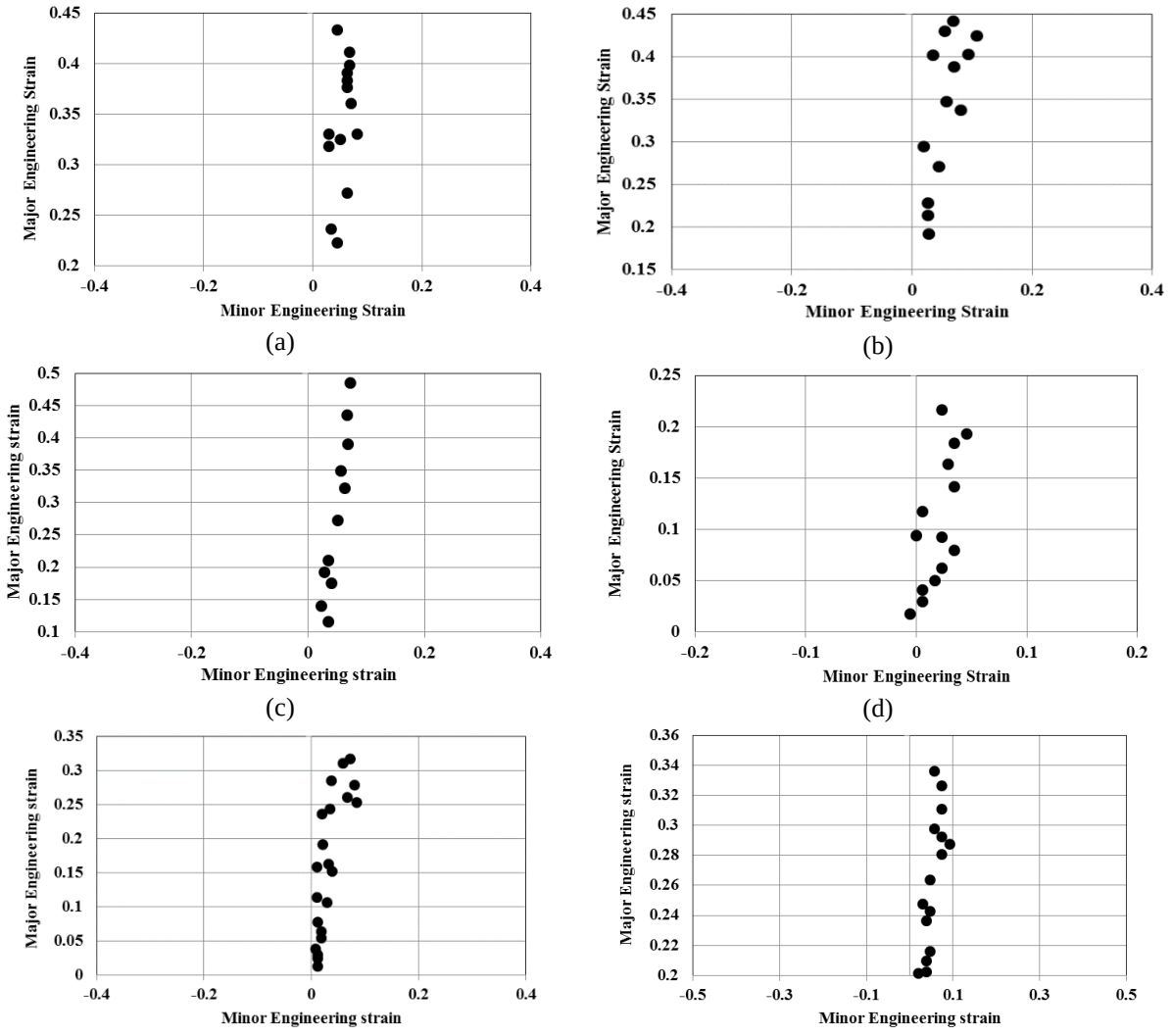

Figure 7.6 Measured strains at fracture for 75° wall angle at (a)6RPM (b)5RPM (c)4RPM, 80° wall angle at (d)6RPM (e)5RPM (f)4RPM at 15° inclination angle

Forming depth achieved in ISF and RAISF experiments have been shown in the Figure 7.7(a).

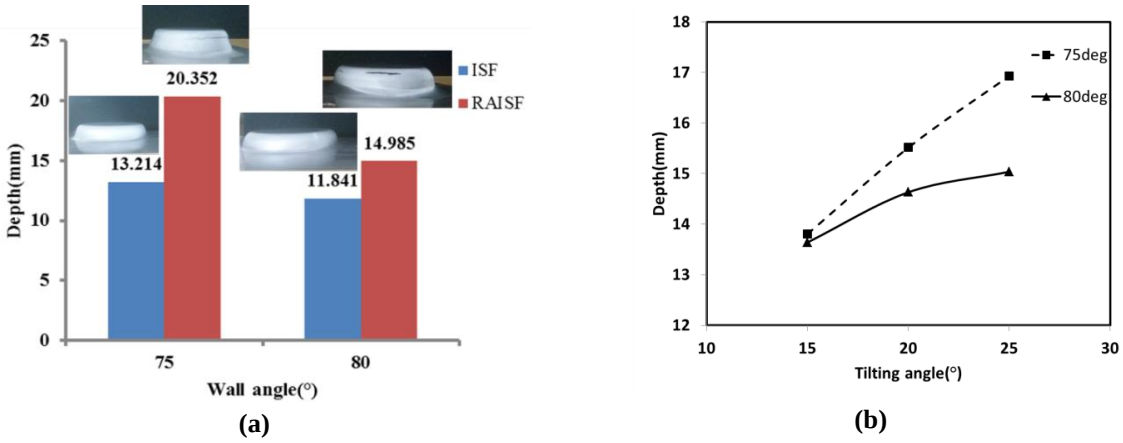

Figure 7.7 Forming depth (a) in ISF and RAISF (b) for increasing inclination and wall angle

In RAISF experiments, parts were formed at constant sheet rotational speed, inclination angle and tool velocity. In RAISF, time taken to achieve peak force is more than ISF which delays the steady state force. Both wall angle parts have been formed at different inclination angle. Figure 7.7(b) shows that by increasing the inclination angle formability of the sheet improves and better forming depth can be achieved at higher inclination angle. Strain distribution for deformed sheet has been investigated at different titling angle for 75° and 80° wall angle parts. Figure 7.8 shows that with increase in inclination angle fracture limit increases for both the wall angle parts. This reveals that by inclination the part, formability of the sheet increases.

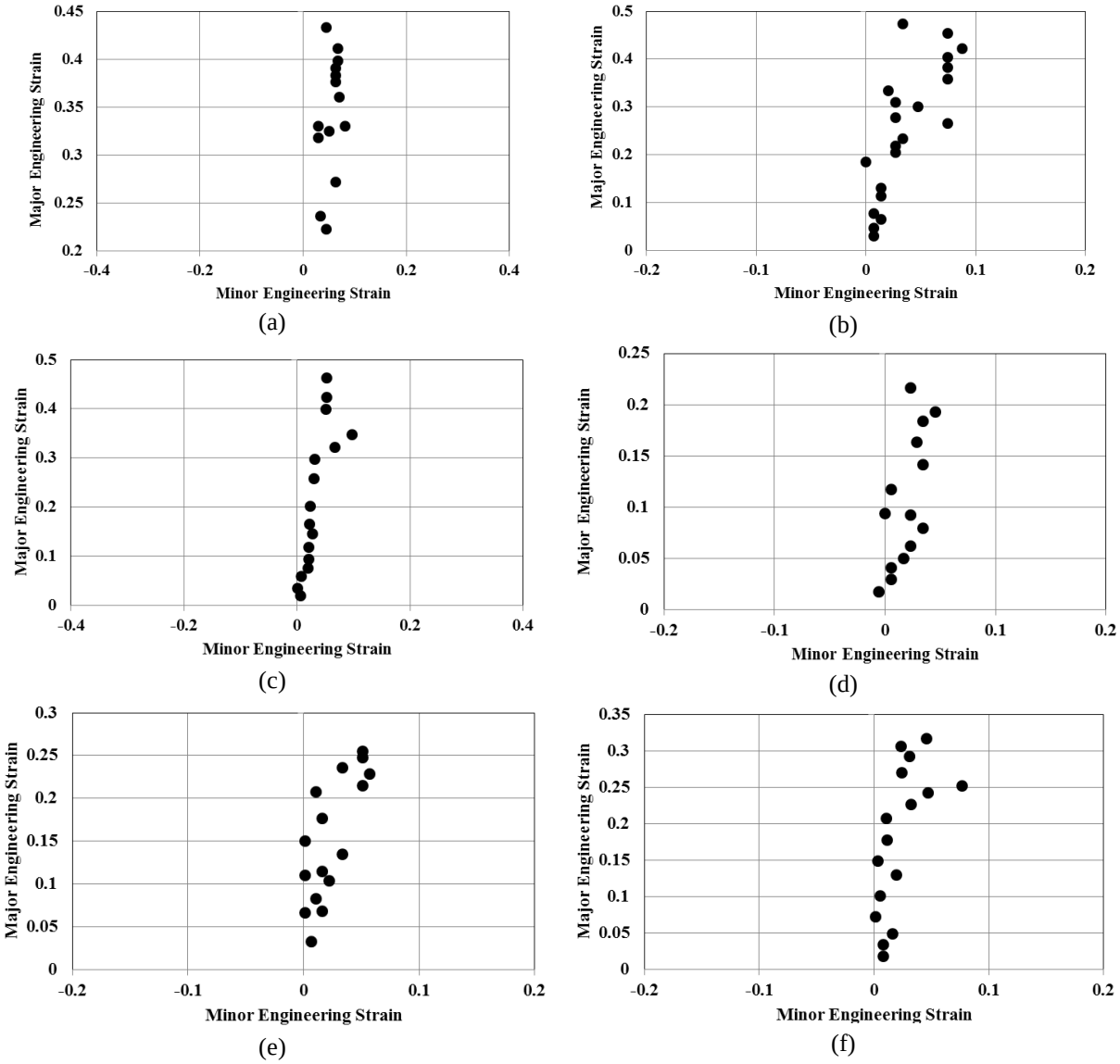

Figure 7.8 Measured strains at fracture for 75° wall angle at (a)15° (b)20° (c)25° inclination angle, 80° wall angle at (d)15° (e)20° (f)25° inclination angle (at 4RPM)

7.5 Summery

This chapter explains the effect of inclination and sheet rotation on the formability of the sheet. Experimental as well as numerical comparison of results obtained in RAISF has been compared. The formability of the material has been analyzed in terms of forming depth, thinning and fracture strain. Effect of new process parameters on sheet thinning, strain distribution and forming depth has been studied in this chapter. It can be concluded from this chapter that inclination angle of the sheet is the most significant factor for thinning and fracture strain. Interaction of wall angle with inclination angle has also significant effect on the output. However, step depth is the least significant factor for formability. Therefore, formability of the sheet can be improved by inclination the sheet by required angle. Formability increases with increase in inclination angle and decrease in sheet rotational speed. The effect of all the input parameters on formability has been investigated by planning the experiment using DOE and the results have been analyzed by implementing ANOVA and regression analysis.

CHAPTER 8

CONCLUSION AND FUTURE SCOPE

8.1 Conclusions

The thesis work was aimed at improving the material formability by manipulating the sheet in incremental sheet metal forming. Based on the work done in this research and results obtained in both experiment and simulation the following conclusions have been drawn.

- A new tool path has been designed to form the sheet incrementally on the manipulator.

The novelty of the tool path designed in the present work is that the total tool path has been subdivided between the forming tool and the robotic manipulator.

- Based on tool path planning, kinematic and dynamic analysis has been done to design a 2-DOF manipulator. The designed manipulator has been successfully fabricated and installed on 3-axis CNC vertical milling machine for RAISF experiments.

Instead of using off-the-shelf robotic manipulators, a dedicated robotic manipulator has been designed with a thorough analysis taking into account the forming forces and envelope volume. Detailed inverse kinematics has been worked out and dynamic analysis and design has been done.

- Effect of additional process parameters on the formability, forming force, thinning have been studied using numerical simulation.

Finite element method based explicit simulation model has been developed to study the parametric dependence of crucial process response variables.

- Due to inclination of the sheet, delay in bending force was observed which led to postponement of fracture in the sheet and a slight increase in peak force was observed due to sheet inclination. Sheet rotation speed has minor effect on peak forming force.
- At higher inclination angle, due to increase in scallop distance, surface roughness decreases. Combined variation in inclination angle and rotational speed increases surface roughness.
- With increase in step interval of the spiral tool path, surface quality reduces. Therefore, a controlled step internal is recommended.
- Due to increase in the scallop height at increasing inclination angle and rotational speed, surface roughness increases.

- For same wall angle, surface quality was found to be better in RAISF than ISF due to decrease in relative wall angle at tilted angle.
- Inclination angle is the most significant factor for thinning and strain distribution. Formability of the sheet increases at higher inclination angle and decreases at higher rotational speed.

8.2 Specific contribution to the research

The work done in the present thesis contributed to the problem of the incremental sheet metal forming in the following ways:

- In this thesis work one of the major advancements were to perform the incremental sheet metal forming by manipulating the sheet metal using a 2DOF manipulator and combining it with the vertical CNC milling machine. Due to addition of 2DOF to the existing process, improvement in forming has been observed.
- The deformation behavior of the sheet due to inclination and rotation of the sheet has been studied using numerical simulation and has been compared with experimental as well as ISF results.
- The effect of additional process parameters on surface quality, formability and forming force has been studied in RAISF experimentally.

8.3 Recommendation for the future work

Analysis and experimentations from this research reveals several areas that need further study. This research could be continued further in the following direction as recommended below:

- The future research can focus on forming of various other shapes in RAISF by changing the tool path algorithm. Higher inclination angle can also be tested in RAISF.
- This research can also be continued to study the deformation behavior of other materials by adding additional 2-DOF.
- There is also the need of understanding the spring back and the effect of tool vibration on the sheet deformation in RAISF.

References

[1] T. Lamminen and I. Huhtaniemi, “Hydroforming of sheet metal pairs from aluminium alloys,” *J. Mater. Process. Technol.*, vol. 115, no. 1, pp. 65–69, 2001.

[2] Y. Murakoshi, M. Takahashi, T. Sano, K. Hanada, and H. Negishi, “Inside bead forming of aluminum tube by electro-magnetic forming,” *J. Mater. Process. Technol.*, vol. 80–81, pp. 695–699, 1998.

[3] P. J. Cheng and S. C. Lin, “An analytical model for the temperature field in the laser forming of sheet metal,” *J. Mater. Process. Technol.*, vol. 101, no. 1–3, pp. 260–267, 2000.

[4] J. Jeswiet, F. Micari, G. Hirt, A. Bramley, J. Duflou, and J. Allwood, “Asymmetric Single Point Incremental Forming of Sheet Metal,” *CIRP Ann.*, vol. 54, no. 2, pp. 88–114, 2005.

[5] F. Micari, G. Ambrogio, and L. Filice, “Shape and dimensional accuracy in Single Point Incremental Forming: State of the art and future trends,” *J. Mater. Process. Technol.*, vol. 191, no. 1–3, pp. 390–395, 2007.

[6] M. Tisza, “General overview of sheet incremental forming,” *Manuf. Eng.*, vol. 55, no. 1, pp. 113–120, 2012.

[7] H. Arai, “Robotic Metal Spinning − Forming Non-axisymmetric Products Using Force Control −,” *Int. Conf. Robot. Autom. 2005 IEEE*, no. April, pp. 691–696, 2005.

[8] L. Filice, L. Fratini, and F. Micari, “Analysis of material formability in incremental forming,” *CIRP Ann. - Manuf. Technol.*, vol. 51, no. 1, pp. 199–202, 2002.

[9] J. Kim, F. C. Park, and J. M. Lee, “A New Parallel Mechanism Machine Tool Capable of Five-Face Machining,” *CIRP Ann. - Manuf. Technol.*, vol. 48, no. 1, pp. 337–340, Jan. 1999.

[10] L. Lamminen, “Incremental Sheet Forming with an Industrial Robot – Forming Limits and Their Effect on Component Design,” *Adv. Mater. Res.*, vol. 6–8, pp. 457–464, 2005.

[11] X. Liao and G. G. Wang, “Evolutionary path planning for robot assisted part handling

in sheet metal bending," *Robot. Comput. Integr. Manuf.*, vol. 19, no. 5, pp. 425–430, Oct. 2003.

[12] T. Schafer and R. D. Schraft, "Incremental sheet metal forming by industrial robots," *Rapid Prototyp. J.*, vol. 11, no. 5, pp. 278–286, 2005.

[13] L. Vihtonen, A. Puzik, and T. Katajarinne, "Comparing Two Robot Assisted Incremental Forming Methods : Incremental Forming by Pressing and Incremental Hammering," *Int. J. Mater. Form.*, vol. 1, Suppl-1, pp. 3–6, 2008.

[14] J. Belchior, M. Guillo, E. Courteille, P. Maurine, L. Leotoing, and D. Guines, "Off-line compensation of the tool path deviations on robotic machining : Application to incremental sheet forming," *Robot. Comput. Integr. Manuf.*, vol. 29, no. 4, pp. 58–69, 2013.

[15] M. Callegari, A. Gabrielli, M.-C. Palpacelli, and M. Principi, "Incremental Forming of Sheet Metal by Means of Parallel Kinematics Machines," *J. Manuf. Sci. Eng.*, vol. 130, no. 5, p. 54501, 2008.

[16] A. Puzik, "Incremental Sheet Forming with a Robot System for an Industrial Application," *Manuf. Syst. Technol. New …*, pp. 421–424, 2008.

[17] H. Meier, B. Buff, R. Laurischkat, and V. Smukala, "Increasing the part accuracy in dieless robot-based incremental sheet metal forming," *CIRP Ann. - Manuf. Technol.*, vol. 58, no. 1, pp. 233–238, 2009.

[18] H. Meier, J. Zhu, B. Buff, and R. Laurischkat, "CAx Process Chain for Two Robots Based Incremental Sheet Metal Forming," *Procedia CIRP*, vol. 3, pp. 37–42, 2012.

[19] H. Meier, S. Reese, Y. Kiliclar, and R. Laurischkat, "Increase of the Dimensional Accuracy of Sheet Metal Parts Utilizing a Model-Based Path Planning for Robot-Based Incremental Forming," *Process Mach. Interact.*, pp. 459–473, 2013.

[20] I. Chera, O. Bologa, G. Racz, and R. Breaz, "Robot-Forming - An Incremental Forming Process Using an Industrial Robot by Means of DELMIA Software Package," *Appl. Mech. Mater.*, vol. 371, pp. 416–420, 2013.

[21] J. Belchior, L. Leotoing, D. Guines, E. Courteille, and P. Maurine, "A Process / Machine coupling approach : Application to Robotized Incremental Sheet Forming," *J.*

Mater. Process. Technol., vol. 214, pp. 1605–1616, 2014.

[22] I. Paniti and M. T. A. Sztaki, "A novel , single-robot based two sided incremental sheet forming system Two robot based ISF systems Single robot based ISF system Concept of the system," pp. 547–553, 2014.

[23] K. Jackson and J. Allwood, "The mechanics of incremental sheet forming," *J. Mater. Process. Technol.*, vol. 209, no. 3, pp. 1158–1174, 2009.

[24] M. B. Silva, P. S. Nielsen, N. Bay, and P. a F. Martins, "Failure mechanisms in single-point incremental forming of metals," *Int. J. Adv. Manuf. Technol.*, vol. 56, no. 9–12, pp. 893–903, 2011.

[25] M. B. Silva, M. Skjoedt, P. a F. Martins, and N. Bay, "Revisiting the fundamentals of single point incremental forming by means of membrane analysis," *Int. J. Mach. Tools Manuf.*, vol. 48, no. 1, pp. 73–83, 2008.

[26] P. a F. Martins, N. Bay, M. Skjoedt, and M. B. Silva, "Theory of single point incremental forming," *CIRP Ann. - Manuf. Technol.*, vol. 57, no. 1, pp. 247–252, 2008.

[27] W. C. Emmens and A. H. van den Boogaard, "An overview of stabilizing deformation mechanisms in incremental sheet forming," *J. Mater. Process. Technol.*, vol. 209, no. 8, pp. 3688–3695, 2009.

[28] M. B. Silva, M. Skjoedt, a G. Atkins, N. Bay, and P. a F. Martins, "Single-point incremental forming and formability–failure diagrams," *J. Strain Anal. Eng. Des.*, vol. 43, no. 1, pp. 15–35, 2008.

[29] Y. Kiliclar, R. Laurischkat, S. Reese, and H. Meier, "The Simulation of Robot Based Incremental Sheet Metal Forming by Means of a New Solid-Shell Finite Element Technology and a Finite Elastoplastic Model with Combined Hardening," *Key Eng. Mater.*, vol. 473, pp. 875–880, 2011.

[30] T. . Kim and D. Yang, "Improvement of formability for the incremental sheet metal forming process," *Int. J. Mech. Sci.*, vol. 42, no. 7, pp. 1271–1286, 2000.

[31] J. Jeswiet and D. Young, "Forming limit diagrams for single-point incremental forming of aluminium sheet," *Proc. Inst. Mech. Eng. Part B J. Eng. Manuf.*, vol. 219, pp. 359–364, 2005.

[32] Y. Li, W. J. T. Daniel, and P. A. Meehan, “Deformation analysis in single-point incremental forming through finite element simulation,” *Int. J. Adv. Manuf. Technol.*, 2016.

[33] S. Ai, B. Lu, J. Chen, H. Long, and H. Ou, “Evaluation of deformation stability and fracture mechanism in incremental sheet forming,” *Int. J. Mech. Sci.*, vol. 124–125, pp. 174–184, 2017.

[34] Y. Li, Z. Liu, H. Lu, W. J. T. Daniel, S. Liu, and P. A. Meehan, “Efficient force prediction for incremental sheet forming and experimental validation,” *Int. J. Adv. Manuf. Technol.*, vol. 73, no. 1–4, pp. 571–587, 2014.

[35] Y. Li, W. J. T. Daniel, Z. Liu, H. Lu, and P. A. Meehan, “Deformation mechanics and efficient force prediction in single point incremental forming,” vol. 221, pp. 100–111, 2015.

[36] R. Aerens, P. Eyckens, A. Van Bael, and J. R. Duflou, “Force prediction for single point incremental forming deduced from experimental and FEM observations,” *Int. J. Adv. Manuf. Technol.*, vol. 46, no. 9–12, pp. 969–982, 2010.

[37] B. Saidi, A. Boulila, M. Ayadi, and R. Nasri, “Experimental force measurements in single point incremental sheet forming SPIF,” *Mech. Ind.*, vol. 16, no. 4, p. 410, 2015.

[38] R. Aerens, J. R. Duflou, P. Eyckens, and A. Van Bael, “Advances in force modelling for SPIF,” *Int. J. Mater. Form.*, vol. 2, no. 1, pp. 25–28, 2009.

[39] Z. Liu, Y. Li, and P. A. Meehan, “Experimental investigation of mechanical properties, formability and force measurement for AA7075-O aluminum alloy sheets formed by incremental forming,” *Int. J. Precis. Eng. Manuf.*, vol. 14, no. 11, pp. 1891–1899, 2013.

[40] A. Blaga and V. Oleksik, “A Study on the Influence of the Forming Strategy on the Main Strains, Thickness Reduction and Forces in a Single Point Incremental Forming Process,” *Adv. Mater. Sci. Eng.*, vol. 2013, no. 382635, 2013.

[41] A. Petek, K. Kuzman, and J. Kopaè, “Deformations and forces analysis of single point incremental sheet metal forming,” *Mater. Manuf. Eng.*, vol. 35, no. 2, pp. 107–116, 2009.

[42] C. H. Wang, W. J. T. Daniel, H. B. Lu, S. Liu, and P. A. Meehan, “An Experimental and Numerical Study on Forming Force, Fracture Behavior, and Strain States in Two Point Incremental Forming Process,” *Key Eng. Mater.*, vol. 725, pp. 586–591, 2016.

[43] I. Bagudanch, G. Centeno, C. Vallellano, and M. L. Garcia-Romeu, “Forming force in Single Point Incremental Forming under different bending conditions,” *Procedia Eng.*, vol. 63, pp. 354–360, 2013.

[44] G. Centeno, I. Bagudanch, A. J. Martínez-Donaire, M. L. García-Romeu, and C. Vallellano, “Critical analysis of necking and fracture limit strains and forming forces in single-point incremental forming,” *Mater. Des.*, vol. 63, pp. 20–29, 2014.

[45] I. Bagudanch, M. L. Garcia-Romeu, G. Centeno, a. Elías-Zúñiga, and J. Ciurana, “Forming Force and Temperature Effects on Single Point Incremental Forming of Polyvinylchloride,” *J. Mater. Process. Technol.*, vol. 219, pp. 221-229, 2015.

[46] K. A. Al-Ghamdi and G. Hussain, “Forming forces in incremental forming of a geometry with corner feature: investigation into the effect of forming parameters using response surface approach,” *Int. J. Adv. Manuf. Technol.*, vol. 76, no. 9–12, pp. 2185–2197, 2014.

[47] P. Shrivastava and P. Tandon, “Investigation of the Effect of Grain Size on Forming Forces in Single Point Incremental Sheet Forming,” *Procedia Manuf.*, vol. 2, pp. 41–45, 2015.

[48] J. Wang, M. Nair, and Y. Zhang, “An Efficient Force Prediction Strategy in Single Point Incremental Sheet Forming,” *Procedia Manuf.*, vol. 5, pp. 761–771, 2016.

[49] A. Singh and A. Agrawal, “Comparison of deforming forces, residual stresses and geometrical accuracy of deformation machining with conventional bending and forming,” *J. Mater. Process. Technol.*, vol. 234, pp. 259–271, 2016.

[50] P. Li, J. He, Q. Liu, M. Yang, Q. Wang, Q. Yuan, and Y. Li, “Evaluation of forming forces in ultrasonic incremental sheet metal forming,” *Aerosp. Sci. Technol.*, vol. 63, pp. 132-139, 2017.

[51] J. Li, J. Hu, J. Pan, and P. Geng, “Thickness distribution and design of a multi-stage process for sheet metal incremental forming,” *Int. J. Adv. Manuf. Technol.*, vol. 62, no.

9–12, pp. 981–988, 2011.

[52] M. S. Shim and J. J. Park, “The formability of aluminum sheet in incremental forming,” *J. Mater. Process. Technol.*, vol. 113, no. 1–3, pp. 654–658, 2001.

[53] J. M. Allwood, D. R. Shouler, and A. E. Tekkaya, “The Increased Forming Limits of Incremental Sheet Forming Processes,” *Key Eng. Mater.*, vol. 344, pp. 621–628, 2007.

[54] J. Li, P. Geng, and J. Shen, “Numerical simulation and experimental investigation of multistage incremental sheet forming,” *Int. J. Adv. Manuf. Technol.*, vol. 68, no. 9–12, pp. 2637–2644, 2013.

[55] A. Bhattacharya, K. Maneesh, N. V. Reddy, and J. Cao, “Formability and Surface Finish Studies in Single Point Incremental Forming,” *J. Manuf. Sci. Eng.*, vol. 133, no. 6, p. 61020, 2011.

[56] M. Ham and J. Jeswiet, “Single point incremental forming and the forming criteria for AA3003,” *CIRP Ann. - Manuf. Technol.*, vol. 55, no. 1, pp. 241–244, 2006.

[57] Y. Li, Z. Liu, H. Lu, W. J. T. B. Daniel, and P. A. Meehan, “Experimental Study and Efficient Prediction on Forming Forces in Incremental Sheet Forming,” vol. 939, pp. 313–321, 2014.

[58] J. R. Duflou, B. Callebaut, J. Verbert, and H. De Baerdemaeker, “Laser assisted incremental forming: Formability and accuracy improvement,” *CIRP Ann. - Manuf. Technol.*, vol. 56, no. 1, pp. 273–276, 2007.

[59] G. Fan, L. Gao, G. Hussain, and Z. Wu, “Electric hot incremental forming: A novel technique,” *Int. J. Mach. Tools Manuf.*, vol. 48, no. 15, pp. 1688–1692, 2008.

[60] R. Liu, B. Lu, D. Xu, J. Chen, F. Chen, and H. Ou, “Development of novel tools for electricity-assisted incremental sheet forming of titanium alloy,” vol. 85, no. 5-8, pp.1137-1144, 2015.

[61] D. Fritzen, A. Daleffe, J. Castelan, and L. Schaeffer, “Brass 70/30 and Incremental Sheet Forming Process,” *Key Eng. Mater.*, vol. 554–557, pp. 1419–1431, 2013.

[62] G. Buffa, D. Campanella, and L. Fratini, “On the improvement of material formability in SPIF operation through tool stirring action,” *Int. J. Adv. Manuf. Technol.*, vol. 66,

no. 9–12, pp. 1343–1351, 2013.

[63] G. Hussain, L. Gao, N. Hayat, and N. U. Dar, “The formability of annealed and pre-aged AA-2024 sheets in single-point incremental forming,” *Int. J. Adv. Manuf. Technol.*, vol. 46, no. 5–8, pp. 543–549, 2010.

[64] G. Ambrogio and F. Gagliardi, “Temperature variation during high speed incremental forming on different lightweight alloys,” *Int. J. Adv. Manuf. Technol.*, vol. 76, no. 9–12, pp. 1819–1825, 2014.

[65] C. Lu, “Study on prediction of surface quality in machining process,” *J. Mater. Process. Technol.*, vol. 205, no. 1–3, pp. 439–450, 2008.

[66] E. Hagan and J. Jeswiet, “Analysis of surface roughness for parts formed by computer numerical controlled incremental forming,” *Proc. Inst. Mech. Eng. Part B J. Eng. Manuf.*, vol. 218, no. 10, pp. 1307–1312, 2004.

[67] A. Attanasio, E. Ceretti, C. Giardini, and L. Mazzoni, “Asymmetric two points incremental forming: Improving surface quality and geometric accuracy by tool path optimization,” *J. Mater. Process. Technol.*, vol. 197, no. 1–3, pp. 59–67, 2008.

[68] G. Ambrogio, L. Filice, and G. L. Manco, “Considerations on the incremental forming of deep geometries,” *Int. J. Mater. Form.*, vol. 1, no. SUPPL-1, pp. 1143–1146, 2008.

[69] M. C. Radu and I. Cristea, “Processing Metal Sheets by SPIF and Analysis of Parts Quality,” *Mater. Manuf. Process.*, vol. 28, no. 3, pp. 287–293, 2013.

[70] V. Mugendiran, a. Gnanavelbabu, and R. Ramadoss, “Parameter Optimization for Surface Roughness and Wall Thickness on AA5052 Aluminium alloy by Incremental Forming using Response Surface Methodology,” *Procedia Eng.*, vol. 97, pp. 1991–2000, 2014.

[71] Z. Liu, S. Liu, Y. Li, and P. A. Meehan, “Modeling and Optimization of Surface Roughness in Incremental Sheet Forming using a Multi-objective Function,” *Mater. Manuf. Process.*, vol. 29, no. 7, pp. 808–818, 2014.

[72] S. Kurra, N. Hifzur Rahman, S. P. Regalla, and A. K. Gupta, “Modeling and optimization of surface roughness in single point incremental forming process,” *J. Mater. Res. Technol.*, vol. 4, no. 3, pp. 304–313, 2015.

[73] H. Khalatbari, A. Iqbal, X. Shi, L. Gao, G. Hussain, and M. Hashemipour, “High-Speed Incremental Forming Process: A Trade-Off Between Formability and Time Efficiency,” *Mater. Manuf. Process.*, vol. 30, no. 11, pp. 1354–1363, 2015.

[74] S. A. Najafabady and A. Ghaei, “An experimental study on dimensional accuracy, surface quality, and hardness of Ti-6Al-4 V titanium alloy sheet in hot incremental forming,” *Int. J. Adv. Manuf. Technol.*, vol. 87, no. 9–12, pp. 3579–3588, 2016.

[75] V. Gulati, A. Aryal, P. Katyal, and A. Goswami, “Process Parameters Optimization in Single Point Incremental Forming,” *J. Inst. Eng. Ser. C*, vol. 97, no. 2, pp. 221–229, 2015.

[76] A. Mulay, S. Ben, S. Ismail, and A. Kocanda, “Experimental investigations into the effects of SPIF forming conditions on surface roughness and formability by design of experiments,” *J. Brazilian Soc. Mech. Sci. Eng.*, vol. 39, no. 1, pp. 3997-4010, 2017.

[77] S. Gatea, H. Ou, and G. McCartney, “Review on the influence of process parameters in incremental sheet forming,” *Int. J. Adv. Manuf. Technol.*, vol. 87, pp. 1–21, 2016.

[78] A. Formisano, L. Boccarusso, L. Carrino, M. Durante, A. Langella, F. M. C. Minutolo, and A. Squillace, “Formability and surface quality of incrementally formed grade 1 titanium thin sheets,” *Key Eng. Mater.*, vol. 716, pp. 99–106, 2016.

[79] W. K. H. Sarraji, J. Hussain, and W.-X. Ren, “Experimental Investigations on Forming Time in Negative Incremental Sheet Metal Forming Process,” *Mater. Manuf. Process.*, vol. 27, no. 5, pp. 499–506, 2012.

[80] O. Lasunon and W. A. Knight, “Comparative investigation of single-point and double-point incremental sheet metal forming processes,” *Proc. Inst. Mech. Eng. Part B J. Eng. Manuf.*, vol. 221, no. 12, pp. 1725–1732, 2007.

[81] L. W. Ma and J. H. Mo, “Three-dimensional finite element method simulation of sheet metal single-point incremental forming and the deformation pattern analysis,” *Proc. Inst. Mech. Eng. Part B J. Eng. Manuf.*, vol. 222, no. 3, pp. 373–380, 2008.

[82] S. Dejardin, S. Thibaud, J. C. Gelin, and G. Michel, “Experimental investigations and numerical analysis for improving knowledge of incremental sheet forming process for sheet metal parts,” *J. Mater. Process. Technol.*, vol. 210, no. 2, pp. 363–369, 2010.

[83] P. Flores, L. Duchêne, C. Bouffioux, T. Lelotte, C. Henrard, N. Pernin, A. Van Bael, S. He, J. Duflou, and A.M. Habraken, “Model identification and FE simulations: Effect of different yield loci and hardening laws in sheet forming,” *Int. J. Plast.*, vol. 23, no. 3, pp. 420–449, 2007.

[84] M. B. Silva, M. Skjoedt, N. Bay, and P. A. F. Martins, “Revisiting single-point incremental forming and formability/failure diagrams by means of finite elements and experimentation,” *J. Strain Anal. Eng. Des.*, vol. 44, no. 4, pp. 221–234, 2009.

[85] M. Bambach, “Performance Assessment of Element Formulations and Constitutive Laws for the Simulation of Incremental Sheet Forming (ISF),” *Proc. VIII Int.*, pp. 1–4, 2005.

[86] R. Malhotra, L. Xue, T. Belytschko, and J. Cao, “Mechanics of fracture in single point incremental forming,” *J. Mater. Process. Technol.*, vol. 212, no. 7, pp. 1573–1590, 2012.

[87] J. Smith, R. Malhotra, W. K. Liu, and J. Cao, “Deformation mechanics in single-point and accumulative double-sided incremental forming,” *Int. J. Adv. Manuf. Technol.*, vol. 69, no. 5–8, pp. 1185–1201, 2013.

[88] C. Robert, A. Delamézire, P. Dal Santo, and J. L. Batoz, “Comparison between incremental deformation theory and flow rule to simulate sheet-metal forming processes,” *J. Mater. Process. Technol.*, vol. 212, no. 5, pp. 1123–1131, 2012.

[89] C. Robert, P. Dal Santo, A. Delamézière, A. Potiron, and J. L. Batoz, “On some computational aspects for incremental sheet metal forming simulations,” *Int. J. Mater. Form.*, vol. 1, no. SUPPL. 1, pp. 1195–1198, 2008.

[90] J. I. V. Sena, C. Lequesne, L. Duchene, A. M. Habraken, R. A.F. Valente, R. J. A. de Sousa, "Single point incremental forming simulation with adaptive remeshing technique using solid-shell elements", *Engineering Computations*, vol. 33 no. 5, pp.1388-1421, 2016.

[91] S. Kurra and S. P. Regalla, “Effect of mesh parameters in finite element simulation of single point incremental sheet forming process,” *Procedia Mater. Sci.*, vol. 6, pp. 376–382, 2014.

[92] S. Kurra and S. P. Regalla, “Effect of Time Scaling and Mass Scaling in Numerical Simulation of Incremental Forming,” *Appl. Mech. Mater.*, vol. 612, pp. 105–110, 2014.

[93] L. Filice, G. Ambrogio, and M. Gaudioso, “Optimised tool-path design to reduce thinning in incremental sheet forming process,” *Int. J. Mater. Form.*, vol. 6, no. 1, pp. 173–178, 2013.

[94] S. Kurra, A. Khan, and S. P. Regalla, “Tool Path Definition for Numerical Simulation of Single Point Incremental Forming,” *Procedia Eng.*, vol. 64, pp. 536–545, 2013.

[95] L. Fratini, G. Ambrogio, R. Di Lorenzo, L. Filice, and F. Micari, “Influence of mechanical properties of the sheet material on formability in single point incremental forming,” *CIRP Ann. - Manuf. Technol.*, vol. 53, no. 1, pp. 207–210, 2004.

[96] G. Ambrogio, L. Filice, and F. Micari, “A force measuring based strategy for failure prevention in incremental forming,” *J. Mater. Process. Technol.*, vol. 177, no. 1–3, pp. 413–416, 2006.

[97] S. He, J. Gu, H. Sol, A. Van Bael, P. van Houtte, Y. Tunckol, and J. R. Duflou, “Determination of Strain in Incremental Sheet Forming Process,” *Key Eng. Mater.*, vol. 344, pp. 503–510, 2007.

[98] Y. H. Ji and J. J. Park, “Formability of magnesium AZ31 sheet in the incremental forming at warm temperature,” *J. Mater. Process. Technol.*, vol. 201, no. 1–3, pp. 354–358, 2008.

[99] M. Bambach, “A geometrical model of the kinematics of incremental sheet forming for the prediction of membrane strains and sheet thickness,” *J. Mater. Process. Technol.*, vol. 210, no. 12, pp. 1562–1573, 2010.

[100] A. Fatemi and B. M. Dariani, “The effect of normal and through thickness shear stresses on the formability of isotropic sheet metals,” *J. Brazilian Soc. Mech. Sci. Eng.*, vol. 38, no. 1, pp. 119–131, 2016.

[101] S. Wojciechowski, “The estimation of cutting forces and specific force coefficients during finishing ball end milling of inclined surfaces,” *Int. J. Mach. Tools Manuf.*, vol. 89, pp. 110–123, 2015.

[102] M. J. B. Fard and E. V. Bordatchev, “Experimental study of the effect of tool orientation in five-axis micro-milling of brass using ball-end mills,” *Int. J. Adv. Manuf. Technol.*, vol. 67, no. 5–8, pp. 1079–1089, 2013.

[103] Y. Fang, B. Lu, J. Chen, D. K. Xu, and H. Ou, “Analytical and experimental investigations on deformation mechanism and fracture behavior in single point incremental forming,” *J. Mater. Process. Technol.*, vol. 214, no. 8, pp. 1503–1515, 2014.

[104] A. Bansal, R. Lingam, S. K. Yadav, and N. V. Reddy, “Prediction of forming forces in single point incremental forming,” *J. Manuf. Process.*, vol. 28, no.3, pp. 486-496, 2017.

[105] B. Lu, Y. Fang, D.K. Xu, J. Chen, H. Ou, N.H. Moser, and J. Cao, “Mechanism investigation of friction-related effects in single point incremental forming using a developed oblique roller-ball tool,” *Int. J. Mach. Tools Manuf.*, vol. 85, pp. 14–29, 2014.

[106] K. P. Jackson, J. M. Allwood, and M. Landert, “Incremental forming of sandwich panels,” *J. Mater. Process. Technol.*, vol. 204, no. 1–3, pp. 290–303, 2008.

[107] G. Hussain, L. Gao, and N. Hayat, “Forming Parameters and Forming Defects in Incremental Forming of an Aluminum Sheet: Correlation, Empirical Modeling, and Optimization: Part A,” *Mater. Manuf. Process.*, vol. 26, no. 12, pp. 1546–1553, 2011.

[108] Y. Li, Z. Liu, W. J. T. (Bill. Daniel, and P. a. Meehan, “Simulation and Experimental Observations of Effect of Different Contact Interfaces on the Incremental Sheet Forming Process,” *Mater. Manuf. Process.*, vol. 29, pp. 121–128, 2014.

[109] R. Malhotra, N. V. Reddy, and J. Cao, “Automatic 3D Spiral Toolpath Generation for Single Point Incremental Forming,” *J. Manuf. Sci. Eng.*, vol. 132, no. 6, p. 61003, 2010.

[110] A. Blaga, O. Bologa, V. Oleksik, and R. Breaz, “Influence of tool path on main strains, thickness reduction and forces in single point incremental forming process,” *Proc. Manuf. Syst.*, vol. 6, no. 4, pp. 2–7, 2011.

[111] T. McAnulty, J. Jeswiet, and M. Doolan, “Formability in single point incremental

forming: A comparative analysis of the state of the art," *CIRP J. Manuf. Sci. Technol.*, vol. 16, pp. 43–54, 2017.

[112] J. Jeswiet, "Asymmetric Incremental Sheet Forming," *Adv. Mater. Res.*, vol. 6–8, pp. 35–58, 2005.

Appendix

Appendix A (Manipulator)

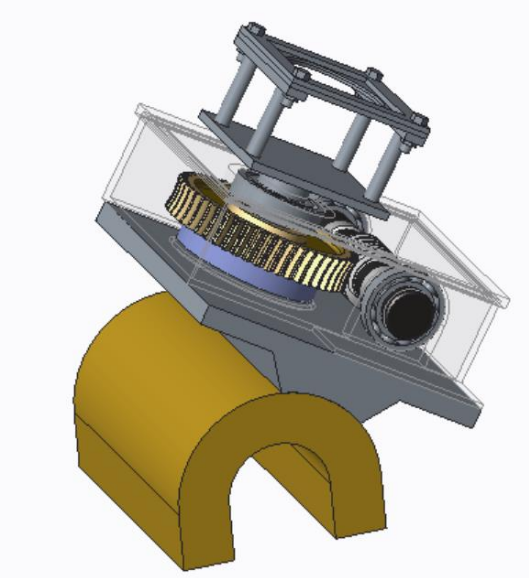

Manipulator

Inclination table

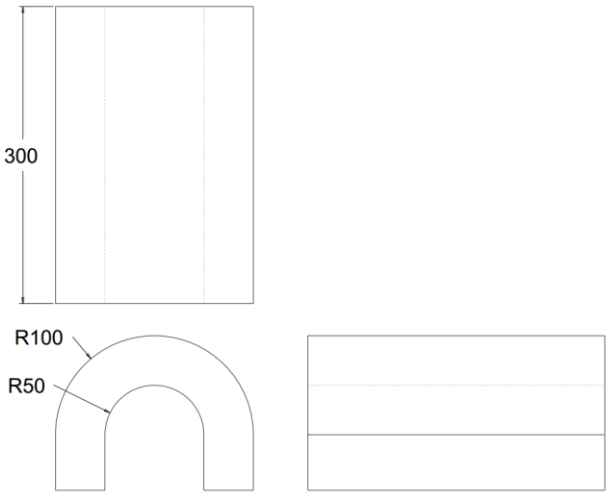

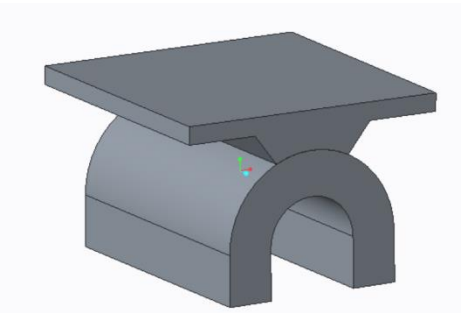

Link-1

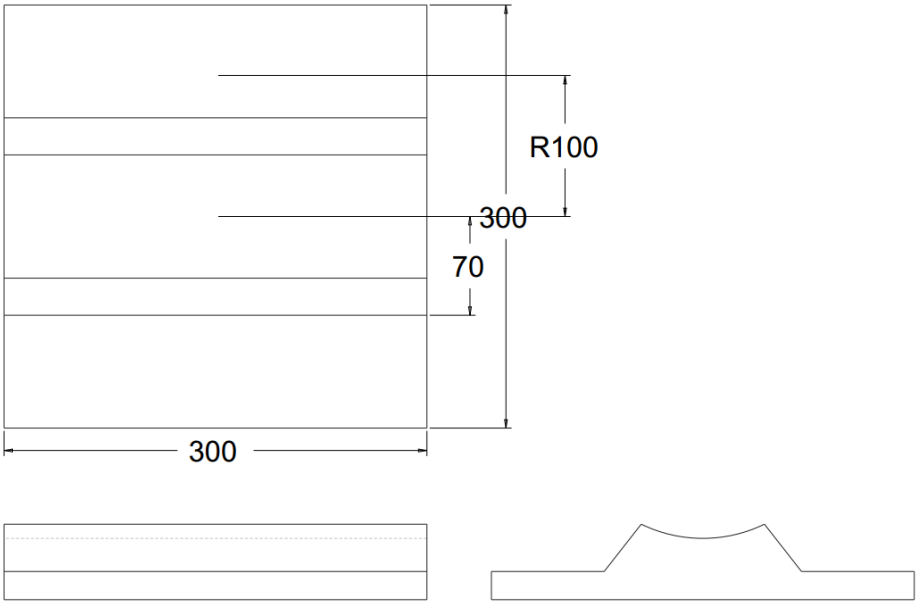

Link-2

Inclination table Link-1 and 2

End Effector

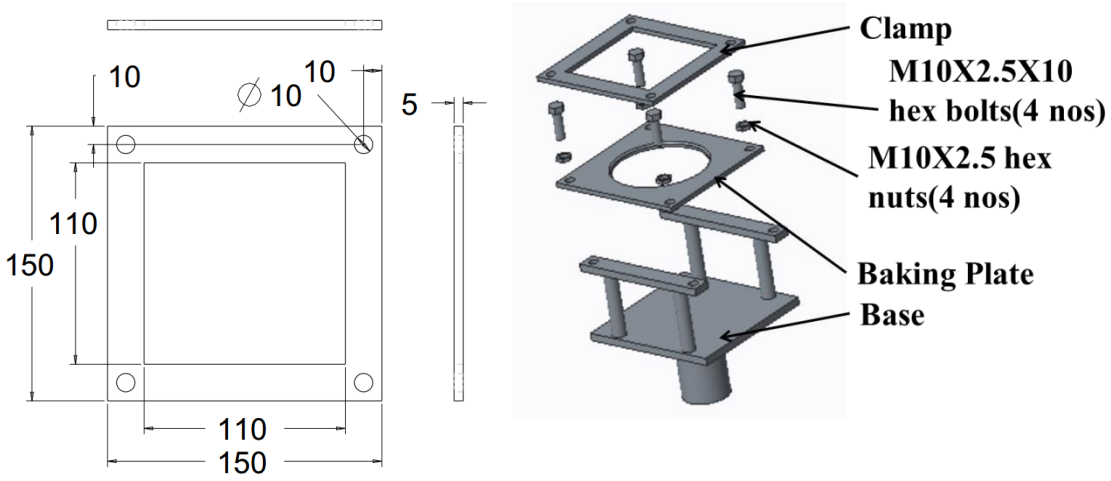

Clamp

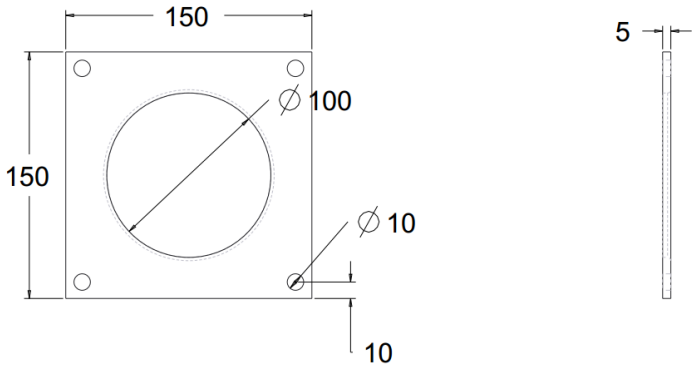

Baking Plate

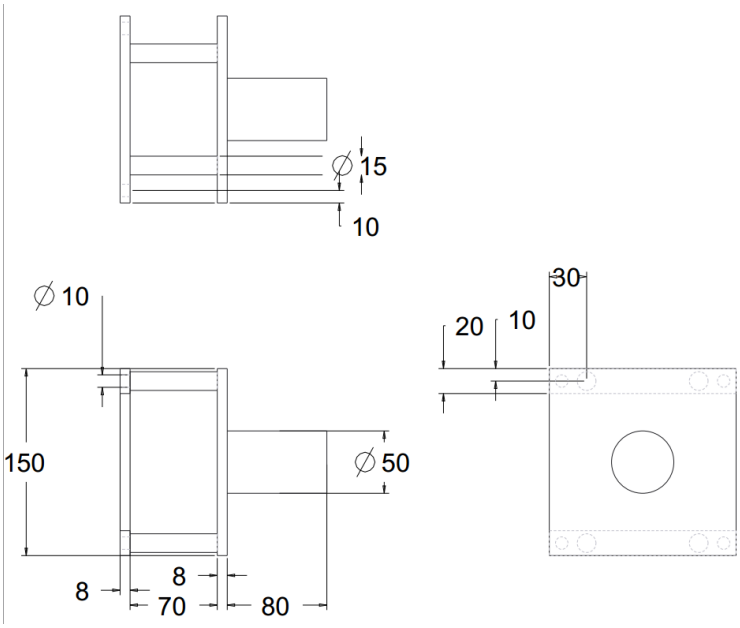

Base

Gear box

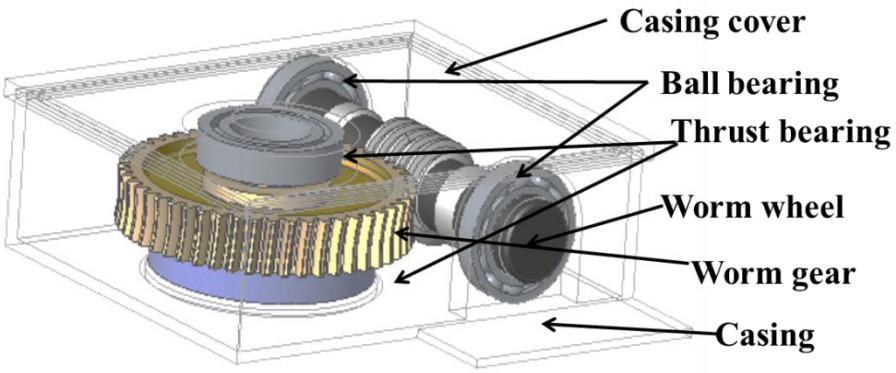

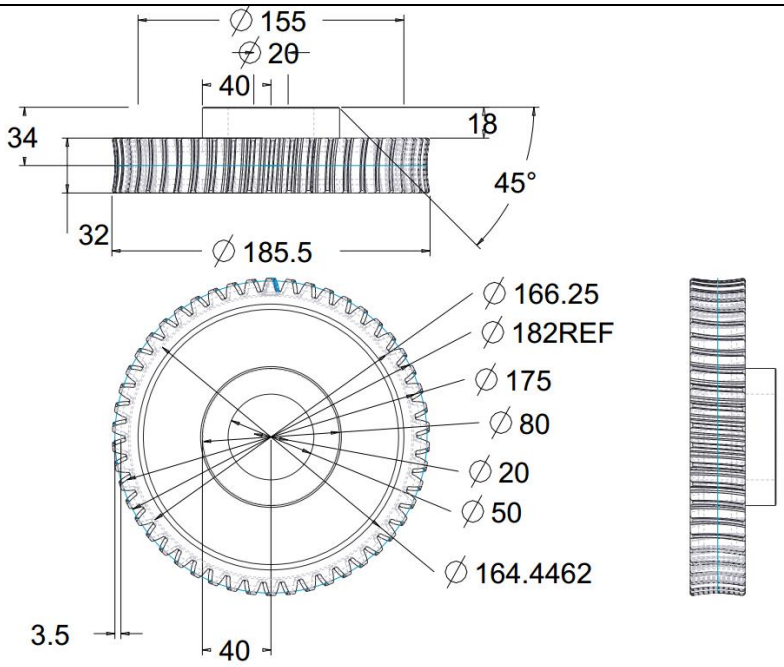

Duplex gear

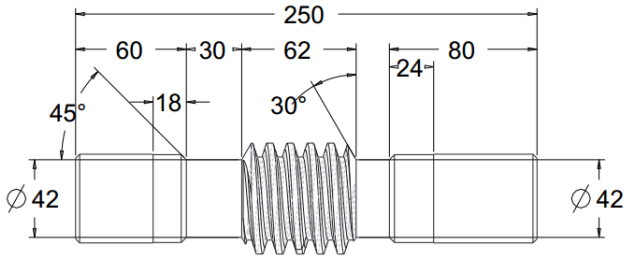

Worm Wheel

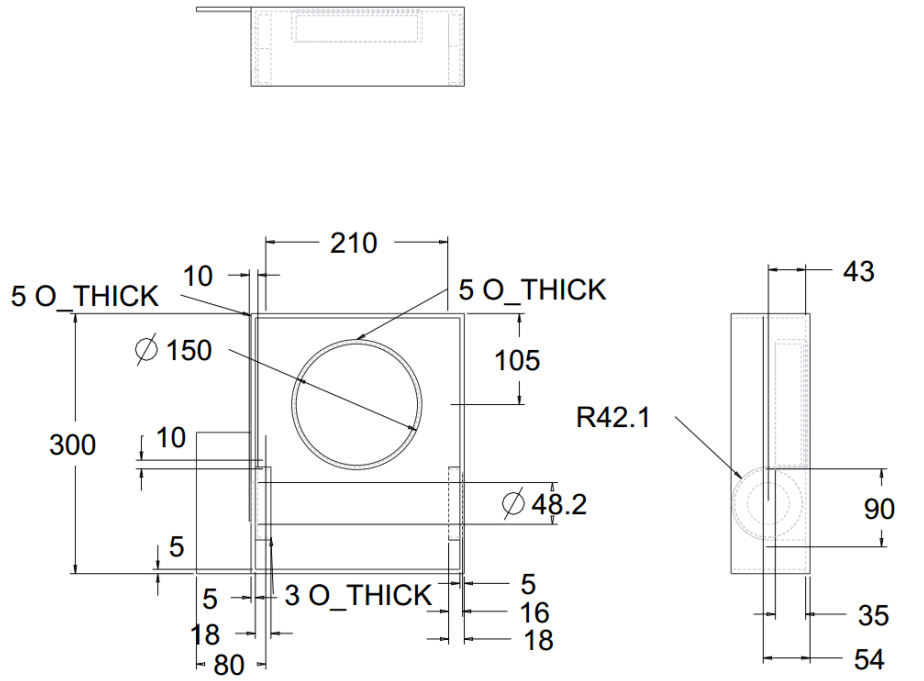

Casing

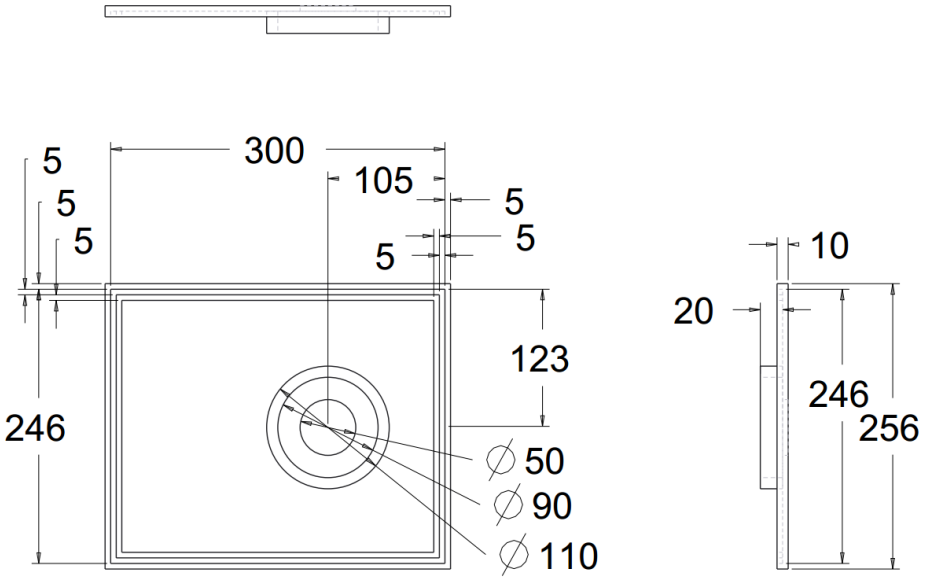

Casing cover

Control system

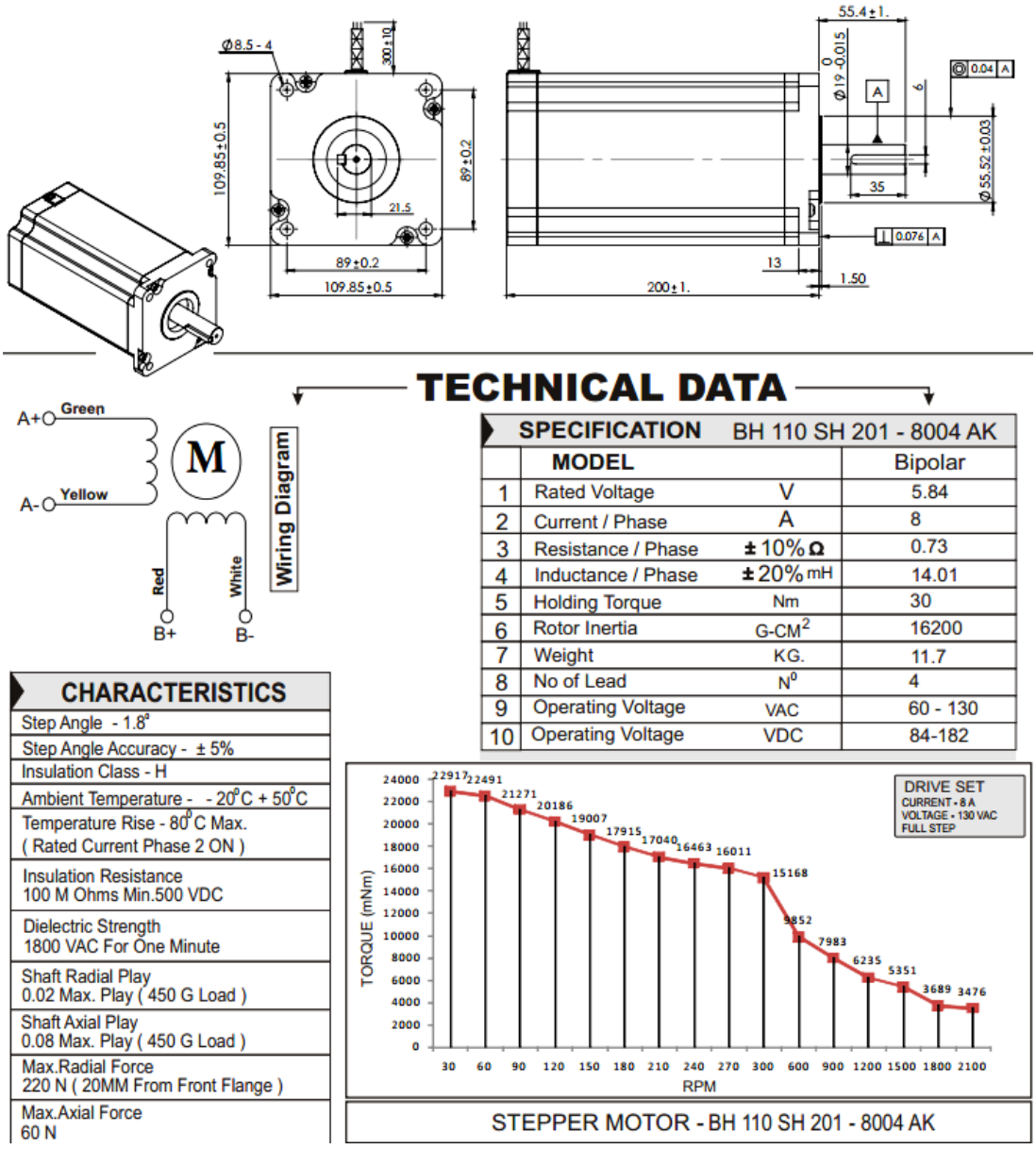

Technical specification of Stepper motor

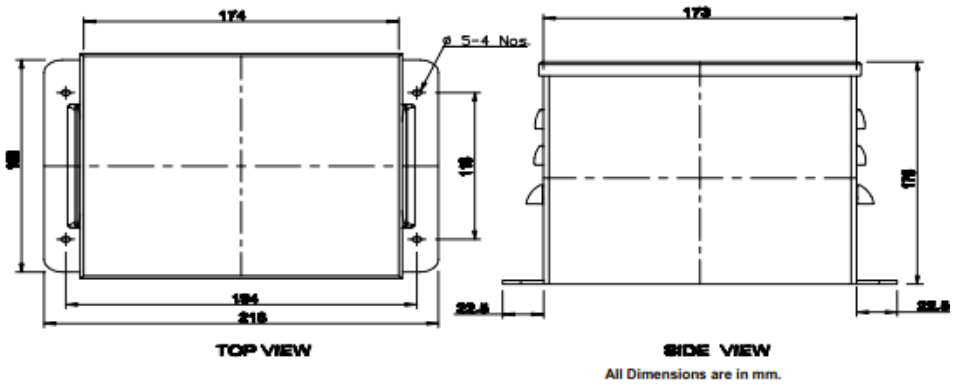

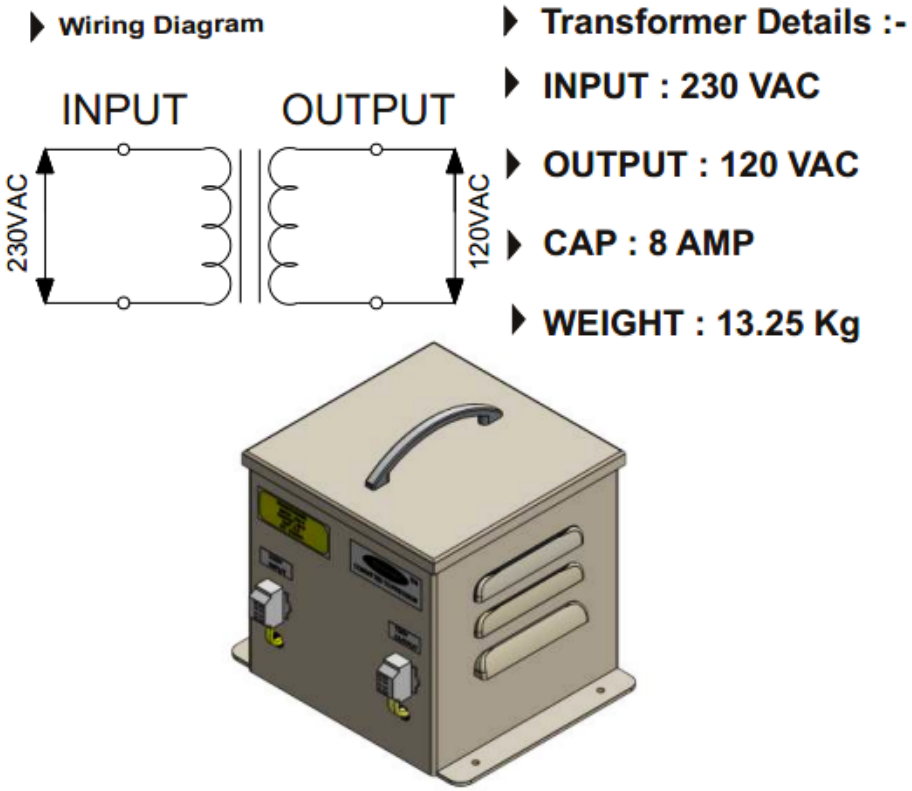

Technical specification of 120V Transformer

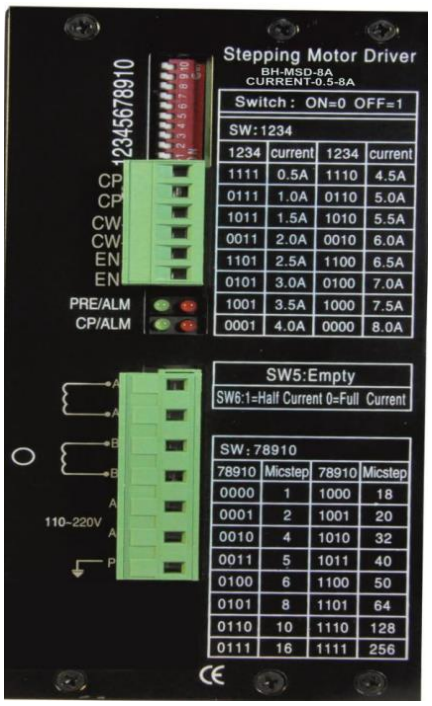

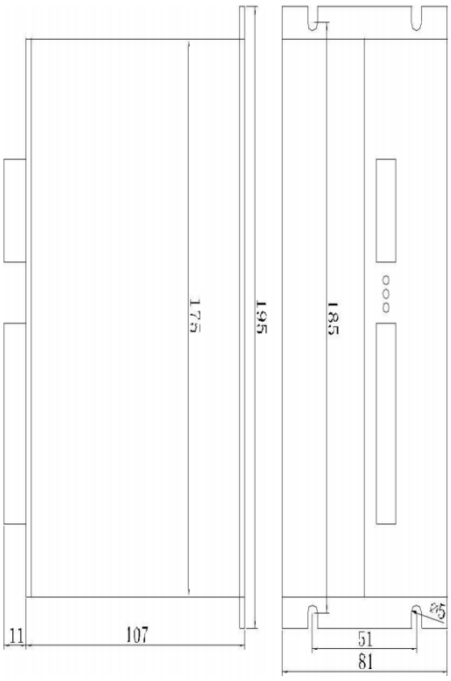

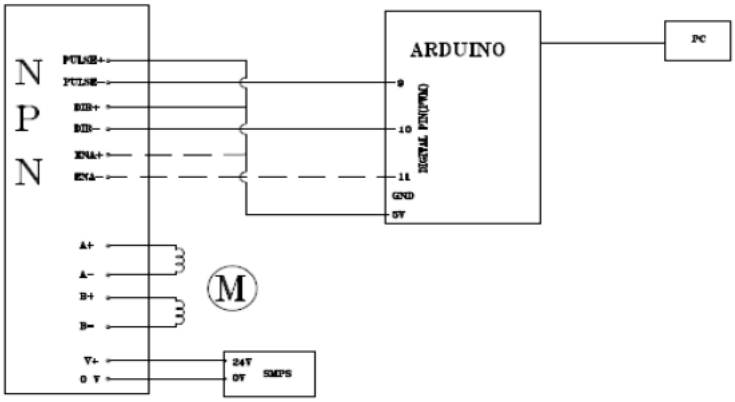

Technical specification of 8A Micro stepping driver

Appendix B (Sample Code)

```
N10G71G94G75G90
75degcircular   9-7-2017
SRF_MILL1
TOOL NUMBER:1
SPINDLE RPM:150'
G0Y0.Z0.T1M6
S150
Y-38.637Z-9.434
G1Z-9.434F2.5.
Y-38.637Z-10.352F2.5
Y-38.575Z-10.439
Y-38.514Z-10.527
Y-38.453Z-10.614
Y-38.392Z-10.701
Y-38.331Z-10.788
Y-38.27Z-10.875
Y-38.209Z-10.962
Y-38.148Z-11.05
Y-38.087Z-11.137
Y-38.026Z-11.224
Y-37.965Z-11.311
Y-37.904Z-11.398
Y-37.843Z-11.486
Y-37.782Z-11.573
Y-37.721Z-11.66
Y-37.66Z-11.747
Y-37.599Z-11.834
Y-37.538Z-11.921
Y-37.477Z-12.009
Y-37.416Z-12.096
Y-37.355Z-12.183
Y-37.294Z-12.27
Y-37.233Z-12.357
Y-37.172Z-12.444
Y-37.111Z-12.532
Y-37.05Z-12.619
Y-36.988Z-12.706
Y-36.927Z-12.793
Y-36.866Z-12.88
Y-36.805Z-12.967
Y-36.744Z-13.055
Y-36.683Z-13.142
Y-36.622Z-13.229
Y-36.561Z-13.316
Y-36.5Z-13.403
Y-36.439Z-13.49
Y-36.378Z-13.578
Y-36.317Z-13.665
Y-36.256Z-13.752
Y-36.195Z-13.839
Y-36.134Z-13.926
Y-36.073Z-14.014
Y-36.012Z-14.101
Y-35.951Z-14.188
Y-35.89Z-14.275
Y-35.829Z-14.362
Y-35.768Z-14.449
Y-35.707Z-14.537
Y-35.646Z-14.624
Y-35.585Z-14.711
Y-35.524Z-14.798
Y-35.463Z-14.885
Y-35.401Z-14.972
Y-35.34Z-15.06
Y-35.279Z-15.147
Y-35.218Z-15.234
Y-35.157Z-15.321
Y-35.096Z-15.408
Y-35.035Z-15.495
Y-34.974Z-15.583
Y-34.913Z-15.67
Y-34.852Z-15.757
Y-34.791Z-15.844
Y-34.73Z-15.931
Y-34.669Z-16.018
Y-34.608Z-16.106
Y-34.547Z-16.193
Y-34.486Z-16.28
Y-34.425Z-16.367
Y-34.364Z-16.454
Y-34.303Z-16.541
Y-34.242Z-16.629
Y-34.181Z-16.716
Y-34.12Z-16.803
Y-34.059Z-16.89
Y-33.998Z-16.977
Y-33.937Z-17.065
Y-33.876Z-17.152
Y-33.814Z-17.239
Y-33.753Z-17.326
Y-33.692Z-17.413
Y-33.631Z-17.5
Y-33.57Z-17.588
Y-33.509Z-17.675
Y-33.448Z-17.762
Y-33.387Z-17.849
Y-33.326Z-17.936
Y-33.265Z-18.023
Y-33.204Z-18.111
Y-33.143Z-18.198
Y-33.082Z-18.285
Y-33.021Z-18.372
Y-32.96Z-18.459
Y-32.899Z-18.546
Y-32.838Z-18.634
Y-32.777Z-18.721
Y-32.716Z-18.808
Y-32.655Z-18.895
Y-32.594Z-18.982
Y-32.533Z-19.069
Y-32.472Z-19.157
Y-32.411Z-19.244
Y-32.35Z-19.331
Y-32.289Z-19.418
Y-32.227Z-19.505
Y-32.166Z-19.593
Y-32.105Z-19.68
Y-32.044Z-19.767
Y-31.983Z-19.854
Y-31.922Z-19.941
Y-31.861Z-20.028
Y-31.8Z-20.116
Y-31.739Z-20.203
Y-31.678Z-20.29
Y-31.617Z-20.377
Y-31.556Z-20.464
Y-31.495Z-20.551
Y-31.434Z-20.639
Y-31.373Z-20.726
Y-31.312Z-20.813
Y-31.251Z-20.9
Y-31.19Z-20.987
Y-31.129Z-21.074
Y-31.068Z-21.162
Y-31.007Z-21.249
Y-30.946Z-21.336
Y-30.885Z-21.423
----------

----------
G0Z25.0
X0.Y0.M2
```

LIST OF PUBLICATIONS AND PRESENTATIONS

1. Mohanty S, Regalla SP, Daseswara DR (2018) Investigation of influence of part inclination and rotation on surface quality in robot assisted incremental sheet metal forming (RAISF). CIRP J Manuf Sci Technol 22:37–48 . doi: 10.1016/j.cirpj.2018.04.005

2. Mohanty S, Regalla SP, Rao YVD, Robot assisted incremental sheet metal forming under different forming condition, Journal of the Brazilian Society of Mechanical Sciences and Engineering,Springer (Under Review)

3. Mohanty S, Regalla SP, Rao YVD ,Influence Of Process Parameters On Surface Roughness And Forming Time Of Al-1100 Sheet In Incremental Sheet Metal Forming, Jordan journal of mechanical and industrial engineering (Under Review)

4. Mohanty S, Regalla SP, Rao YVD, Improvement of formability in incremental sheet metal forming using a robotic manipulator, Journal of advanced manufacturing technology (submitted)

Conference

1. Mohanty S, Regalla SP, Rao YVD (2015) Multi-stage and robot assisted incremental sheet metal forming. Proc 2015 Conf Adv Robot - AIR '15 1–5 . doi: 10.1145/2783449.2783457
2. Mohanty S, Regalla SP, Rao YVD (2016) Dynamic analysis of robotic manipulator for Incremental Sheet metal forming. 6th Int 27th All India Manuf Technol Des Res Conf (AIMTDR-2016), December 16-18, 2016 Coll Eng Pune, Maharashtra, INDIA 2–6
3. Mohanty S, Regalla SP, Daseswara Rao YV (2017) Tool Path Planning for manufacturing of Asymmetric parts by incremental sheet metal forming by means of Robotic manipulator. Mater Today Proc 4:811–819 . doi: 10.1016/j.matpr.2017.01.090

Book Chapter

Mohanty S., Regalla S.P., Daseswara Rao Y.V. (2018) Dynamic Analysis of Robotic Manipulator for Incremental Sheet Metal Forming. In: Dixit U., Kant R. (eds) Simulations for Design and Manufacturing. Lecture Notes on Multidisciplinary Industrial Engineering. Springer, Singapore

BRIEF BIOGRAPHY OF THE CANDIDATE

Swagatika Mohanty is a research scholar at Birla Institute of Technology and Science Pilani, Hyderabad Campus, India. She obtained her bachelor's degree in mechanical engineering from C.V. Raman College of engineering Bhubaneswar, Odisha in 2011. She worked in Asia Motor Works, Bhuj, Gujarat from 2011 to 2013. Her research area includes incremental forming and robotics.

BRIEF BIOGRAPHY OF THE SUPERVISOR

Dr. Srinivasa Prakash Regalla is a full professor and coordinator of the product design and realization laboratory in the department of mechanical engineering at the BITS Pilani, Hyderabad campus. He was the first head of the department. He was also previously associate dean of work integrated learning programmes (WILP) and assistant dean of research & consultancy at the same institute. Before joining BITS Pilani, he was a guest researcher at NIST, Gaithersburg, MD, USA. He recently completed as principal investigator & project coordinator a BIRAC/BIG-5 project on 'innovative and affordable 3D printing technologies to manufacture artificial limbs for disabled in India'. This work led to continuing collaboration with Share/India – Mediciti institute of medical sciences and a startup company, pspr-3d-tech, dedicated to innovative medical engineering of medical devices, of which he is one of the founders. He published more than 40 peer-reviewed international journal papers, presented in over 35 international conferences, authored 2 books, delivered several invited talks and filed 3 patents. He guided 3 PhDs and is currently guiding 6 PhDs. His research areas are additive manufacturing, sheet metal forming, CAD/CAM, innovative medical devices, metalworking tribology. He has PhD from IIT Delhi, M.Tech from IIT Kanpur and B.Tech. from Kakatiya University, Warangal, all in mechanical engineering.

BRIEF BIOGRAPHY OF THE CO-SUPERVISOR

Dr. Yendluri Venkata Daseswara Rao obtained Ph.D from NIT Raipur in mechanical engineering and M.Tech from IIT Delhi in Design engineering. He was head of department of mechanical engineering in BITS Hyderabad. He was Director of Sri Chaitanya College of Engineering and Technology. He is currently associate professor in mechanical engineering department at BITS Pilani, Hyderabad campus. He has 33 years of experience in teaching and research. He has 21 publications in international journals and 26 in international conferences. His current research areas include Kinematics of Machines and Robotics, Structural Dynamics, Biomaterials, Fluid induced Vibrations, Mechatronics.